uOttawa

L'Université canadienne
Canada's university

FACULTÉ DES ÉTUDES SUPÉRIEURES ET POSTOCTORALES

uOttawa

L'Université canadienne
Canada's university

FACULTY OF GRADUATE AND POSDOCTORAL STUDIES

Kaela Esseghaier

AUTEUR DE LA THÈSE / AUTHOR OF THESIS

M.A.Sc. (Civil Engineering)

GRADE / DEGREE

Department of Civil Engineering

FACULTÉ, ÉCOLE, DÉPARTEMENT / FACULTY, SCHOOL, DEPARTMENT

Early Age Hydration of Portland Cement Systems Containing Cement Kiln Dust

TITRE DE LA THÈSE / TITLE OF THESIS

Dr. James Beaudoin

DIRECTEUR (DIRECTRICE) DE LA THÈSE / THESIS SUPERVISOR

CO-DIRECTEUR (CO-DIRECTRICE) DE LA THÈSE / THESIS CO-SUPERVISOR

EXAMINATEURS (EXAMINATRICES) DE LA THÈSE / THESIS EXAMINERS

Dr. B. Isgor

Dr. M. Fall

Gary W. Slater

Le Doyen de la Faculté des études supérieures et postdoctorales / Dean of the Faculty of Graduate and Postdoctoral Studies

Early Age Hydration of Portland Cement Systems Containing Cement Kiln Dust

by

Kaela Esseghaier

A thesis
Presented to the University of Ottawa
in partial fulfillment of the requirements of the
Master of Applied Science
in Civil Engineering

Department of Civil Engineering
University of Ottawa
Ottawa, Canada

The M.A.Sc. in Civil Engineering is a joint program
with Carleton University administered by the
Ottawa-Carleton Institute for Civil Engineering

Your file Votre référence
ISBN: 978-0-494-51645-4
Our file Notre référence
ISBN: 978-0-494-51645-4

Acknowledgements

I would like to sincerely thank my supervisor Dr. J.J. Beaudoin, Research Emeritus, at the Institute for Research in Construction, National Research Council Canada and Adjunct Professor at the Department of Civil Engineering, University of Ottawa, for his guidance, advice, valuable suggestions, kindness, and understanding in all aspects of my research, degree, and time at NRC.

I would also like to thank the following researchers and technical officers for their technical support and help with the laboratory work and analysis: Mr. Gordon Chan, Mr. Glendon Pye, Mr. Ken Trischuk, Dr. Tai Sato, Dr. Lyndon Mitchell, Dr. Jon Makar, and Mr. Jocelyn Henrie from the Institute of Research in Construction, and Mrs. Bussaraporn Patarachao from the Institute for Chemical Process and Environmental Technology, both institutions belong to the National Research Council, Canada.

I would also like to express special gratitude to my husband and my family for their support and encouragement throughout my degree.

Abstract

Cement kiln dust (CKD) has been used in combination with ordinary Portland cement (OPC). It has also been shown that this generally results in a reduction in strength. In some cases hydration is retarded. The objectives of this study were to use nano-calicum carbonate (CC) and metakaolinite (MK) particles in cement systems containing OPC and CKD to improve its hydration, strength, and pore structure. Calorimetry results showed that both the addition of the CC and MK particles significantly accelerated the hydration of the system. The addition of CC and the MK particles were generally effective in improving the strength of the system. Analysis of AC impedance measurements suggested that CC or MK addition resulted in a refinement of the pore structure of the system. Results from X-ray diffractometry measurements and SEM imaging were in general agreement with results obtained from the other testing techniques.

Contents

List of Tables

List of Figures

Glossary

A	cross-sectional area, mm^2
C	capacitance, F (farad)
C_d	total capacitance of the solid-liquid interface, Farad
C_f	capacitance of the solid-liquid interface for one element, Farad
d	day
F	frequency, Hz
i(t)	current, A
j	$\sqrt{-1}$
m_d	dry mass, g
m_{disp}	mass of the displaced fluid, g
m_s	submerged mass, g
m_w	wet mass, g
N	number of elements
n	depression angle parameter
P	concentrically applied load, N
P	porosity
p_i	intrusion volume (%) for a given pressure, i
ρ_{disp}	the density of the displaced fluid in g/cm^3
R	resistance, or resistance due to R_S and R_L in parallel, Ω
R_1	total resistance of the liquid, Ω
R_2	total resistance due to the solid-liquid interface, Ω
R^2	regression value
r_o	mean pore size
r_i	pore diameter, μm, for a given pressure, i
R_f	resistance of the solid-liquid interface, Ω
R_S	resistance in the solids, Ω
R_L	resistance in the liquid, Ω
S	area of the solid element normal to the electric field, mm^2
S_1	the area of the liquid phase, mm^2
t_p	time to reach the peak value of the heat of hydration
V_{disp}	volume of the displaced fluid, cm^3
V_p	volume of the pores in the sample, m^3
V_t	total volume of the sample, m^3
v(t)	voltage applied to the system, V
|Z|	magnitude of impedance, Ω
Z'	real part of impedance
Z''	imaginary part of impedance
Z_1	total impedance of the parallel circuit containing R_S and R_L, Ω
Z_2	total impedance of the parallel circuit containing R_f and C_f, Ω
Z_C	impedance due to a capacitor, Ω
Z_T	total impedance, Ω
Δx	the width of the N electrical elements, mm
φ	porosity
φ_{dep}	depression angle

ω	angular frequency of the applied current, rad/s
σ	engineering stress, MPa
σ_l	the electrical conductivity of the liquid phase, $\Omega^{-1}m^{-1}$
ψ_s	the area fraction of the solid phase, mm^2

Abbreviations

AC	alternating current
ACIS	alternating current impedance spectroscopy
A	Al_2O_3, aluminum oxide
C	CaO, calcium oxide
$CaCO_3$	calcium carbonate
CC*	calcium carbonate
CKD	cement kiln dust
CPE	constant phase element
C-S-H	Calcium Silicate Hydrate
F	Fe_2O_3, iron oxide
GGBFS	ground granulated blast furnace slag
H	H_2O
HFA	high frequency arc
MK	metakaolinite
OPC	ordinary Portland cement
psi	pounds per square inch
S	SiO_2, silicon dioxide
SEM	scanning electron microscopy
SCM	supplementary cementing material
XRD	X-ray diffractometry
XRF	X-ray fluorescence

*Cement chemistry nomenclature abbreviates calcium carbonate as $C\overline{C}$, where $\overline{C}$= CO_2.

Chapter 1

Introduction

1.1 Portland Cement and Cement Kiln Dust

Concrete, the engineering building material of choice, consists of Ordinary Portland Cement (OPC), coarse and fine aggregate, and water. There are three main reasons that concrete is the most widely used engineering material. Firstly, it has a high resistance to damage that can be sustained due to water and fire (unlike both steel and wood structures). The second reason is that it can be molded into as many shapes as can be imagined. And the third main reason is due to the fact that it is one of the cheapest and most readily available building materials (Mehta and Monteiro, 2006).

Approximately 11 billion metric tones of concrete are consumed around the world every year. Naturally, with all this concrete production also comes a lot of waste. One type of waste is produced during the manufacturing of the OPC used in concrete. The waste comes in the form of a dust. This dust is called Cement Kiln Dust (CKD) and it is accumulated as raw materials are put through a kiln during the process of cement manufacturing. It has been estimated that the cement plants around the world generate around 30 million tons of CKD every year (Dyer et al., 1999). The exact composition of the dust varies just as the composition of the cement varies from plant to plant. Overall, the CKD can be composed of a mixture of calcined (materials heated to high temperatures to change its physical properties to be used as a cementing material) and uncalcined feed materials, fine cement clinker (a cement material which appears during the cement manufacturing process that has not yet been ground down to the finer particle size of OPC), fuel combustion by-products, and condensed alkali compounds (compounds containing sodium or potassium) (ASTM D5050, 2008).

It has been suggested that CKD is responsible for significant financial losses suffered by the cement industry; its collection and disposal are among the costs that have contributed to these losses (Konsta-Gdoutos and Shah, 2003). Clearly, finding ways to make use of the CKD would not only be financially beneficial but would also cut down on disposal and hence, the negative impacts that disposal can have on the local environment. One solution would be to recycle the CKD directly back into the kiln during cement production. However, direct recycling of CKD has been known to cause damage to kiln refractories; in addition, it causes an unfavored clinker phase to be formed during the firing of the kiln (during cement manufacturing) which is attributed to the effect the high alkalinity contents of the dust have on the nature of the clinker phases (Shoaib et al., 2000). Another intuitive solution to this problem is to recycle the CKD and use it in combination with the OPC to make concrete; this is especially relevant in these times when the recycling of materials and the use of sustainable materials should be among the priorities of building designers. However, one disadvantage associated with the replacement of OPC with CKD is that it appears to be responsible for decreased early and advanced age compressive strengths (i.e. early and overall strength development) (Bhatty, 1984). On occasion it has been known to increase cement paste setting times. Loss in early strength and increased setting times both translate into an undesirably longer amount of time necessary before formwork on construction sites can be stripped.

In order to counter slow setting and reduced strength, an accelerator would need to be used in addition to the CKD and OPC. Calcium carbonate, $CaCO_3$, which in cement chemistry nomenclature is abbreviated as, $C\bar{C}$ (where C= CaO and $\bar{C}$ = CO_2), has been used in the past as an accelerator in cement systems. Nano-calcium carbonate, (which will be referred to as nano-CC or simply 'CC' for the remainder of the discussions) are particles of calcium carbonate with a maximum particle size of a few nanometers. In recent studies, its addition to cement systems has improved the strength and accelerated the setting times of systems containing the following: 1) OPC, 2) mixes containing OPC and ground granulated blast furnace slag (GGBFS, a

by-product in iron and steel manufacturing), and 3) OPC and fly ash (a by-product of pulverized coal) (Sato and Beaudoin, 2006, 2007). The research showed that 10% and 20% additions of the nano-CC to the OPC greatly accelerated the early hydration and strength of all three systems. In addition, it was found that the larger the amount of nano-CC that was added, the greater the accelerating effect that was observed. It was suggested that the reason for this accelerating effect was due to the small particle size of the nano-CC, which was believed to have acted as a nucleation site (a site that enables the growth of C-S-H (calcium silicate hydrate) nuclei to take place resulting in an acceleration of the cement hydration process). For the reasons mentioned, it was thought that the nano-CC could be used in conjunction with the OPC+CKD mix to possibly aid in accelerating the hydration process and improve its strength development. There appears to be, to the author's knowledge, no research conducted to determine whether adding nano-CC to a cement mix that has already been partly replaced by CKD is beneficial with regard to strength and its hydration process.

In the past, natural pozzolans (materials that when finely ground and used in combination with calcium hydroxide and water exhibit cementitious properties) such as metakaolinite (MK) have also been shown to increase the strength of OPC. For example, Malhotra (1987) showed that the use of 10% of a natural pozzolan increased the overall strength of OPC paste. Another study showed that when MK was added to OPC, it promoted a decrease in the porosity, and the formation of a finer pore size distribution of the cement paste (Guneyisi et al., 2008). For the current work, it was thought that using MK in combination with the OPC+CKD and the OPC+CKD+nano-CC mixes might benefit their respective strength developments and microstructures. To the author's knowledge no research in the past has combined OPC, CKD, and MK nor OPC, CKD, MK, and nano-CC.

1.2 Research Objectives

The objectives of the research were to:

1. Determine the effects of the addition of nano-CC on the replacement of OPC with CKD and/or MK with emphasis on:
   -early hydration (first 24 hours),
   -strength development, and strength-porosity relationship (at 1, 3, 7, 28 days of hydration),
   through the use of calorimetry, strength, and porosity measurements.

2. Use A.C. impedance methods (from 0-24 hours) along with porosity (at 5, 8, 16, and 24 hours) and mercury instrusion porosimetry measurements (at 8 hours) as a means of further investigating early-age hydration behavior of the binary, ternary, quaternary systems containing CKD. Supplement the interpretation of the AC impedance spectra (at early ages) using physical measurements:
   - for example: pore size distribution and porosity of the mixes.

3. Assess, to the extent possible, the influence of CKD composition on the early hydration kinetics of the cement systems under study. The CKDs selected had the following specific characteristics: Bath CKD (high in chloride and low in alkali); Alpena CKD (high in sulfate and high in alkali); and Ashgrove CKD (high in alkali). Employ investigative tools such as X-Ray Diffraction (XRD) spectroscopy and Scanning Electron Microscopy (SEM) to further understand the development of the microstructure and its contribution to engineering performance of the systems studied.

4. Assess the compatibility of MK in cement systems containing CKD; as MK has been shown to be an excellent supplementary cementing material.

Meeting these objectives is expected to provide a better understanding of the combined effects of the materials studied on the early strength development and hydration kinetics. In addition it should aid in further investigating the varying effects that the materials have on the cement systems in terms of microstructural descriptions such as: porosity, pore structure, conductivity of the pore solution, and pore size distribution. It should also aid in optimizing the quantities of the CKD, MK, and nano-CC that might serve as effective replacements or additions to OPC.

Chapter 2

Literature Review and Background Information

2.1 Introduction to OPC

Portland cement is defined in the American Society for Testing and Materials, (ASTM) Standard C150 as a hydraulic cement (meaning it reacts with moisture) that is produced by pulverizing clinker that consists of calcium silicates usually containing one or more of the forms of calcium sulfate as an inter-ground addition (ASTM C150, 2007). Clinker is made up of solid particles, produced after a raw mixture of materials is heated to high temperatures as part of the cement manufacturing process. During this process, chemical reactions take place between raw materials of limestone and clay in the cement kiln. This produces the four primary compounds of OPC: tricalcium silicate (C_3S), dicalcium silicate (C_2S), tricalcium almuniate (C_3A), and tetracalcium aluminoferrite (C_4AF). When water is added to OPC, the C_3A hydrates immediately; this can cause pre-mature setting of the cement paste. For this reason, gypsum (chemical formula: $CaSO_4 \cdot 2H_2O$) is added to the cement paste so that it reacts with the C_3A. This reaction produces needle-like crystals called ettringite (Taylor, 1997). The chemical formula for each of the main compounds found in OPC can be seen in Table 2.1-1. These compounds make up around 90% of the cement mass. Gypsum and other minor compounds make up the remainder of the mass. Alkalis (compounds which contain sodium or potassium) in OPC are present due to the addition of the clay components that are in the raw mix and added coal (Mehta and Monteiro, 2006).

Table 2.1-1: Primary compounds in OPC with their corresponding chemical formulas

Compound	Chemical Formula
C_3S	$3CaO{\cdot}SiO_2$
C_2S	$2CaO{\cdot}SiO_2$
C_3A	$3CaO{\cdot}Al_2O_3$
C_4AF	$4CaO{\cdot}Al_2O_3{\cdot}Fe_2O_3$

2.1.1 Hydration of OPC

OPC is a manufactured powder that requires water to be added for it to bind sand and rock in concrete. When water is added to OPC it undergoes a chemical reaction, referred to as hydration, that leads to the formation of products that possess setting and hardening characteristics (Mehta and Monteiro, 2006). The hydration reactions of OPC compounds are exothermic. The data from the heat of hydration can be used to characterize the setting and hardening behavior of cements (Mehta and Monteiro, 2006). A calorimeter is commonly used to measure the heat given off by a sample of cement paste as it hydrates. A typical output curve for OPC at a water/cement ratio of 0.5 can be seen in Fig. 2.1-1. The data used in Fig. 2.1-1 was collected during this study. In this figure, the y-axis displays the heat of hydration measured in calories of heat /gram of sample/ hour (cal/g/hr) while the x-axis displays the time after the sample has been mixed. It should be noted that details on calorimetry are discussed further in Chapters 4 and 5.

It can be seen from this figure that the data initially peaks within the first few minutes of hydration (see "1" on Fig. 2.1-1). This first peak is thought to be due to the heat of solution of aluminates and sulfates (Mehta and Monteiro, 2006) and the initial formation of ettringite (chemical formula: $C_3A{\cdot}3CaSO_4{\cdot}32H_2O$). Ettringite is formed when C_3A and gypsum react, it is part of what is termed the AFt phase group (the 't' stands for tri, as in containing three molecules of calcium sulfate) (Taylor, 1997).

The third peak (see "3" on Fig. 2.1-1) is typically associated with the reaction of C_3A and it has been suggested that it corresponds to the renewed formation of ettringite

(Pratt and Ghose, 1983). It is the second peak (see "2" on Fig. 2.1-1) that is of great interest in cement science. Initial setting of OPC occurs during the ascension of peak 2. It is during this period when the OPC begins to stiffen and solidify. The second peak itself, occurring typically between four and eight hours, is due to the heat of rapid formation of $Ca(OH)_2$ and hydrated silicate phases, due to the reaction between C_3S and C_2S, whose chemical formula is assumed to be approximately $C_3S_2H_3$ (Taylor, 1997). It should be noted that the stoichiometry is approximate because its chemical composition varies depending on the OPC's age, temperature, and water/cement ratio (Sato, 2002). The common notation refers to $C_3S_2H_3$ as C-S-H; and it should not be interpreted to mean that it follows any particular structure. Also mixed in with the C-S-H are hydrates in the AFm phase group (the 'm' stands for mono, meaning their composition is made up of only one molecule of calcium sulfate). They are considered poorly crystalline and can be intimately mixed with the C-S-H (Taylor, 1997).

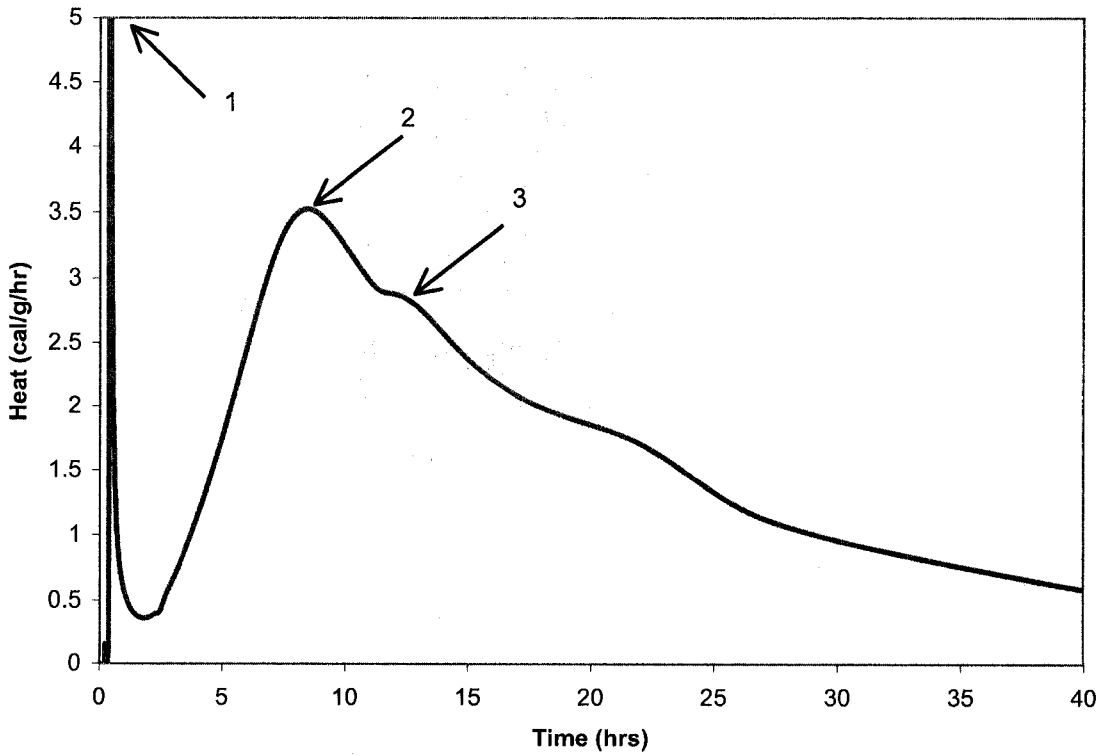

Fig. 2.1-1: Typical output curve for the hydration of OPC with w/c=0.5.

De Silva and Glasser (1990) suggested that peaks 2 and 3 were not actually the result of two exothermic reactions, but of an exothermic one and an endothermic one. They proposed that what is perceived as two separate peaks is actually one broadened peak due to the exothermic reaction of the formation of C-S-H with a superimposed endothermic dip resulting from the reaction during which AFt changes to AFm: giving the illusion of two separate peaks.

Interpretations aside, it is agreed upon that at this point where the second peak occurs the OPC has completed solidifying and begins to harden. The time at which the second peak occurs depends on the compounds present in the mix as well as the water/cement ratio. As this time to the second peak becomes shorter (i.e. the peak shifts to the left), the mix is setting faster; as this time lengthens (i.e. the peak shifts to the right), the mix is setting more slowly.

2.2 Introduction to CKD

The CKD, as was mentioned earlier, is a waste by-product produced during the manufacturing of cement. It is estimated that the cement manufacturing plants around the world generate around 30 million tons of CKD every year (Konsta-Gdoutos and Shah, 2003). Shoaib et al. (2000) provide a useful description of how CKD is formed. During cement manufacturing, a mixture of limestone, shale, clay, and sand are ground together. This mixture is fed through a kiln at high temperature which fuses the materials together. Small-sized balls called clinker and fine solid particles of the raw material and semi-finish dust then form in the kiln. It is during the cement plant's drying process that CKD is generated. Approximately 12% of the mass of the materials fed into the kiln exit as dust (Shoaib et al., 2000).

The CKD can be composed of a mixture of calcined and uncalcined feed materials, fine cement clinker, fuel combustion by-products and condensed alkali compounds (ASTM D5050, 2008). Physically, the dust looks like a powder that is usually slightly darker or lighter in colour than OPC. The chemical compounds found in the CKD

vary from plant to plant. Because CKD is a by-product of OPC, it naturally contains some of the compounds present in OPC such as calcite ($CaCO_3$) which is a filler used in OPC. The actual chemical composition of the CKD depends on both the raw materials used in the production of the cement as well as the type and source of carbon-based fuel used to heat the materials in the kiln (Siddique, 2006). The alkalis present in the CKD come from the clay compounds that are present in the raw mix as well as the coal used in the cement manufacturing process (Mehta and Moneiro, 2006). The exact chemical compositions of the CKDs used in the current work will be discussed in Chapter 3.

Effectively replacing OPC with CKD in combination with CC (and in some cases in combination with MK) is the ultimate goal of the research that will be presented. It should be noted that there are a few other ways in which CKD is currently being re-used such as: in soil stabilization (as way of improving soil strength), in waste treatment (used for solidifying and stabilizing waste), and in asphalt pavement (as a replacement to reduce asphalt cement requirements) (Siddique, 2006).

2.2.1 Previous Research on Cement Systems Containing CKD

Studies have been conducted on the use of CKD over the last three decades. Research has been performed on the use of CKD with cement systems (i.e. OPC or OPC mixes containing other supplementary cementing materials (SCMs) such as fly ash, a by-product of pulverized coal, and ground granulated blast furnace slag, GGBFS, a by-product of smelting iron or steel). The studies have focused on compressive strength measurements and the hydration process.

2.2.1.1 CKD Addition: Effect of on Strength Development of Cement Systems

The effect CKD addition has on the compressive strength of cement systems has been researched in the past. It has been found to decrease early and later age strength. The

research conducted by Shoaib et al. (2000) showed that the compressive strength of OPC decreased with increasing quantities of CKD present in the mix. Replacements of 10%, 20%, 30% and 40% of OPC with CKD resulted in a decrease in compressive strengths throughout its hydration (1, 3, 6 months). The higher the amount of OPC that was replaced with CKD the greater the decrease in compressive strength that was observed. This is in agreement with experiments conducted by Bhatty (1984) where the replacement of 10%, 15%, and 20% of OPC with CKD generally lowered strength values as the percentage of CKD increased. This decrease was generally attributed to the replacement of cement clinker, which is mainly responsible for strength development. In addition, the larger amounts of chloride present in the CKD resulted in a sort of crystallization of the hydration products. This resulted in an opening of the pore systems, which led to a reduction of strength. The increased abundance of alkalis and sulfates in the mix (due to the CKD) was also thought to be a reason for the decrease in strength. Siddique (2006) suggested that an increase in these compounds (the alkalis, sulfates, and chlorides) affect the amount of C-S-H and aluminate hydrates, which leads to the formation of considerable amounts of hydrated sulpho-aluminates and chloro-aluminates, which causes softening of the mix.

However, research conducted by Bhatty (1984) showed that a CKD with high amounts of potassium chloride (KCl), an alkali chloride, at a replacement percentage of 20% had a higher compressive strength than replacements with 10% or 15%. It was suggested that KCl might behave similarly to calcium chloride ($CaCl_2$), which is known to increase concrete strength especially at 1 to 3 days of curing (Bhatty, 1984). Bhatty (1985) also showed that cement mixes containing a CKD with a high sulfate composition developed higher strengths when compared to CKDs with less sulfate present. The research conducted involved compressive strength testing on mixes containing 10%, and 20% replacements of CKD for 1-inch cement cubes at a water/solids ratio of 0.45 with testing conducted at 1, 7, 28, 90, and 365 days. The results showed that mixes that contained higher amounts of sulfate and free lime (CaO) developed higher strengths.

The effects of the water/cement ratio on the strength development of concrete and cement pastes containing OPC and CKD have also been investigated. In the research conducted by Al-Harthy et al. (2003) seven mixtures were tested with CKD replacement percentages of 5%, 10%, 15%, 20%, 25%, and 30%. Three water/cement ratios were used: 0.7, 0.6, and 0.5. Mixtures containing lower percentages (5%) of CKD produced compressive strengths close to the control mix. This was especially true at a lower water/cement ratio of 0.5. It was concluded that a lower water/cement ratio might aid in lowering the detrimental effects caused by the replacement of OPC with CKD.

In addition to the possibilities of decreased strength there is another concern in using CKD to replace OPC in concrete. Increased alkali-aggregate reactions (reactions where aggregates in the concrete react with the alkali hydroxides in the mix which leads to expansion and cracking) and chloride corrosion of reinforcing steel due to the increased alkalis and chlorides in the CKD are possibilities. It was thought by Bhatty (1984) that these negative impacts caused by the addition of the CKD might be controlled by the addition of fly ash or slag. In this study mixes were cast as one-inch cubes with a water/solids ratio of 0.5 using five different types of CKDs: some low in alkali and chloride and others higher. Mixes were made with 10% CKD and 10% (and later with 20%) of fly ash, as well as 10% CKD with 10% (and later with 20%) of slag. The mixes containing fly ash were generally weaker than mixes containing simply OPC and CKD. Fly ash mixes that contained CKDs with low alkali contents faired better than those with higher alkali contents. And fly ash mixes containing CKDs with high alkali and high chloride contents generally faired worse than mixes containing other CKDs. In general, the mixes that contained high amounts of chloride present in the CKD used with fly ash caused a lower overall gain in strength as compared with the CKDs that did not contain an abundance of chloride. As for mixes that contained slag, they tended to have higher strengths than those containing fly ash. They also produced higher strengths than mixes that contained simply CKD and OPC. In addition, increased amounts of slag tended to increase the strength of the CKD and OPC mix.

Konsta-Gdoutos and Shah (2003) researched the possible use of CKD as an activator for granulated ground blast furnace slag (GGBFS). They suggested that CKD's high alkali and sulfate content could make it an activator for pozzolanic materials. A pozzolanic material is one which when combined with calcium hydroxide ($CaOH_2$) and moisture, chemically reacts to form compounds that possess cementitious properties. Four different CKDs were used in the mixes whose proportions were follows: 100% OPC, 50% OPC+ 50% slag, 50% CKD+50 % slag. They measured the compressive strength of mixes of cylindrical mortar specimens (75 x 150 mm) at 7, 28, and 56 days. The strengths for all mixes that contained CKD were always lower than the OPC or OPC+slag mixes. The CKD of the CKD+slag mix that was the weakest lacked adequate quantities of lime for a pozzolanic reaction to occur. The CKD of the CKD+slag mix that was the strongest was composed of fine and uniformly distributed particles that provided a higher surface area and promoted an intense reaction to take place.

Other additives such as sodium hydroxide (NaOH) have been added to mixes containing CKD and fly ash in hopes that it would add to the alkali concentration of the mix (in addition to those provided by the CKD) and activate the fly ash with the objective of improving compressive strengths. Wang et al. (2004) added NaOH (2% and 5%) to pastes containing 50% CKD and 50% fly ash at a water/solids ratio of 0.52. They found that at a temperature of 38°C the addition of 2% NaOH to the 50% CKD, 50% fly ash mix resulted in the highest compressive strength value (of 27 MPa). However, it was thought that the higher curing temperature might have been the dominant variable (over the effects of the added NaOH) that was responsible for the increase in strength.

2.2.1.2 CKD Addition: Effect on Hydration of Cement Systems

The substitution of OPC with CKD has been known to have varying effects on its hydration. Siddique (2006) reported that an addition of 5% CKD to an OPC paste slightly retarded its setting time. Heikal et al. (2002) found that when 2.5% CKD was

added to a mix containing OPC and slag (at both 70%/30% and 50%/50% proportions of OPC and slag), it increased the setting time of the mix. The CKD used in that research was high in both sulfates and chlorides.

Konsta-Gdoutos and Shah (2003) also researched the effects on the hydration of mixes containing simply OPC and OPC with 50% slag, and then with 50% slag and 50% CKD: using five different CKDs. Firstly, they found the addition of the slag increased the setting time of OPC by 50 minutes. Secondly, they found that the slag and CKD mix whose CKD contained a high amount of sulfate decreased the setting time; whereas the four other CKDs which, were low in sulfate, all had increased setting times. Thirdly, the hydration of the slag and CKD mix whose CKD content was high in chloride showed an earlier peak in the heat evolution curve which indicated that its hydration was accelerated by this CKD. The mixes with the other CKDs, which all had lower chloride contents, showed delayed peaks in their heat evolution curves. This conflicts somewhat with research conducted by Bhatty (1984). The results there showed that samples containing 10%, 15%, and 20% replacements of CKD decreased the setting time even for the CKD high in chloride.

To the author's knowledge, there has not been any research conducted which combined OPC, CKD, and nano-CC and/or MK. Background information on CC is discussed next.

2.3 Introduction to the Use of Calcium Carbonate in Cements

Limestone, which is mainly composed of calcium carbonate (CC), can occur in the form of a dust that is produced in quarrying operations. It poses disposal and environmental problems (Ramachandran and Chun-mei, 1986). It is used as a common replacement to OPC so as to reduce the amount necessary for concrete applications. Originally, the aim behind using CC as a replacement to OPC was simply to replace a valuable material (the OPC) with a less valuable material (the CC); however, as further research was conducted, there were indications of positive

effects that the CC had on the OPC in terms of its hydration and strength (Sato and Beaudoin, 2007).

Standards in several countries allow for certain concentrations of limestone to be present in the OPC. ASTM C150 allows for up to 5% of the cement paste used in concrete to be made up of limestone so long as it is naturally occurring, finely ground, and contains at least 70% by mass of one or more of the mineral forms of calcium carbonate (ASTM C150, 2007); this has only been the case since the year 2004. The Canadian Standards Association (CSA) has allowed OPC to contain a maximum of 5% of limestone since 1983 (CSA, 2008). In addition, the CSA Standard A3001-08, defines a "Portland-limestone cement" as a product obtained by blending Portland cement and limestone (CSA, 2008). This standard allows for a proportion of 5% to 15% of limestone to be present in the Portland-limestone cement where the CC content must be at least 75% by mass (CSA, 2008). The British / European Standard, BS EN 197-1, also specifies a "Portland limestone cement". There it can contain from 6% to 35% of ground limestone (BS EN, 2000). Countries such as South Africa and Mexico both allow up to 35% limestone addition; while, New Zealand and Brazil allow up to 15% and 10% additions of limestone, respectively (Hooton et al., 2007).

2.3.1 Previous Research with Calcium Carbonate and Nano-Calcium Carbonate

2.3.1.1 The Effect of Added CC on the Compressive Strength of Cement Systems

The addition of CC has been known to increase the compressive strength of mixes made with OPC and cement mortars. Research conducted by Soroka and Setter (1977) showed that the addition of finely ground limestone (10%, 20%, 30%, and 40%) in combination with OPC, and a 1:2.75 ratio of cement to sand, improved its compressive strength. In general, compressive strengths improved as the fineness and amount of limestone increased. They attributed the increase in strength to an increase in the mix density, and lower air content that is associated with the use of fillers such

as limestone. Ingram and Daugherty (1991) reported that a 7.5% addition of CC resulted in an increase of compressive strength of OPC at one day after mixing. They mention that this ratio of carbonate to the amount of C_3A in the system might give more of the monocarboaluminate species, which is known to add strength to cement. Péra et al. (1999) concluded that cylinders (20 mm x 40 mm) of OPC paste with CC percentages of 10%, 20% and 40% (although they had lower compressive strengths than the control mix) faired well in comparison with the controls. A replacement of 10% had values nearest to the compression strengths of the control mix at all ages (7, 28, and 60 days). Soroka and Stern (1976) also conducted research that involved the addition of ground limestone and reagent grade quality CC (i.e. pure CC) (added in percentages of 10%, 20%, 30%, and 40%) in combination with OPC and sand (with cement to mortar ratio of 1:2.75). They found that strength improvements of the mortar cubes were mostly seen in the early ages of cement hydration rather than at later stages (such as at 28 and 90 days hydration). This is characteristic of strength development when the hydration of cement is accelerated. The reagent grade CC, with higher specific surface values, showed a more pronounced effect on the early stages of strength development. They suggested that fine fillers such as CC act as crystallization nuclei, or seeds, for accelerating the hydration of cement.

2.3.1.2 The Effect of CC Addition on the Hydration of Cement Systems

The addition of CC to C_3S and OPC systems is known to accelerate the hydration process. Ramachandran and Chun-mei (1986) studied the effects of the addition of CC on the hydration of C_3S. C_3S is known to be responsible for strength development in OPC. An understanding of the effects the addition of CC had on the hydration of C_3S is the first step in attempting to understand why CC aids in strength development of OPC. The idea that the CC acts as a nucleation site (a site that enables a reaction to take place) for hydration products, was first suggested by Soroka and Stern (1976). This idea was also discussed by Ramachandran and Chun-mei (1986). Their research showed that the main calorimetry peak shifted toward earlier times for C_3S mixes

with added CC. The time to reach the peak also decreased with increasing CC concentrations (5%, 10%, 15%, 20%): indicating hydration was accelerated. Research conducted on OPC pastes with added CC indicated the same accelerating effects observed with the C_3S pastes. Péra et al. (1999) reported research on the effects of CC on the hydration of OPC. The results showed that the rate of heat evolution curves for the hydration of the mixes containing 50% CC indicated the hydration was accelerated by an hour.

Ramachandran and Chun-mei's (1986) microhardness data showed an increase in hardness of C_3S paste as the concentration of CC increased. They attributed this to the fact that the CC may add strength by contributing to the bonding of the C-S-H particles during hydration. They also showed that the density of samples containing CC increased as the hydration progressed as compared to the density of samples without added CC. Pore size distribution curves for the samples showed that for up to 7 days, the sample containing 15% CC exhibited a structure with more fine pores as compared with the mix without added CC. They suggested that the pores were being filled with the fine-sized, high surface area particles of CC. Scanning electron microscopy (SEM) imaging was performed on samples of C_3S with 50% CC at 1 day and 28 days hydration. It could be seen in these images that fibrous particles of C-S-H grew on both the C_3S and the CC particles. They concluded from this that it was possible that the CC was acting as a nucleating agent. From this they were able to also conclude that the accelerating effect of CC may be related to its nucleating effects.

2.3.1.3 Previous Research on Cement Systems Containing nano-Calcium Carbonate Particles

It is clear from past research that CC additions have aided in accelerating the hydration and improving the early strength development of cement systems. As was mentioned earlier, it is the belief that the CC's fine particle size and high surface area provide it with the means of behaving as a nucleation site for the growth of hydration

products such as C-S-H. Research conducted by Sato and Beaudoin (2006) took this idea further by using nano-calcium carbonate (nano-CC), (particles of calcium carbonate with a particle size distribution indicating a range of particle sizes of around 50-100 nanometers) in cement systems. This provided the cement systems with an even finer carbonate addition having an increased surface area.

Sato and Beaudoin (2006) conducted research on samples of OPC, and OPC with 10% and 20% additions of both micro-sized and nano-sized CC. Both the micro-CC and nano-CC accelerated the hydration of the OPC. However, it was the nano-CC that greatly accelerated the hydration. From the heat of hydration curves (results from calorimetry measurements) it could be seen that the nano-CC halved the time to the major peak of the heat of hydration curve of OPC. In addition, it was observed that the accelerating effect increased with increasing concentrations of both micro and nano-CC that were added. They also conducted experiments on mixes with 50% OPC, 50% slag (and others with 50% fly ash in another study (Sato and Beaudoin, 2007)) with 10% and 20% additions of micro-CC and nano-CC. The additions of the 10% and 20% micro-CC had a very small accelerating effect (based on the calorimetric curves) on the hydration of the mix as compared with the significant effect that was observed with the additions of nano-CC.

Sato and Beaudoin's (2006, 2007) microhardness testing results indicated that the addition of the nano-CC had a greater impact than the micro-CC in improving the hardness of the OPC/slag and OPC/fly ash mixes. It was suggested that the reason for greater improvements seen when using nano-CC as compared to micro-CC was due to the smaller particle size of the nano-CC particles that may have acted as nucleation sites. Early and longer-term strengths of OPC/slag and OPC/fly ash mixes were both remarkably improved with the addition of 20% nano-CC.

The positive impacts of nano-CC addition on accelerating hydration times and improving strength of OPC supplementary cementing materials (slag and fly ash) provided the basis for its use in this research. It was thought that the nano-CC might

also have the same positive effects on mixes containing OPC and CKD. It follows that one of the objectives of the research that will be presented in the chapters that follow is to determine if these positive results can be extended to the OPC-CKD system.

2.4 Introduction to the Use of Metakaolinite in Cement Systems

Metakaolinite (MK) is a natural pozzolan. A pozzolan is a material which when combined with calcium hydroxide ($CaOH_2$) and moisture, chemically reacts to form compounds that possess cementitious properties. It is a commonly used supplementary cementing material. It has an amorphous composition (a solid compound without a defined crystalline structure) and high surface area (Lagier and Kurtis, 2007). It is produced by the calcination of pure or refined kaolin clay at the temperature between 650°C and 850°C; this is followed by grinding the material to an average particle size of approximately 1 to 2μm (Sato, 2006). Ranges for the chemical composition of MK used in this study were provided by the manufacturing company and can be seen in Table 2.4-1.

Table 2.4-1: Typical chemical composition of MK (% by mass).

SiO_2	Al_2O_3	CaO	Fe_2O_3	MgO	SO_3	Na_2O	K_2O
52-53	42-43	0.02-0.1	0.5-1	0-1.0	0-0.1	0-0.05	0.4-1.5

2.4.1 Previous Research on the Use of Metakaolinite in Cement Systems

2.4.1.1 The Effect of MK Addition on the Strength and Pore Structure of Cement Systems

The addition of MK to concrete has been shown to improve its strength and pore structure. Research conducted by Guneyisi et al. (2008) concluded that the addition of MK (in 10% and 20% additions by mass of OPC) to OPC at two different water/cement ratios (0.35 and 0.55) increased their compressive strength values

substantially. Strength increased with increasing concentrations of added MK. Early-age effects of the MK on the paste's strength and pore structure refinement was described by Poon et al. (2001): higher compressive strengths and pore structure refinement of samples were attributed to MK's high initial reactivity. Similar results were found by Malhotra (1987). This research showed that the use of 10% of a natural pozzolan increased the 28-day strength of OPC paste. Guneyisi et al. (2008) also found substantial improvements in strength at later hydration times, for example at 120 days. They argued that the increase in concrete strength was due to the improvement of the bond between the cement paste and the aggregate particles as well as the increased density of the cement paste. The density of the samples improved due to the ultra-fine particles of the MK filling the voids in the hydrated cement.

Guneyisi et al. (2008) also studied the microstructure of samples containing MK. Mercury intrusion porosimetry was performed on samples, without coarse aggregate, to determine the porosity and pore size distributions of the mixes at 120 days hydration. It should be noted that mercury intrusion porosimetry will be discussed in detail in Chapters 4 and 5. The results showed that for similar pore sizes the pore volume of the samples without MK was higher than those with MK. Also, the samples containing MK had lower total porosities with increasing amounts of MK and finer pore size distributions as compared to those without MK. This was in agreement with research conducted by Khatib and Wild (1996) who found that the addition of MK to OPC lead to a refinement of the pore structure.

2.4.1.2 The Effect of MK Addition on the Hydration of Cement Systems

The addition of MK to cement systems has been known to accelerate its hydration. During the hydration process, the MK reacts with $Ca(OH)_2$ (which is produced during the hydration of the calcium silicate phases in the cement, (Lagier and Kurtis, 2007)) to form C-A-S-H and aluminate phases, C_2ASH_8 and C_2AH_{13} (Rojas and Cabrera,

2002). It is believed that the formation of the C-A-S-H during the hydration process reduces the total porosity and refines the pore structure which ultimately improves the strength of the cementitious matrix (Khatib and Wild, 1996). Justice and Kurtis (2007) conducted calorimetry measurements on samples containing OPC and OPC with an 8% addition of MK (composed of both a medium and high surface area material). They found that the MK had an accelerating effect on the hydration of the OPC which increased with the increasing surface area of the MK. Lagier and Kurtis (2007) suggested that the MK had a catalyzing effect on cement hydration. The reason for this may be because the MK provided well-dispersed sites for nucleation of hydration products. This was an argument for the addition of nano-CC to OPC mixes discussed in section 2.3.1.2.

There has been no research reported on the effects of the addition of MK to an OPC+CKD mix. The objective is to add MK to the OPC+CKD system as well as the OPC+CKD+CC system to benefit from possible positive effects on porosity and strength. The high reactivity and surface area of MK and the previous synergism obtained with CC addition to OPC systems containing slag and fly ash support an investigation of ternary and quaternary systems containing this pozzolan.

2.5 Statement of Original Research Conducted in this Study

Previous research has included investigation of the hydration and strength development of OPC and CKD with and without other SCMs such as slag and fly ash. No studies have included additions of nano-CC or MK. In addition, studies have not yet been conducted on the effect such combinations have on the early-age microstructure development, for example porosity, etc. In brief, the early-age behavior of these systems as quantified by calorimetry, compressive strength data, porosity, and electrical impedance measurements have not been performed on ternary and quaternary mixes containing combinations of OPC and CKD with CC and/or MK.

The original research reported in this study used calorimetry to investigate the early age hydration of OPC-CKD systems containing the additives described. Also, calorimetry measurements provided an indication of the action of the various additions on the relative rate and extent of hydration during the first 24 hours. In addition, 1-28 day compressive strength determinations with corresponding porosity measurements were obtained to investigate the longer term effects CC and MK additions had on these parameters. Further, AC impedance spectroscopies, corresponding porosity measurements, and mercury intrusion porosimetry pore size distributions over the first 24 hours of the hydration process were obtained. These methods provide estimates of the early-age porosity, pore size distributions, pore solution conductivity, and the overall early microstructure development of the mixes. This research is intended to serve as an initial means of gaining insight and understanding into characterizing the OPC-CKD systems behavior at early ages. This initial research could potentially lead to a more detailed understanding of these OPC-CKD systems and provide useful information for CKD selection and use.

Chapter 3

Background Information on the Cement Systems Selected for Study

3.1 Materials and Sample Proportions

Three different CKDs from three different cement plants were chosen for the investigation. These were Bath CKD (supplied by the Lafarge Bath Cement Plant in Bath, Ontario), Alpena CKD (supplied by the Lafarge Alpena Cement plant in Alpena, Michigan, U.S.A), and Ashgrove CKD (supplied by The Ash Grove Cement Company in Chanute Kansas, U.S.A.). These three CKDs were chosen based on the fact that their chemical compositions were all quite different as will be described in section 3.2. The nano-calcium carbonate, which will be de-noted as 'CC' for the remainder of the discussions, was provided by READE in Riverside, Rhode Island, U.S.A. The MK was supplied by Engelhard Corporation in Iselin, New Jersey, U.S.A. The OPC was provided by cement manufacturing company St-Lawrence Cement (Holcim Ltd.) in Mississauga, Ontario, Canada. Originally a batch of OPC from the year 2005 was used in the mixes. The supply of this OPC became depleted as the project progressed. A batch of St-Lawrence OPC from the year 2008 was used for mixes containing Ashgrove CKD and MK. Eighteen different mixes, all with a water/solids ratio of 0.5, were tested in all aspects of the research. Mix identification and the corresponding constituents proportions (in parts) can be seen in Table 3.1-1. CKD, as indicated in the table, was used as a replacement to OPC. MK was then used as a replacement to CKD. CC was used as an added supplementary material.

Table 3.1-1: List of mixes and solid constituents.

Mix Identification	Solids Constituents (in parts)			
	OPC	CKD	MK	CC
2005 OPC Controls				
1 OPC	1	--	--	--
1 OPC, 0.1 CC	1	--	--	0.1
1 OPC, 0.2 CC	1	--	--	0.2
Bath CKD + 2005 OPC				
0.7 OPC, 0.3 Bath	0.7	0.3	--	--
0.7 OPC, 0.3 Bath, 0.1 CC	0.7	0.3	--	0.1
0.7 OPC, 0.3 Bath, 0.2 CC	0.7	0.3	--	0.2
Alpena CKD + 2005 OPC				
0.7 OPC, 0.3 Alpena	0.7	0.3	--	--
0.7 OPC, 0.3 Alpena, 0.1 CC	0.7	0.3	--	0.1
0.7 OPC, 0.3 Alpena, 0.2 CC	0.7	0.3	--	0.2
Ashgrove CKD + 2008 OPC				
OPC 2008 St-L	1	--	--	--
0.7 OPC, 0.3 Ashgrove	0.7	0.3	--	--
0.7 OPC, 0.3 Ashgrove, 0.1 CC	0.7	0.3	--	0.1
0.7 OPC, 0.3 Ashgrove, 0.2 CC	0.7	0.3	--	0.2
0.7 OPC, 0.15 Ashgrove, 0.15 MK	0.7	0.15	0.15	
0.7 OPC, 0.15 Ashgrove, 0.15 MK, 0.1 CC	0.7	0.15	0.15	0.1
0.7 OPC, 0.15 Ashgrove, 0.15 MK, 0.2 CC	0.7	0.15	0.15	0.2
0.7 OPC, 0.3 MK	0.7	--	0.3	--
0.7 OPC, 0.3 MK, 0.1 CC	0.7	--	0.3	0.1

3.2 Raw Materials Analysis: XRD

The purpose of this section is to identify the general composition of the raw materials. It is important to establish the composition of the materials so that their behavior in the various experiments can be better understood and explained (for example, in Chapters 6, 7, and 8 where the results of the experiments are discussed).

X-ray diffractometry (XRD) is a well-known method that is used to identify the crystalline compounds (solids in which atoms are structured in a regular and repeating pattern) within a material. The raw materials are sieved using a 275 μm^2 micro-sieve and placed onto the sample holder and then into the XRD instrument (see Fig. 3.2-1). This technique was used to aid in identifying the phases present within each of the raw materials: the 2005 OPC, 2008 OPC, Bath, Alpena, and Ashgrove CKDs.

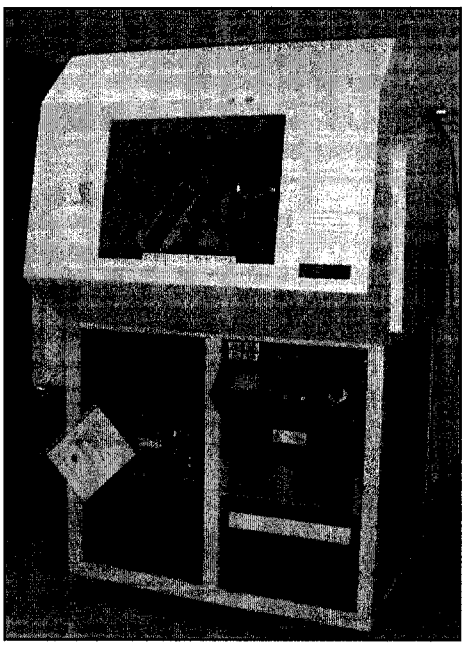

Fig. 3.2-1: The XRD Instrument.

For the purposes of this research, a qualitative analysis was performed. The abundance of the compound identified was output as a percentage of the relative crystalline quantities found within the sample. The abundance was then assigned to be "Low", "Medium", "High", or "Very High" based on where the percentage fell within the ranges shown in Table 3.2-1. These ranges were arbitrarily assigned for comparison purposes. If it appeared that a certain compound may be present, but only in extremely small amounts, it was assigned as "Trace". Compounds found within the samples and their corresponding chemical formulas, for information purposes, are presented in Table 3.2-2. The results from the qualitative XRD analysis for 2005

OPC, 2008 OPC, Bath CKD, Alpena CKD, and Ashgrove CKD are presented in Tables 3.2-3, 3.2-4, 3.2-5, 3.2-6, and 3.2-7, respectively.

Table 3.2-1: Percentage ranges and assigned values.

Assigned Value	Percentage Range
Low	0-10%
Medium	10-30%
High	30-70%
Very High	>70%

Table 3.2-2: Compounds and their chemical formulas.

Compound	Chemical Formula
Bassanite	$2CaSO_4 \cdot (H_2O)$
Bayerite	$Al(OH)_3$
C_2S	$2CaO \cdot SiO_2$
C_3A	$3CaO \cdot Al_2O_3$
C_3S	$3CaO \cdot SiO_2$
C_4AF	$4CaO \cdot Al_2O_3 \cdot Fe_2O_3$
Calcite	$CaCO_3$
Calcium Sulfate	$CaSO_4$
Corundum	Al_2O_3
Gypsum	$CaSO_4 \cdot 2H_2O$
Lime	CaO
Portlandite	$Ca(OH)_2$
Potassium Silicate	K_4SiO_4
Quartz	SiO_2
Sylvite	KCl

Table 3.2-3: XRD results for 2005 OPC

Compound	Assigned Category
Calcite	Low
C_3A	Low
C_4AF	Low
C_3S	High
C_2S	Medium
Gypsum	Low
Corundum	Low
Quartz	Low

Table 3.2-4: XRD results for 2008 OPC.

Compound	Assigned Category
Calcite	Medium
C_3A	Low
C_4AF	Low
C_3S	High
C_2S	Medium
Gypsum	Low
Bassanite	Low

Table 3.2-5: XRD results for Bath CKD

Compound	Assigned Category
Calcite	Very High
Quartz	Medium
Sylvite	Low

Table 3.2-6: XRD results for Ashgrove CKD

Compound	Assigned Category
Lime	High
Calcium Sulfite	Trace
Bayerite	Medium

Table 3.2-7: XRD results for Alpena CKD

Compound	Assigned Category
Lime	High
Calcite	High
Portlandite	Low
Calcium sulfate	Trace
Quartz	Low
Potassium silicate	Possible trace amounts
Corundum	Low

The results from the XRD measurements showed typical cement compounds were found in the OPCs. The Bath CKD contained the highest amount of CC. Alpena CKD contained high amounts of both CC and lime. Ashgrove CKD did not contain any CC. It also did not contain high amounts of lime. Ashgrove CKD was known to be more amorphous by nature and might therefore prove to be a more reactive CKD contributing to strength development; as ill-crystallized materials are known to have good bonding properties (Feldman and Beaudoin, 1976). It is important to note that, as mentioned earlier, only crystalline structures can be identified through XRD measurements. This means that amorphous compounds go undetected by the XRD instrument.

Oxide analysis data for all three CKDs were also collected. This type of analysis determines the concentration of certain compounds using an X-ray fluorescence (XRF) machine. Noteworthy results are mentioned here while the complete data sets for each of the CKDs can be seen in Table 3.2-1 in the Appendix. An automated Bruker AXS S4 Pioneer XRF was used in the analysis for Ashgrove CKD. The work was performed by the Institute for Chemical Process and Environmental Technology (ICPET) at the National Research Council, Canada (NRC). The results showed that the Ashgrove CKD contained a high amount of the alkali potassium oxide, K_2O. A previously performed oxide analysis on Alpena CKD showed that it contained a high amount of sulfate. Lastly, an oxide analysis on Bath CKD showed that it contained a high percentage of chloride. This was verified by performing a chloride titration, which showed that it contained approximately 1% of chloride (which is a high percentage of chloride for a cementitious material).

3.3 XRD Analysis of Samples at 8 Hours Hydration

XRD measurements were also performed on a selection of mixes at eight hours hydration. These measurements provided further characterization of the samples after they had begun to harden as well as reference information for the discussion of experiments presented in later chapters. Each sample was ground using a mortar and

pestle, passed through the micro-sieve, placed in the sample holder, and then placed into the XRD instrument. Ideally, a sample from every mix would have been tested. This was not feasible. Therefore eleven samples were chosen. The following is a list of the samples tested and any noteworthy results (plots of the XRD output data can be seen in Fig. 3.3-1 and Fig. 3.3-2):

1) 2005 OPC: A dominant presence of calcium hydroxide, $Ca(OH)_2$, and C_3S was found. There is a possibility of the presence of some gypsum and potassium sulfate.
2) 2005 OPC, 0.1 CC: Results showed that the presence of $Ca(OH)_2$ is even more dominant than the control OPC, while that of C_3S is reduced. This means that C_3S is being consumed; therefore indicating an accelerating effect of the CC particles.
3) 0.7 OPC+0.3 Alpena: A significant amount of gypsum was present. This was expected due to the high amount of sulfate that was detected by the oxide analysis of the raw Alpena CKD. In addition, there appears to be an even more intense presence of $Ca(OH)_2$ than in the previous two mixes; this indicates that the Alpena CKD has an accelerating effect on the hydration of the OPC.
4) 0.7 OPC+0.3 Alpena+0.1CC: There appeared to be a reduced intensity of $Ca(OH)_2$ present when compared with the previous mix which did not contain any added CC. Also, there was a greater amount of C_3S present indicating a slower rate of hydration. This result was not expected and will be cross-checked with the calorimetry measurement results of Chapter 6.
5) 0.7 OPC+ 0.3 Bath: No gypsum was detected in this mix. In addition, the intensity of $Ca(OH)_2$ was only slightly less than those identified in the Alpena CKD mix. A similar intensity of C_3S was seen in this mix as compared with that in the Alpena CKD mix. Quartz and some alumina gel may also be present.

6) 0.7 OPC+0.3 Bath+0.1CC: A reduced intensity of $Ca(OH)_2$ was seen with the added presence of the CC. Some quartz was also detected. Similar amounts of C_3S were seen in this mix as compared with the previous mix.
7) 2008 OPC: Compared to the results of the 2005 OPC, the presence of $Ca(OH)_2$ was significantly greater while the presence of C_3S was less; this indicates that it may hydrate faster than the 2005 OPC. Also, there appeared to be a possibility of some potassium sulfate (K_2SO_4) in this sample.
8) 0.7 OPC+0.3 Ashgrove: Compared with the Alpena and Bath CKD mixes (without CC) the presence of $Ca(OH)_2$ is much less. The presence of C_3S is comparable to those found in the Alpena and Bath CKD mixes. Its hydration may be slower with respect to that of Alpena and Bath CKD mixes. In addition, gypsum and quartz appear to be present.
9) 0.7 OPC+0.3 Ashgrove+0.1 CC: The added CC appears to have accelerated this mix. This was evident in the increased intensity of $Ca(OH)_2$ and the decreased intensity of C_3S. There is the possibility of the presence of the calcium carboaluminate hydrate phase $C_4A\bar{C}H_{11}$.
10) 0.7 OPC+0.15 Ashgrove+0.15 MK: When compared with the previous mix, there appeared to be an increase in the presence of the $Ca(OH)_2$. The C_3S intensities were similar. This may indicate an accelerated hydration. There was the possibility of the presence of another calcium aluminate hydrate, C_4AH_{13} which forms when a pozzolan, such as metakaolinite (MK), is present in the mix.
11) 0.7 OPC+0.15 Ashgrove+0.15 MK+0.1CC: The addition of the CC to the above mix showed similar intensities of the $Ca(OH)_2$ peak while the C_3S peaks were significantly less intense: indicating that the CC addition to the mix containing MK accelerates the hydration even more.

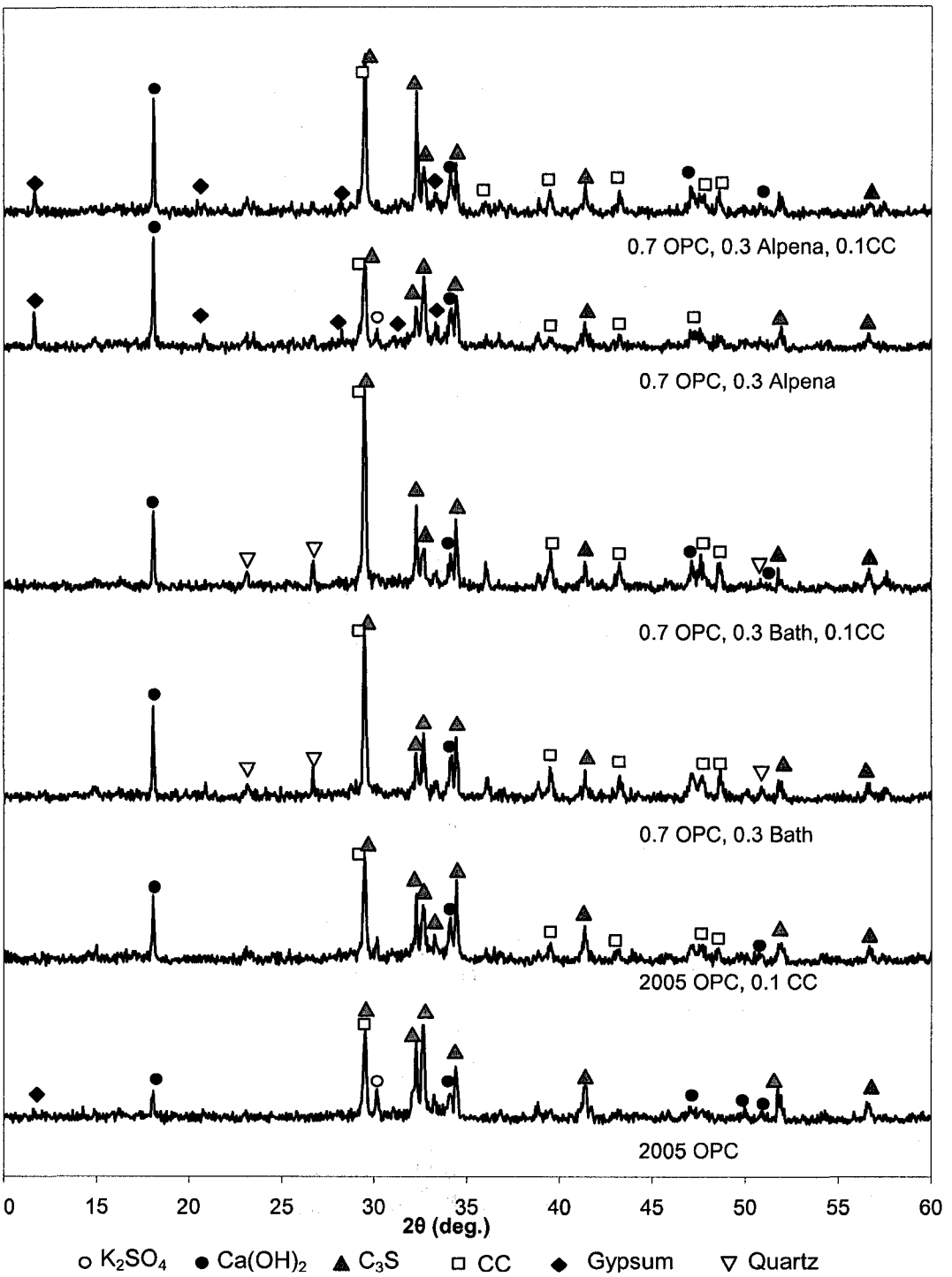

Fig. 3.3-1: Output data from the XRD testing of control, Bath CKD, and Alpena CKD mixes.

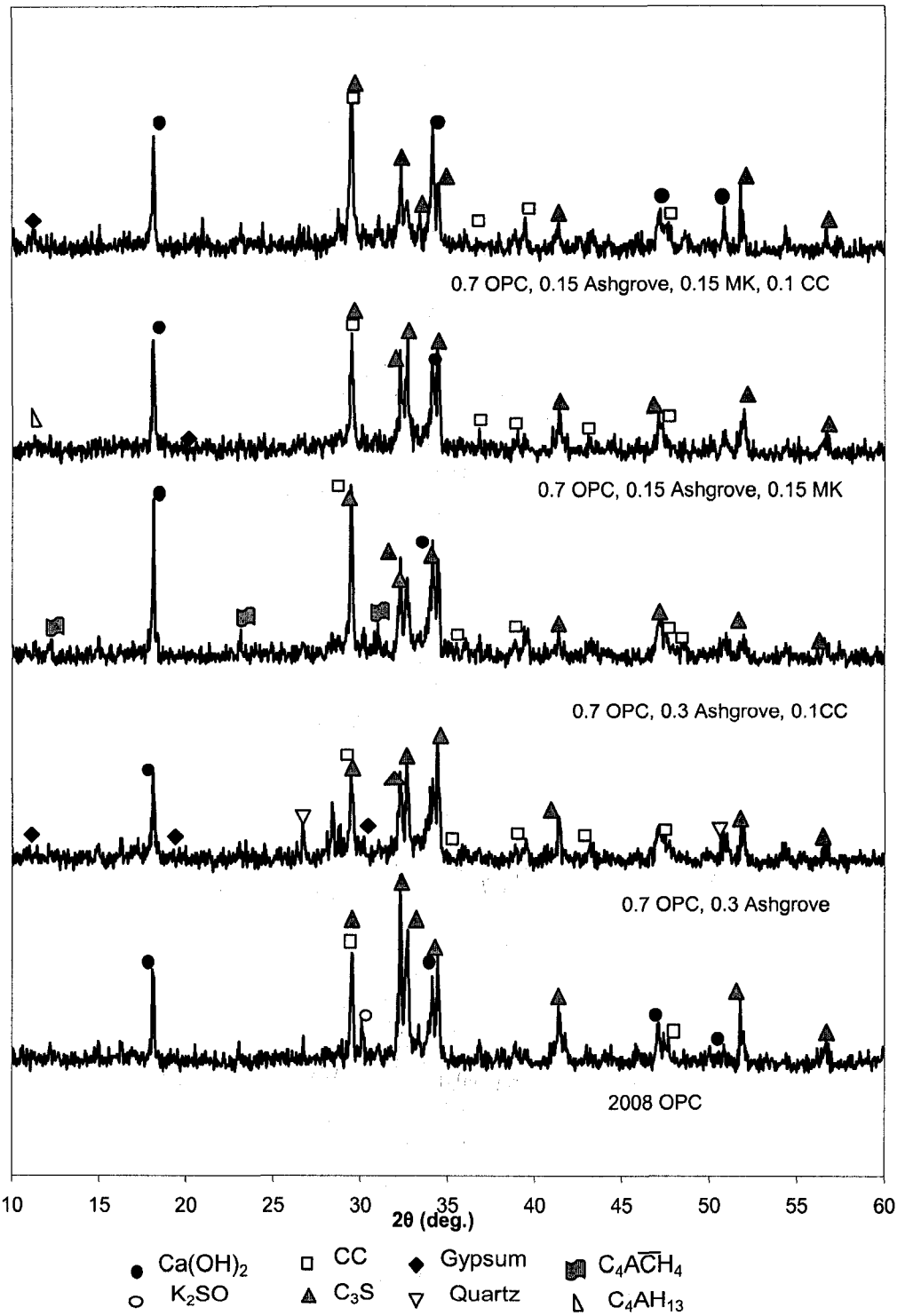

Fig. 3.3-2: Output data from the XRD testing of Ashgrove CKD and MK mixes.

3.4 Selection of SEM Images of Raw Materials and Cement Systems at 8 Hours Hydration

This section serves as additional background information on the raw and hydrated materials. A selection of unhydrated and hydrated cement systems (in particular at 8 hours hydration) will be shown and discussed. A Hitachi S-4800 Field Emission Scanning Electron Microscope, as seen in Fig. 3.4-1, was used to obtain the SEM images. Samples were ground to a powder and placed on an aluminum stub covered in carbon tape (which secured the powder to the stub). The samples used in the SEM imaging were the same as those used in the XRD measurements.

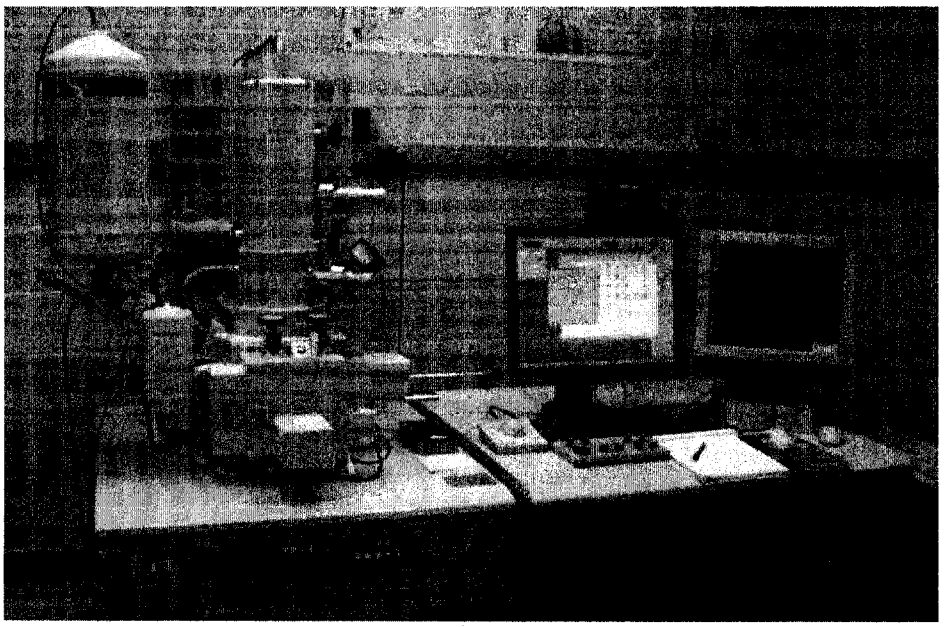

Fig. 3.4-1: The Hitachi S-4800 Field Emission Scanning Electron Microscope.

Before discussing SEM images of hydrated cement systems it is useful to first view images of the raw materials. Fig. 3.4-2 and Fig. 3.4-3 show images of raw CC and MK, respectively. Dimensions have been drawn onto Fig. 3.4-2 to indicate the relative size of the CC particles. The dimensions, although they may be difficult to view on the image, read as follows: 92.4 nm, 119.5 nm, 85.9 nm. Note the contrast in the appearance of the structured CC and amorphous MK.

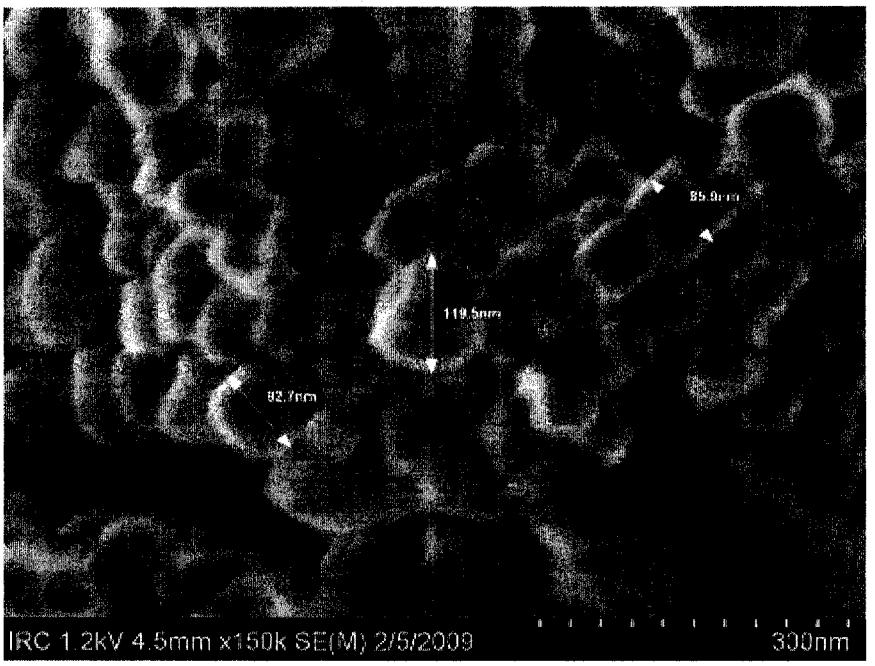

Fig. 3.4-2: SEM image of nano-CC particles.

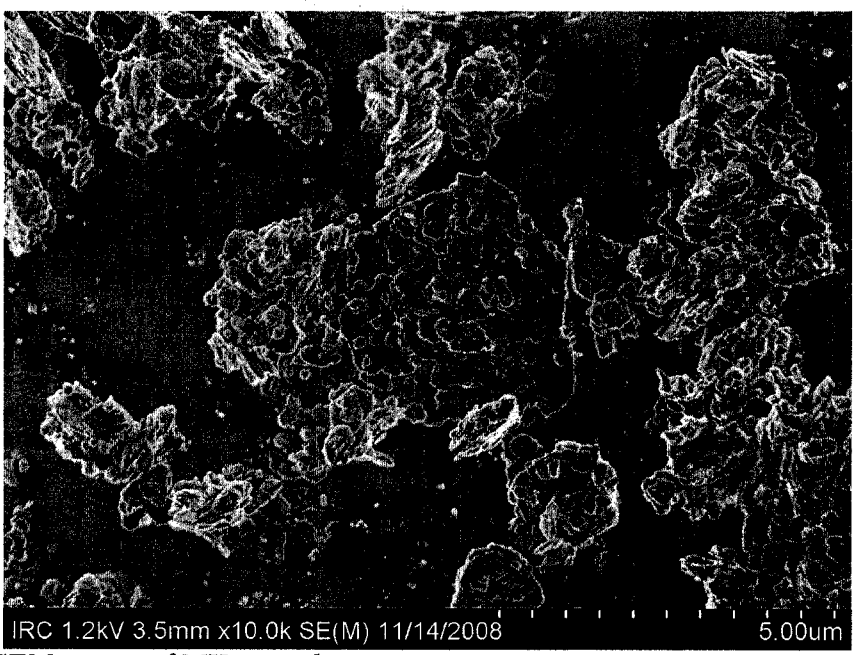

Fig. 3.4-3: SEM image of MK particles.

Fig. 3.4-4 a) and b) show SEM images of raw 2008 OPC particles and the OPC after 8 hours of hydration, respectively. As can be seen in Fig. 3.4-4 b) the growth of hydration products (C-S-H) has begun.

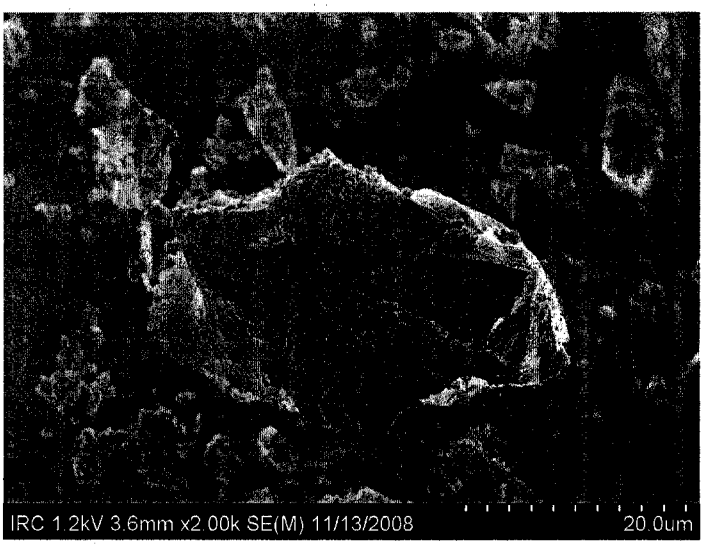

a) Raw OPC

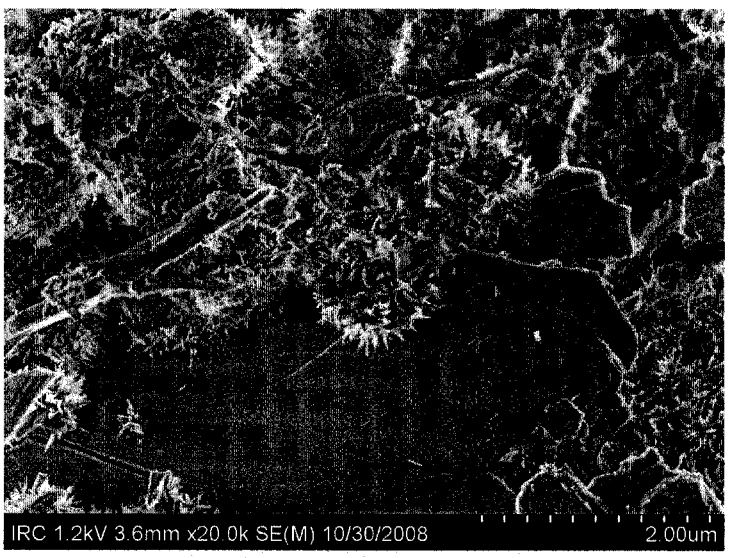

b) OPC hydrated for 8 hours

Fig. 3.4-4: a) SEM image of raw 2008 OPC particles b) OPC hydrated for 8 hours

Fig. 3.4-5 shows an image of an OPC+ 0.1 CC mix that has hydrated for 8 hours. This image shows that hydration products have begun to form around the CC particles. Note the differences in the images shown in Fig. 3.4-2 (the unhydrated CC particles) and Fig. 3.4-5. This may suggest that the CC is acting as a nucleation site, promoting hydration. It would be in agreement with the XRD results.

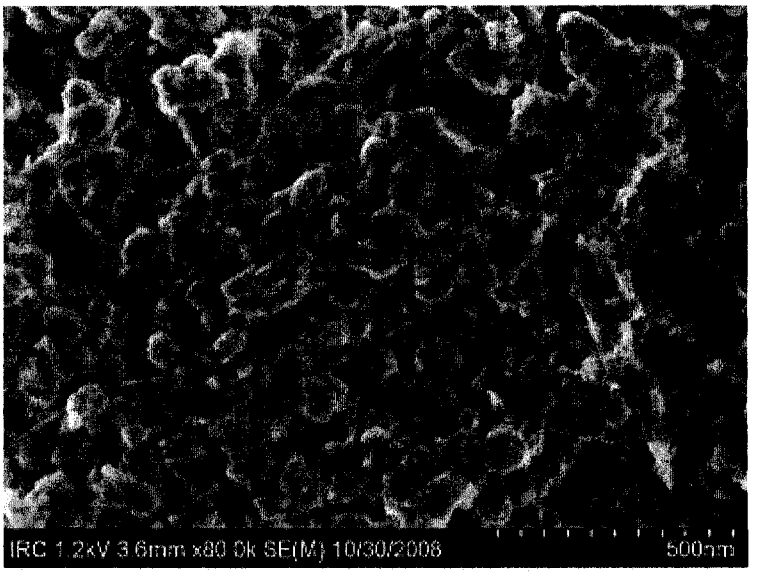

Fig. 3.4-5: SEM image of OPC with added CC particles, hydrated for 8 hours.

Raw Alpena CKD, OPC+Alpena CKD hydrated for 8 hours, and OPC+Alpena CKD+0.1 CC can be seen in Fig. 3.4-6, Fig. 3.4-7, and Fig. 3.4-8, respectively. It appears as though there are some crystalline materials present in this CKD. As will be seen in later images, its appearance is in contrast to Ashgrove CKD. It is interesting to note the hydration product growth in Fig. 3.4-7 and compare this with what appears to be more hydration growth present in Fig. 3.4-8. This could be due to the addition of the CC, which has accelerated the hydration of the system.

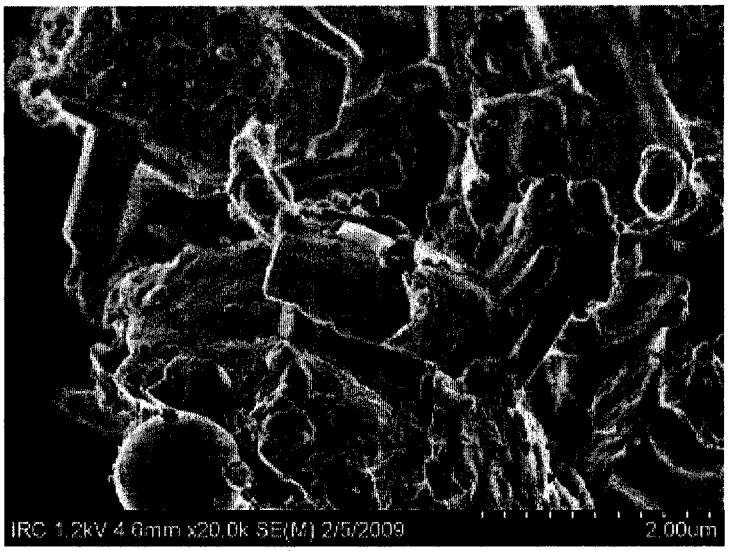

Fig. 3.4-6: SEM image of raw Alpena CKD.

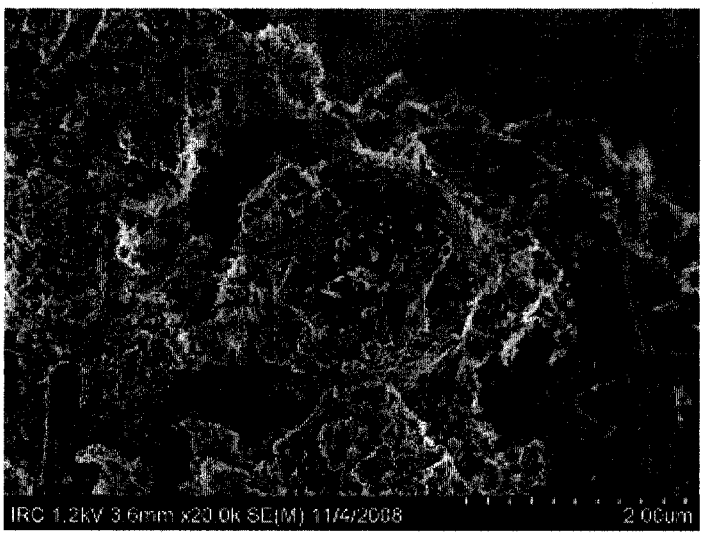

Fig. 3.4-7: SEM image of OPC+Alpena CKD hydrated for 8 hours.

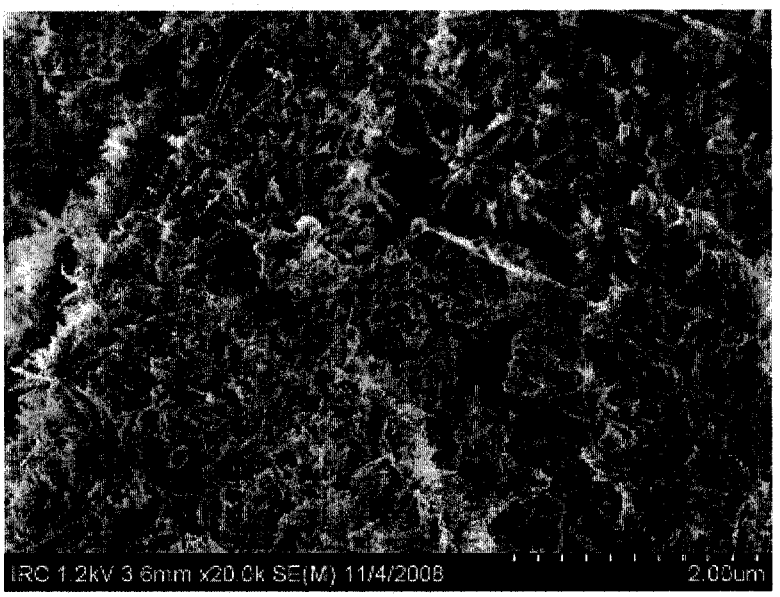

Fig. 3.4-8: SEM image of OPC+Alpena CKD+0.1 CC hydrated for 8 hours.

An image of raw Ashgrove CKD can be seen in Fig. 3.4-9. The image of this raw CKD looks highly irregular and amorphous in nature. It does not appear as though it contains structured crystalline materials as was seen in the image in Fig. 3.4-6 (the raw Alpena CKD). An image of OPC+Ashgrove CKD hydrated for 8 hours can be seen in Fig. 3.4-10. In this image hydration products are visible. An image of OPC+Ashgrove CKD+MK can be seen in Fig. 3.4-11.

The XRD results indicated that the partial replacement of the Ashgrove CKD with MK possibly accelerated its hydration. However, unlike the clarity that was seen with growth on CC particles, it is difficult to determine visually from Fig. 3.4-11 if more hydration products are present as compared with Fig. 3.4-10 where there was no MK present in the mix. This is likely due to the fact that both the Ashgrove CKD and MK are both amorphous and are therefore difficult to distinguish. Therefore, it can only be speculated (on the basis of SEM evidence) that the MK particles act as nucleation sites.

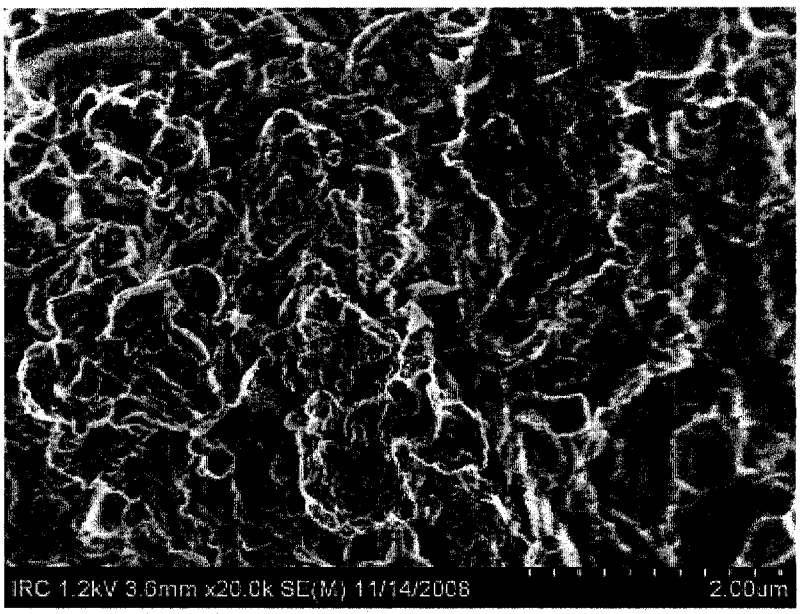

Fig. 3.4-9: SEM image of raw Ashgrove CKD.

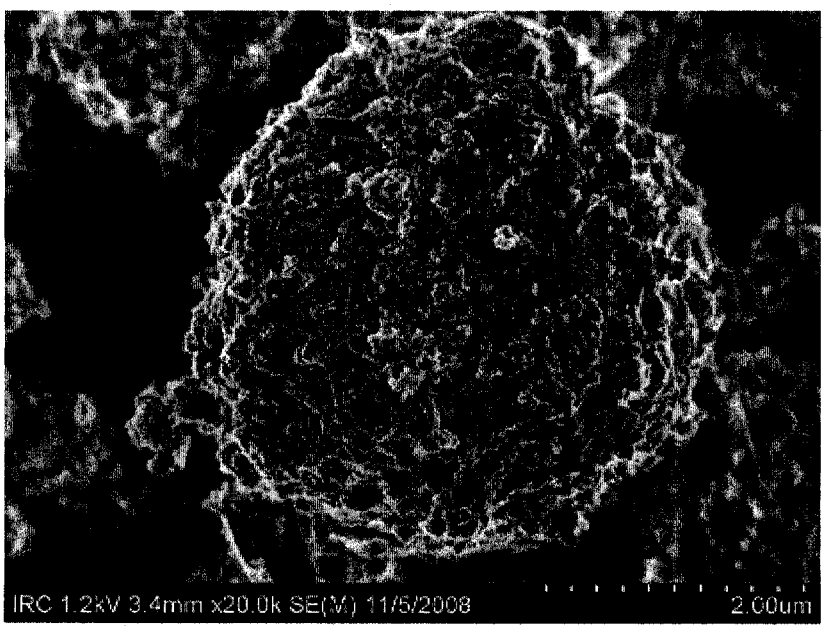

Fig. 3.4-10: SEM image of OPC+Ashgrove CKD hydrated for 8 hours.

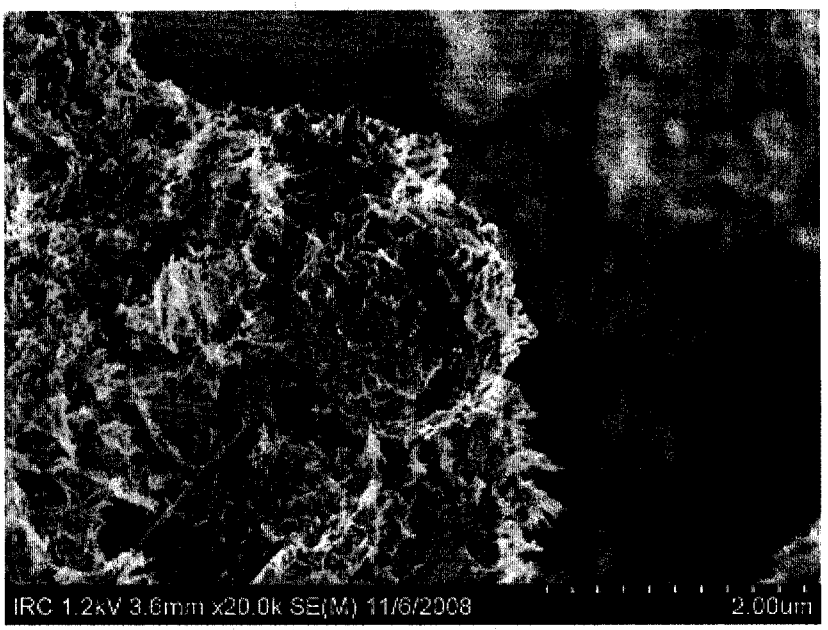

Fig. 3.4-11: SEM image of OPC+Ashgrove CKD+MK hydrated for 8 hours.

Chapter 4

Theory and Objectives: Calorimetry, Strength, Porosity, AC Impedance, and Porosimetry Measurements.

4.1 Calorimetry Measurements

4.1.1 Objectives of Calorimetry Measurements

The objective of the calorimetry measurements was to determine how the varying amounts of CKD, CC, and MK affect the hydration kinetics of OPC at early ages. It will be shown that these materials when combined to form binary, ternary, and quaternary systems, accelerate or retard the early-age cement hydration. All 18 systems listed in Table 3.1-1 were examined in the calorimeter. The rate of heat development curves were compiled in order to compare their respective hydration processes; sample preparation and testing are described in Chapter 5.

4.1.2 Background Information on the Use of Calorimetry in Cement Science

A calorimeter, the apparatus used for calorimetry measurements, is a device used to measure the amount of heat of a chemical reaction. The use of calorimetry is a common and helpful first step in cement research when little is known about how the materials will physically interact and behave when combined. In this case, the calorimeter was used to measure the rate of heat development during hydration (the process whereby a solid forms as the result of cement powder reacting with water) in the first 24 hours. The physical and chemical properties of the cement systems affect the heat they produce while undergoing hydration.

The calorimeter instrument, itself, is made up of a series of channels. The channels are vertical cylindrical openings that extend down into the machine. They are paired off to include one sample channel and its corresponding reference channel. The sample being tested (the contents of which contain a measured amount of solids mixed with the appropriate amount of water) is placed in the sample channel and the reference sample (typically an appropriate amount of small glass beads) is placed in the reference channel. The reference sample can be thought of as a baseline to which the heat given off by the sample that is hydrating is compared. Also, the reference sample serves as a means of eliminating noise that may be in the system. Heat flow sensors, which are imbedded directly underneath the bottom of the channel, measure the heat given off by the sample.

The heat measured by the calorimeter is generally output in milliWatts, mW. The reason it is in mW is because the heat flow sensor measures a voltage signal which is proportional to the heat flow. The data is conventionally converted from mW to cal/g/hr (calories of heat produced / gram of solids within the sample / hour). Typical output data for a sample of OPC with a water/cement ratio of 0.5 was shown in Fig.2.1-1 of Chapter 2.

4.2 Strength and Porosity Measurements

4.2.1 Objectives of Strength and Porosity Measurements

There were three objectives for the strength and corresponding porosity measurements. The first objective was to investigate the effects the CKD, CC, and MK addition in varying concentrations had on strength development of OPC at 1, 3, 7, and 28 days after mixing. The second objective was to measure the porosity changes of the cement systems during hydration. The third objective was to produce strength-porosity curves to compare and analyze the mixes. The latter eliminates time from the comparison and provides more basic information about the nature of the microstructure as it relates to strength development (Ramachandran et al., 1981).

Beaudoin and Feldman (1975) showed that the compressive strength for various cement systems (some with added fly ash and others containing various silica contents) when plotted versus the respective porosity values on a semi-log plot, produced a family of straight lines each with different slopes (see Fig. 4.2-1).

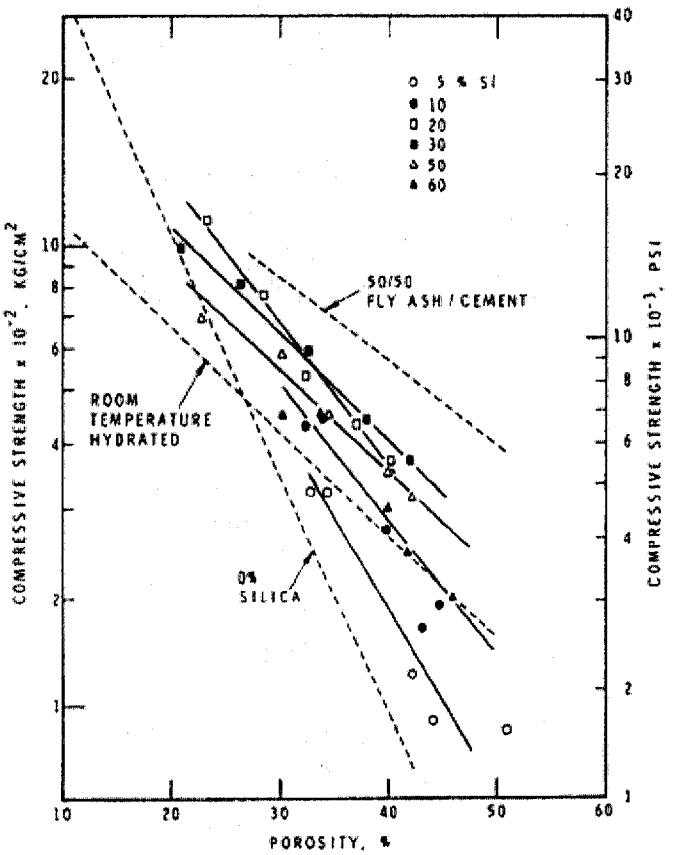

Fig. 4.2-1: Compressive strength versus porosity for various cement systems (Beaudoin and Feldman, 1975).

4.2.2 Background Information on Strength Tests

Compression testing is a technique used for evaluating the engineering performance of concrete, mortars, and cement paste. During this procedure a machine is used to apply concentric loading to a specimen until its ultimate strength is reached. The common engineering equation (Eq. 4.2-1) was used in order to calculate the sample's compressive strength.

$$\sigma = \frac{P}{A} \tag{4.2-1}$$

where: σ= engineering stress, MPa

P= concentrically applied load, N

A= cross-sectional area of the cube, mm^2.

For the current work, cement cubes that measured two inches by two inches by two inches were used. A broken piece of a cube from each mix was saved after the compression testing for porosity measurements. ASTM C-109 was followed in the preparation of the cubes. The sample preparation and compression measurements will be discussed further in Chapter 5.

4.2.3 Background Information on Porosity Measurements

Porous materials, such as hydrating cements, tend to have a heterogeneous microstructure, with a wide range of particle and pore sizes (Sereda, 1972). During the hydration of cement a pore system (as well as solids) is produced (Nagaraj and Banu, 1996). One of the most important characteristics of a pore system is its porosity (Kumar and Bhattacharjee, 2003). It is known to be one of the main factors that determine strength (Odler and Robler, 1985). Porosity is defined as in Eq. 4.2-2:

$$\varphi = \frac{V_p}{V_t} \tag{4.2-2}$$

where: φ= porosity

V_p= volume of the pores in the sample, m^3

V_t= total volume of the sample, m^3

The pore structure of the cement paste is known to govern several properties of mortars and concrete such as the physical and chemical resistance, temperature resistance, and thermal conductivity (Rostasy et. al, 1980).

Porosity and strength are inversely proportional for cement paste. As the hydration of cement progresses, the amount of hydration products increases. The growth of hydration products closes the available void pore volumes which leads to a decrease in total porosity. This leads to an increase of the compressive strength over time (Shoaib et al., 2000). Also, it has been found that for a given porosity, the strength of a cement paste is known to increase with increasing amounts of hydrate phases present (Odler and Robler, 1985).

A piece of the broken cement cube, as mentioned earlier, was saved on each day of the compression testing and placed into a glass container filled with isopropanol. It is known that, by solvent exchange, submersing a cement sample in isopropanol stops the sample from hydrating further. There are important reasons for the use of isopropanol. The composition of the hydrated cement (C-S-H) can be modeled as a layered system. If the sample had been submerged in water, some water would move into the interlayer regions. This would cause the porosity measurement to be inaccurate as interlayer space is considered part of the solid and not as pore space. Isopropanol does not move into the interlayer regions of the sample. When a sample is submerged in isopropanol it stops hydrating and therefore the degree of hydration remains constant. Each saved piece was used for porosity measurements to correlate the sample's compressive strength value with porosity. It was ideal to use the same sample for both the compression and the porosity measurements as this produces the most accurate strength-porosity correlation. The method used in the porosity measurements can be performed on a sample of any size or shape. Further details are given on how to calculate the porosity later in Chapter 5, section 5.2, where the experimental set-up and mass measurements (precursors to the porosity determinations) are explained so that the porosity calculation can be understood.

4.3 AC Impedance Measurements

4.3.1 Objectives of AC Impedance Measurements

The objectives of the AC impedance measurements were to further understand and quantify the microstructural development of the cement systems at early-age (from zero to 24 hours). Microstructural descriptions for example, early-age porosities, pore size character, and pore solution conductivity, can be extracted from impedance spectra. It was expected that this data would be useful in assessing the relative merits of the CKDs and the efficacy of the CC and MK additions.

4.3.2 Background Information on AC Impedance Spectroscopy

AC impedance testing (formally referred to as Alternating Current Impedance Spectroscopy, ACIS) is a non-destructive testing technique primarily used for electrochemical investigations. This technique has been used as early as the 1950s in researching the properties of ceramics (Gu et al., 1993). It is an ideal testing technique to use for early-age cement samples. The reason for this is because the testing can be performed while the sample remains cast in its mould. This way the sample is able to continue the curing process undisturbed while undergoing testing.

The impedance of a sample is measured. The result, depending on the type of sample, can then be interpreted in different ways to determine the sample's properties. For example, the pore size character (i.e. whether it is a narrow or broad pore size distribution) and the conductivity of the pore solution can be estimated from the data. In order to understand and interpret the output data, background information on impedance principles are first introduced.

4.3.3 Introduction to the Concept of Impedance

Impedance is a term that is applied to the variable that relates voltage and current when both are time dependent (this is the case in an Alternating Current, AC, system). Voltage and current are related to impedance as in Eq. 4.3-1:

$$v(t) = i(t) \cdot Z_T \tag{4.3-1}$$

where: v(t)= voltage applied to the system, V

i(t)= current, A

Z_T= total impedance, Ω

The total impedance, Z_T is associated with the combined effects of resistors, capacitors, and inductors that may be in the system. Resistance is a measure of the sample's ability to oppose current flow; capacitance is a measure of the sample's ability to store an electric charge; and inductance is a measure of the sample's ability to generate an electromagnetic field.

4.3.4 Application of AC Impedance Measurements of Hydrating Cement Samples

In this section, a set of example output data obtained from AC impedance measurements will first be presented and then explained in further detail. Prior to testing a cement sample using AC impedance, a set of electrodes is cast into the cement sample mould. A potential difference is applied to the two electrodes which induces a current through the sample. The output data represents the sample's response to the electronic signal. Data is collected using computer software and is presented on a complex plane. Real values are displayed on the x-axis and imaginary values are displayed on the y-axis. An idealized example set of output data obtained from the testing and an image of a cement sample with its cast-in electrodes are presented in Fig 4.3-1.

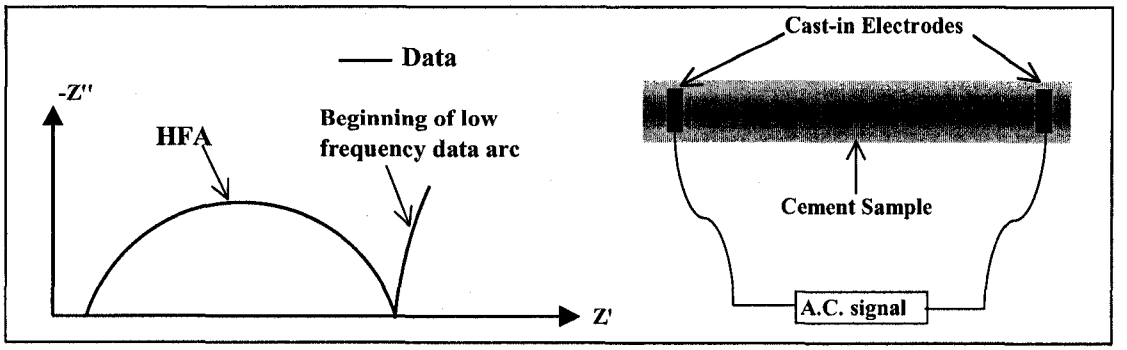

Fig.4.3-1: An example set of output AC impedance data and a sample being tested.

A typical impedance plot output for a cement sample, as can be seen in Fig 4.3-1, contains a semi-circle, or arc, on the left hand side followed by the beginning of another semi-circle on the right. Z' and –Z'' represent the real and imaginary values of impedance, respectively. The negative imaginary values are plotted on what is the conventional positive y-axis; the reason for this is to present a visually simple set of right side up arcs (otherwise, the semi-circles would appear inverted). The first arc is a result of high frequencies being swept and is therefore called the High Frequency Arc (HFA). The second arc appears when the lower frequencies are being swept. The HFA is attributed to the cement paste's impedance behavior (Gu et al., 1994) and is therefore the most important part of the output data. The intercept of the HFA with the Z' axis (on the left hand side of the first arc) and the diameter of this arc will be of great importance and will be discussed later.

In order to fully understand the output AC impedance data, a physical cement model and the idea of an equivalent circuit for cement paste can be introduced and are explained in subsequent sections.

4.3.5 Introduction to the AC Impedance Response of Electrical Elements

A combination of electrical elements, both resistors and capacitors are used to model the data output from the AC Impedance measurements of a cement system. The following symbols are used to represents resistors, capacitors, and the A.C. signal in any electric circuit that will be presented:

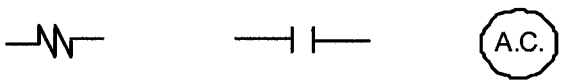

Resistor Capacitor A.C signal

A circuit, termed an equivalent circuit, is modeled so that its impedance fits the data obtained from the testing. By fitting the data to the equivalent circuit, various physical parameters from the cement system can be estimated and interpreted. Those details will be described in the next section (4.3.6). The AC impedance response of resistors and capacitors will first be described so that the response of the equivalent circuit can be better understood.

Sato (2002) provides an explanation of the response of the electrical elements. When an alternating current is applied to a resistor, its impedance is simply equal to the magnitude of the resistor itself (see Fig. 4.3-2 a)). This is due to the fact that the magnitude of a simple resistor is constant. However if the signal is applied to a capacitor, whose value is dependent on frequency, the magnitude of the impedance is as defined in Eq. 4.3-1. A graphic representation of its response can be seen in Fig. 4.3-2 b).

$$|Z| = \frac{1}{\omega C} \tag{4.3-1}$$

where: $|Z|$= magnitude of impedance, Ω

ω= angular frequency of the applied current, rad/s

C= capacitance, F (farad)

Angular frequency, ω, is defined as being equal to 2πf, where 'f' is the frequency of the applied current measured in hertz, Hz.

Later, in section 4.3.6 in a derivation of the total impedance of the cement system, the capacitance will be defined as a vector as in Eq. 4.3-2.

$$Z_c = \frac{-j}{\omega C} \tag{4.3-2}$$

The –j is a vector indicating that the direction of the capacitance's impedance response is along the negative y-axis (which is in the direction of the –Z'' axis in a complex plane). Mathematically, 'j' has a value of $\sqrt{-1}$. Physically, 'j' indicates that the phase shift of current to voltage is out by 90 degrees. It should be noted that a phase shift is a time lag between the peak values of the sinusoidal wave functions of current and voltage.

When a resistor and capacitor are combined in parallel the resulting impedance measurement is as in Fig. 4.3-1 c). As can be seen in this figure, the resulting data output of the resistor and capacitor in parallel displays a semi-circle. Along with the modeling of the equivalent circuit, and a model of the cement system, the mathematical reasons for the semi-circular data output due to the resistor and capacitor in parallel will be described in section 4.3.6.

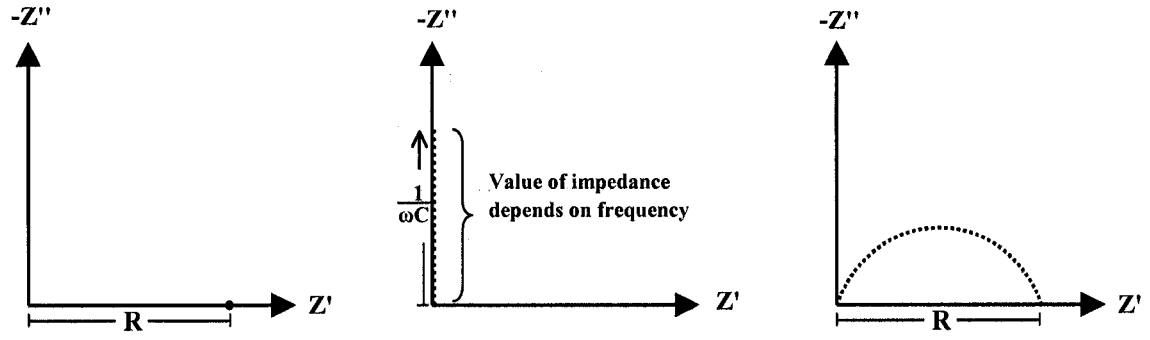

a) resistor b) capacitor c) resistor and capacitor in parallel

Fig.4.3-2: The AC impedance response for a) a resistor, b) a capacitor, c) a resistor and capacitor in parallel.

4.3.6 AC Impedance Modeling and Equivalent Circuits of Cement Samples

The microstructure and pore solution chemistry in a hydrating cement sample are mainly responsible for impedance behavior (Gu et al., 1993 (II)). The impedance is dependent on the resistance and the capacitance in the sample. Solids, liquid, and a solid-liquid interface are key elements. A model of these phases introduced by Xie et al. (1993) can be seen in Fig. 4.3-3. The resistance in the sample is due to the solids, liquid, and the solid-liquid interface; while the capacitance in the sample is due to the solid-liquid interface. In order to calculate the total impedance of the system, the contributions of impedance due to the total resistance in the system (due to the solids, liquids, and the solid-liquid interface) and due to the capacitance (due to the solid-liquid interface) must be summed.

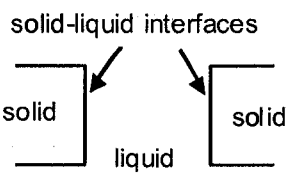

Fig. 4.3-3: A schematic of solids, liquid, and the solid-liquid interfaces of a cement paste after Xie et al., 1993.

Xie et al. (1993) developed a physical and mathematical representation for cement paste. The model represents a saturated cement paste sample subjected to an applied voltage. As seen in Fig 4.3-4 a), it was modeled using N electrical elements with a width of Δx. The white cubes represent solid particles, and the liquid is represented as the black spaces between the cubes. The elements are connected in series as seen in Fig 4.3-4 b), and summed from 1 to N. Fig 4.3-4 c) represents the solid-liquid interface within the sample. The ionic composition of the solid-liquid interface is different than that of the liquid due to the surface adsorption on the solid. It was suggested by Xie et al. (1993) that when the sample is subjected to an A.C. voltage, it causes the separation of opposite charges within the solid and solid-liquid interface: this can also be seen in Fig 4.3-4 c). This separation of opposite charges results in a capacitance behavior. Due to the ionic composition and microstructure of the solid-liquid interface it has a different electrical resistance than the liquid alone. This is accounted for in the electrical model that Xie et al. (1993) developed which can be seen in Fig 4.3-4 d). In this model R_S and R_L represent the resistance in the solids and liquid, respectively, in parallel. While R_f and C_f represent the resistance and capacitance of the solid-liquid interface, also placed in parallel. To re-iterate, the reason the second set of electrical elements (R_f and C_f) are required is due to the fact that the resistance and ionic composition of the solid-liquid interface differs from that of the liquid in the sample.

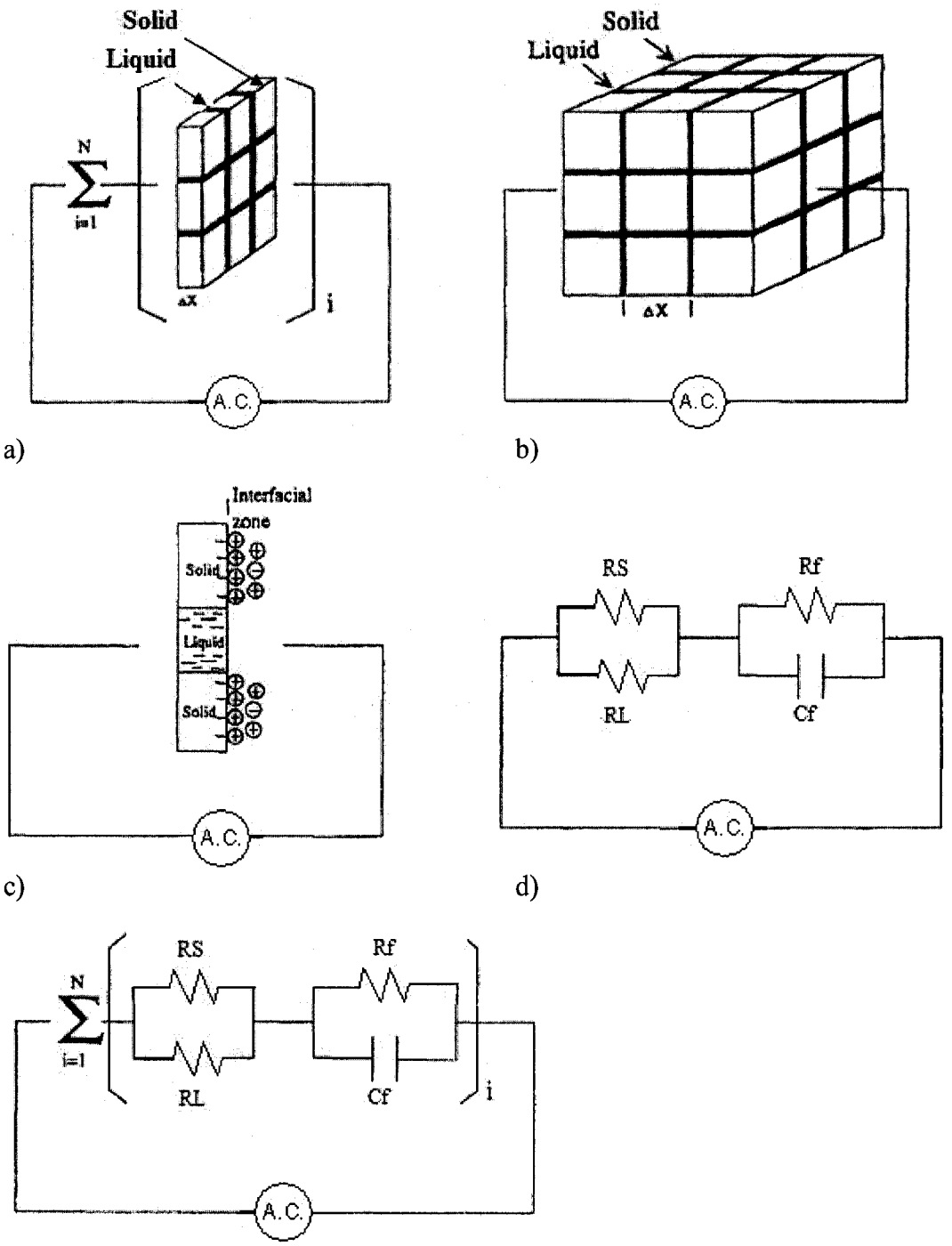

Fig. 4.3-4 a-e): The cement paste model and corresponding equivalent circuits developed by Xie et. al (1993).

The equivalent circuit for the entire sample is simply the summation of the N electrical elements as seen in Fig 4.3-4 e). Xie et al. (1993) further explain that the total impedance, Z_T, can now be calculated based on the model as follows:

$$Z_T = Z_1 + Z_2 \tag{4.3-3}$$

where: Z_1= total impedance of the parallel circuit containing R_S and R_L

Z_2= total impedance of the parallel circuit containing R_f and C_f

The derivation of terms Z_1 and Z_2 lead to the origin of the semi-circles that are seen in the AC impedance output data. The derivations of Z_1 and Z_2 are discussed next.

The impedance of a resistor is simply equal its resistance. This is due to the fact that resistance is not time dependent and so its contribution to the voltage is the same in a D.C. (direct current) or A.C. circuit. This simply means that Z_T of Eq. 4.3-1 (the generalized equation of impedance) can be interchanged with a total resistance, R (in this case R the equivalent resistance due to R_S and R_L in parallel). When calculating the total impedance, Z_1, in the cement sample due to R_S and R_L in parallel summing for all N elements the following equation is used:

$$\frac{1}{Z_1} = \sum_{i=1}^{N} \left(\frac{1}{R_S} + \frac{1}{R_L} \right)_i \tag{4.3-4}$$

Which can be re-arranged to:

$$Z_1 = \sum_{i=1}^{N} \left(\frac{1}{\frac{1}{R_s} + \frac{1}{R_L}} \right)_i$$

R_S is considered to be substantially larger than R_L, which causes the value of $1/R_S$ to approach zero in Eq. 4.3-4 leaving simply:

$$Z_1 = \sum_{i=1}^{N} (R_L)_i = NR_L \tag{4.3-5}$$

Calculating the impedance Z_2 is more complicated and this is due to the fact that the impedance of a capacitor is dependent on frequency, meaning it is time dependent. Xie et al. (1993) expressed the impedance across a capacitor, Z_C as follows:

$$Z_c = \frac{-j}{\omega C} \tag{4.3-6}$$

where: -j= a vector indicating the direction of the capacitance's impedance is in the direction of the –Z'' axis.

This means that the total impedance Z_2 is as seen in Eq. 4.3-7:

$$Z_2 = \sum_{i=1}^{N} \left(\frac{1}{\frac{1}{R_f} + j\omega C_f} \right)_i \tag{4.3-7}$$

This can further be expanded to:

$$Z_2 = \sum_{i=1}^{N} \left(\frac{R_f}{1+(\omega C_f R_f)^2} - j\frac{\omega C_f R_f^{\,2}}{1+(\omega C_f R_f)^2} \right)_i \tag{4.3-8}$$

And further expanded again to:

$$Z_2 = \frac{NR_f}{1+(\omega C_f R_f)^2} - j\frac{N\omega C_f R_f^{\,2}}{1+(\omega C_f R_f)^2} \qquad (4.3\text{-}9)$$

Eq. 4.3-3 ($Z_T = Z_1 + Z_2$) then becomes:

$$Z_T = NR_L + \frac{NR_f}{1+(\omega C_f R_f)^2} - j\frac{N\omega C_f R_f^{\,2}}{1+(\omega C_f R_f)^2} \qquad (4.3\text{-}10)$$

Sato (2002) simplified this equation by letting $R_1 = NR_L$, $R_2 = NR_f$, $C_d = C_f/N$, and Eq. 4.3-10 becomes:

$$Z_T = R_1 + \frac{R_2}{1+(\omega C_d R_2)^2} - j\frac{\omega C_d R_2^{\,2}}{1+(\omega C_d R_2)^2} \qquad (4.3\text{-}11)$$

Xie et al. (1993) set Z' and Z'' as follows:

$$Z' = R_1 + \frac{R_2}{1+(\omega C_d R_2)^2} \qquad Z'' = \frac{\omega C_d R_2^{\,2}}{1+(\omega C_d R_2)^2}$$

then Eq. 4.3-11 becomes:

$$\left(Z' - \left(R_1 + \frac{R_2}{2}\right)\right)^2 + (Z'')^2 = \left(\frac{R_2}{2}\right)^2 \qquad (4.3\text{-}12)$$

Xie et al. (1993) explain further that Eq. 4.3-12 is now in the familiar form of the equation of a semi-circle having a radius of $R_2/2$, a center of $(R_1+R_2/2, 0)$. This is illustrated in Fig 4.3-5 a) along with the corresponding equivalent electric circuit seen in Fig. 4.3-5 b).

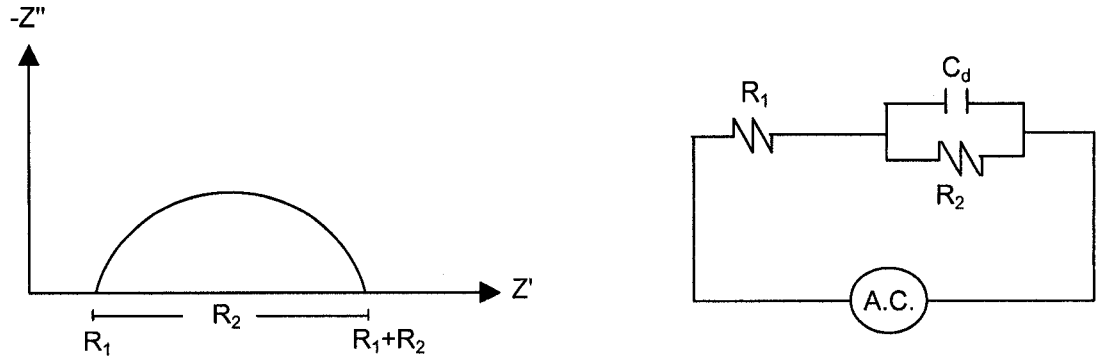

Fig 4.3-5: a) Graphical representation of the resulting AC impedance response due to the equivalent circuit shown in b).

Electrodes are cast into the sample mould for AC impedance measurements. The contact between the electrodes and the hydrating cement produces an additional capacitance behavior as well as an additional resistance. This results in another arc that appears on the right hand side of the HFA. This was mentioned in section 4.3.4 and was shown in Fig. 4.3-1. The information provided by this second arc is generally not used and therefore needs no further discussion. However it was important to mention it due to the fact that the beginning of this second arc can be seen in the output data.

4.3.7 The Depression Angle Parameter

The images in Figs. 4.3-1 and 4.3-5 a) assumed the arcs to be perfect semi-circles with their diameters running along the positive Z' axis. The equivalent circuits have been derived based on these assumptions. This response is rarely observed; in reality, the arc is depressed clockwise below the Z' axis by an angle termed the depression angle, φ_{dep}, as can be seen in Fig. 4.3-6.

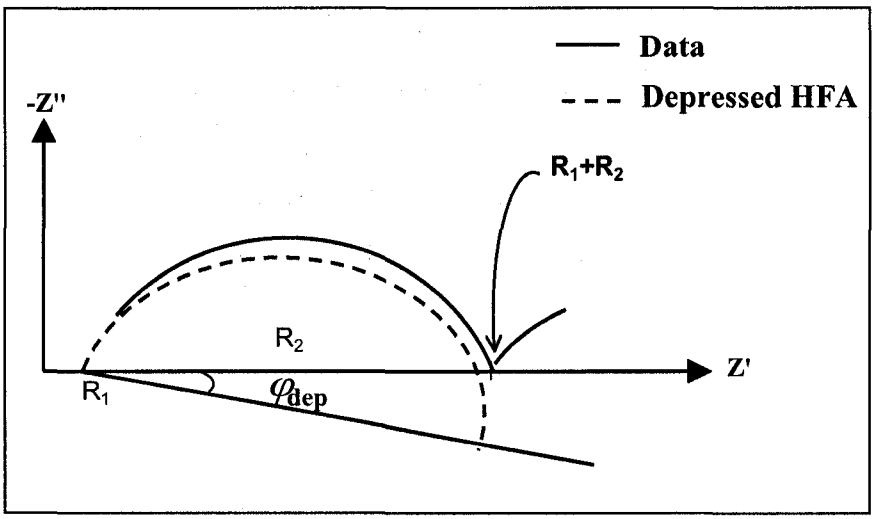

Fig. 4.3-6: Graphical representation of the depression angle.

As can be seen in this figure, the value for R_2 is still measured along the Z' axis (and is therefore no longer equal to the diameter of the semi-circle represented by the data).

The depression angle parameter, n, (a unit-less number physically meaningful between zero and one) is defined in Eq. 4.3-13 (see Skalny and Mindness, 1995, section authored by Gu et al. for the origins of this equation):

$$n = 1 - \frac{2}{\pi}\phi_{dep} \tag{4.3-13}$$

Physically, the depression angle is related to the roughness and heterogeneity of the interface within the sample (Sato, 2002). As the roughness within a sample increases, the depression angle increases as well. As a sample becomes smoother, the depression angle decreases. A depression angle parameter equal to one represents a perfectly smooth sample (as the depression angle would be zero in this case, and the arc's diameter would lie on the Z' axis).

Several causes of the depressed semi-circle have been reported in the past. Gu et al. II (1993) suggested that the depressed arc could be attributed to an uneven current distribution at the interface. In another study, Gu et al. (1993) reported results that related the depression angle to the pore size distribution of a sample. The testing involved conducting AC impedance measurements on samples of cement paste and porous glass. The results showed that the depression angle for cement paste (which had a broad pore size distribution) had a large depression angle as compared with the depression angle of the porous glass (which had a narrow pore size distribution). They concluded that a broad pore size distribution results in a wide spread of relaxation times (the length of time for the dipoles of ions inside the pores of the sample to orientate to follow the A.C. signal) which corresponded to a large depression angle, and therefore a small depression angle parameter, 'n'. It follows that a narrow pore size distribution would result in a reduced spread of relaxation times. This would in turn result in a small depression angle, or a large value of the depression angle parameter 'n'.

Further to this, Gu et al. (1993) suggested that when the AC signal is applied to the system, the dipoles of ions adsorb to the solid-liquid interface of the micropores. This means that the solid-liquid interface, which until now was described as behaving as a perfect capacitor (and was modeled as such in the equivalent circuit of Fig. 4.3-4 b)) actually has a resistance associated with it. In order to accurately model the solid-liquid interface, a resistor is added in parallel to the capacitor of Fig. 4.3-4 b). This new combination of the added resistor with the capacitor is displayed using a new element termed a CPE (Constant Phase Element). The CPE is commonly represented in electrical circuits with the following symbol:

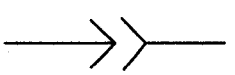

An updated equivalent circuit that includes the CPE is shown in Fig. 4.3-7. The impedance of the CPE is defined with the following equation:

$$Z = \frac{1}{C(j\omega)^n} \tag{4.3-14}$$

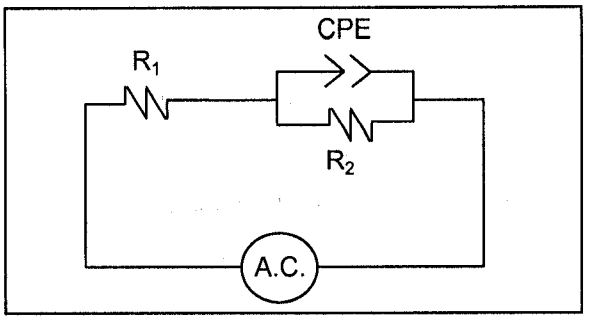

Fig. 4.3-7: The CPE within the model of the equivalent circuit.

The origin of Eq. 4.3-14 can be seen in Skalny and Mindness (1995), in the section authored by Gu et al. It was the circuit in Fig. 4.3-7 that was used to fit all of the output data from the AC impedance testing in the current work. Further details on the parameters that were estimated by fitting the equivalent circuit to the data are described in section 5.3.2.

4.4. Mercury Intrusion Porosimetry

The objective of the mercury intrusion porosimetry was to measure the pore size distribution of six samples that had each hydrated for 8 hours; so that their mean pore sizes, r_o, could be calculated. Naturally, it would have been ideal to measure all 18 mixes using this technique; however for practical reasons it was not feasible to do so. This data will be examined later in section 8.6. It is useful when used in conjunction with AC impedance and porosity measurements. It should be noted that a second set of porosity measurements (the first set were measured in conjunction with compressive strength hydration times as was previously discussed) were made for each mix at hydration times of 5, 8, 16, and 24 hours which will be further discussed in section 5.4.

4.4.1 Background Information on Porosimetry Measurements

In general, the purposes of using mercury intrusion porosimetry can be to determine the pore size distribution, apparent volume, or true volume of solid materials. This

technique involves placing a small sample (typically of a mass between 0.5 g and 1 g) into a glass penetrometer cell. The cell is a glass tube with an opening in which the sample is placed. The sample is immersed in liquid mercury. The contents of the penetrometer cell are then subjected to increasing pressure: first a low pressure analysis (exerting pressures from zero to approximately 15 psi (103 kPa)) is done followed by a high pressure analysis (15 psi to approximately 55,000 psi (103 MPa)). The output data combines data from both to form a seamless set of data. Computer software is used to collect data of the volume of mercury that penetrates into the pores of the sample at a corresponding pressure. An output for OPC hydrated for 8 hours can be seen in Fig. 4.4-1.

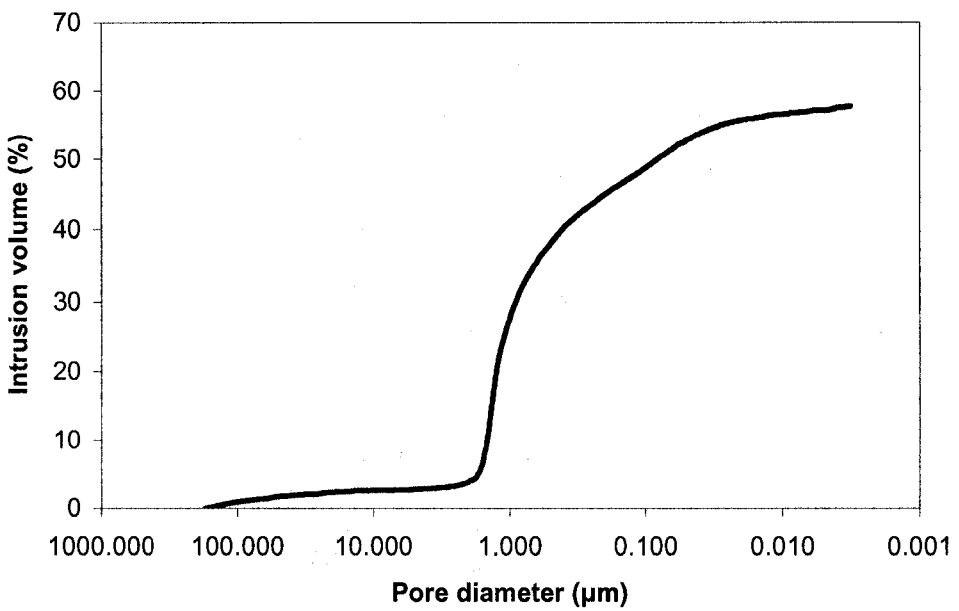

Fig. 4.4-1: A typical pore size distribution curve for (OPC hydrated for 8 hours) measured using mercury intrusion porosimetry.

The collected data is used to calculate a sample's mean pore size diameter. The following equation is used:

$$r_o = \frac{\sum p_i r_i}{\sum p_i} \qquad (4.4\text{-}1)$$

where: p_i= intrusion volume (%) for a given pressure, i

r_i= pore diameter, μm, for a given pressure, i

It should be noted that there are some limitations when it comes to measurements performed by a mercury intrusion porosimeter. Some of these limitations have been published by Beaudoin (1979). It is possible that at high pressures that the intruded mercury damages the pore walls which could lead to an inaccurate representation of the distribution. In addition, it is possible that some pores could be too small for the mercury to penetrate. In this study the water to solids ratio was 0.5 where the limitations are minimal. Further details on the mercury intrusion porosimetry apparatus used in this study are discussed in section 5.5.

Chapter 5

Experimental: Apparatus, Sample Preparation, and Testing Procedures

5.1 Calorimetry Measurements

5.1.1 The Calorimetry Apparatus

A Thermometric TAM Air Isothermal eight-channel Calorimeter (which can be seen in Fig. 5.1-1) was used to conduct the calorimetry experiments. The calorimeter consists of slots, or channels, in which the samples were placed. At the base of the channel there is a heat measuring device that measures the amount of heat the sample emits over time. The data is collected using a program called PicoLog Recorder in mW and then is converted to calories of heat/gram of solids in the sample/hour (cal/g/hr). It was later viewed by using a program called PicoLog Player (both programs are by Pico Technology Limited) and then transferred to Excel for graphics purposes.

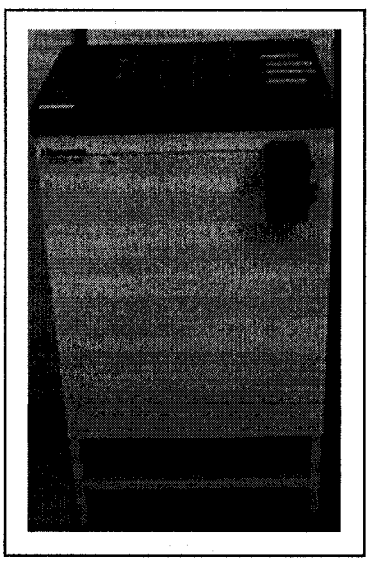

Fig. 5.1-1: The thermometric TAM Air Isothermal Calorimeter.

5.1.2 Sample Preparation and Testing

Samples containing 5 grams of material prepared at a water/solids ratio of 0.5 were used. The appropriate solid amounts of each mix were measured and placed in 30 mL plastic containers. Water was added using a pipette (a device used to draw precise amounts of liquids, see Fig. 5.1-2a)). The contents were mixed for approximately 30 seconds or until the contents appeared thoroughly mixed. Plastic caps were then tightened onto the containers (as can be seen in Fig. 5.1-2 b)). They were placed immediately inside the channels of the calorimeter so as to capture as much data of the heat of hydration as possible. Heat flow data was collected each minute for the duration of the test. The test ran for a period of 24 hours as the important information regarding cement hydration can be obtained within this time period.

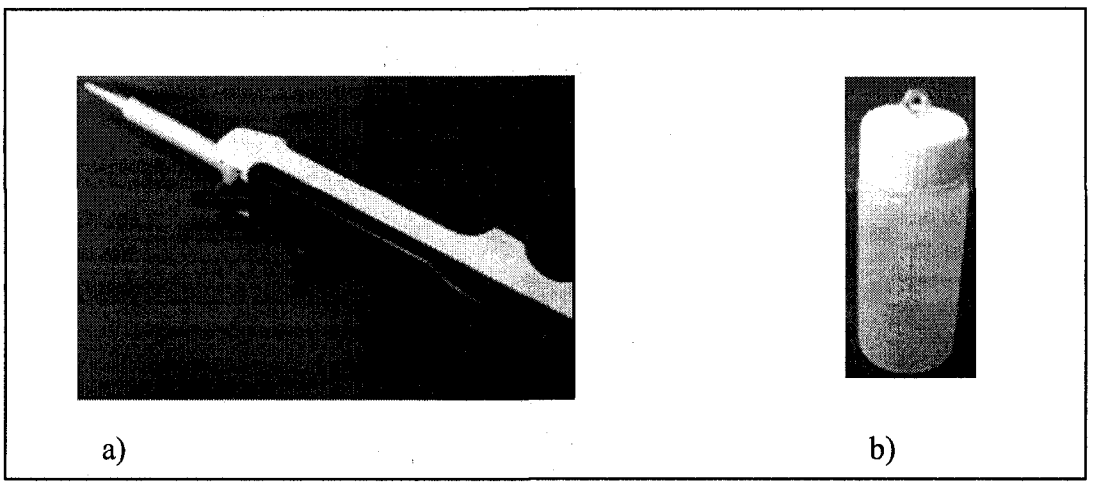

Fig. 5.1-2: a) The pipette used to measure precise amounts of liquid, b) the sample container with screw-on cap in which samples are placed.

5.2 Strength and Porosity Measurements

5.2.1 Sample Preparation for Strength Tests

ASTM C-305 was followed in the mixing process for production of the cement cubes. The mixing bowl was placed in the Hobart mixer as seen in Fig. 5.2-1. First the water

was weighed out on a balance and then it was added to the mixing bowl. The appropriate amounts of solid materials (OPC, CKD, CC, MK) were added to the water and the contents were mixed for one minute at a slow speed. The mixer's speed was then increased to a medium speed for 30 seconds. After this, the mixer was stopped and left to stand for 1.5 minutes. During the first 15 seconds of this time interval, any mortar that had accumulated on the sides of the bowl was scraped down to the bottom of the bowl. Finally, mixing the contents for one minute at medium speed completed the mixing process.

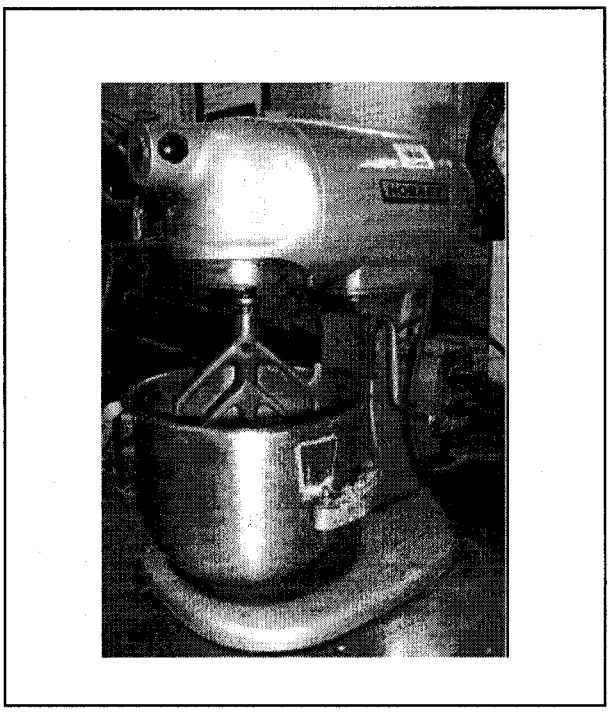

Fig. 5.2-1: The Hobart Mixer used in the mixing process.

ASTM C-109 was followed for the casting and strength measurements of the cement cubes. Brass moulds (see Fig. 5.2-2) with three compartments were used to cast the cement cubes. These moulds were wiped with a layer of Vaseline petroleum jelly so that the cement cubes could later be easily de-moulded.

Twelve cubes were cast (three cubes for each testing day) for each cement mix to allow for testing throughout the stages of the hydration process (1, 3, 7, and 28 days). The casting process began with adding a one-inch thick layer of the cement mix to all three compartments of the mould. The cement was then tamped (with a rubber tamper) 32 times in each cube compartment in four rounds in ten seconds. The order of the rounds can be seen in Fig. 5.2-3. In this figure, the rectangular shapes indicate the orientation of the tamper as it hits the cement and the numbers indicate the numerical order in which the cement was tamped. This process was repeated with another one-inch thick layer of the mix.

After the tamping process was complete, the cement mixture was leveled using a metal straight edge and any excess mortar was wiped clean from the mould. The moulds were then placed in a humid room to cure. The humid room was kept at a relative humidity of not less than 95% and a temperature of 23.5 +/- 1.7 degrees Celsius (following ASTM C-511, 2003). After 24 hours the cubes were de-moulded, and properly labeled according to its particular mix for easy identification. The cubes were then placed back in the humid room to continue the curing process. On each testing day, three cubes for each mix were removed and tested in compression as described in the next section.

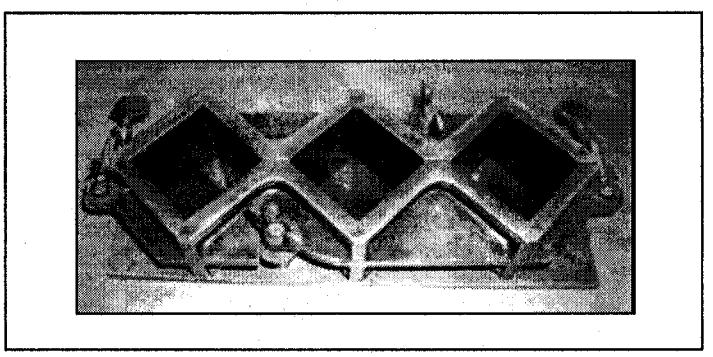

Fig 5.2-2: The brass cube mould in which the mixes were cast.

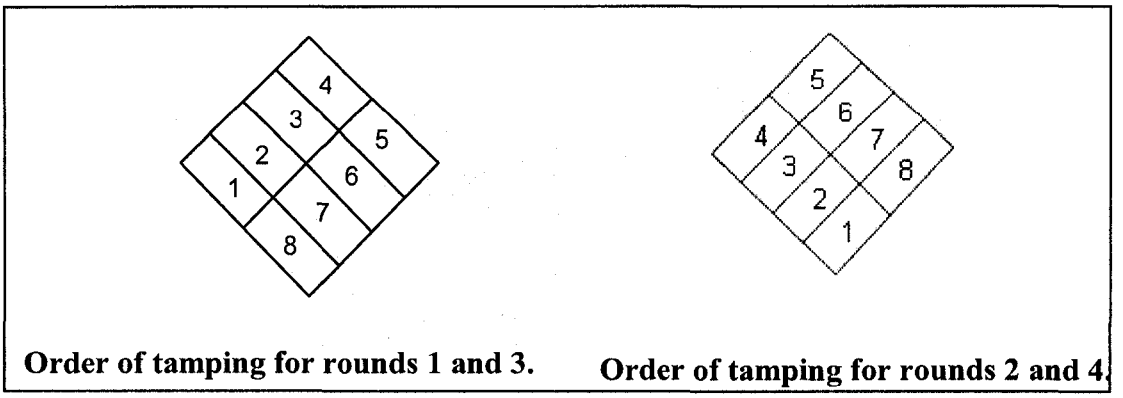

Fig 5.2-3: The order of tamping for rounds 1 to 4.

5.2.2 Strength Test Procedures and the Testing Apparatus

A computer controlled Instron compression testing apparatus was used for the compression testing of the cement cubes. The Instron testing apparatus can be seen in Fig. 5.2-4 a). Testing of three cubes was conducted after they had cured for the following hydration times (in days): 1, 3, 7, and 28. In order to test a cube, the cross head of the Instron was raised and a cube was placed on the loading cell (as seen in Fig. 5.2-4 b)). Before the testing began the surfaces of the cube in contact with the cross head and loading cell were smoothed by rubbing it against these contact surfaces. When conducting compression tests on cement cubes it is important not to place the surface of the cube which was face-up in the mould (i.e. the face that is exposed in the mould) in contact with either the cross head or loading cell. The reason for this is due to the fact that it is the least smooth of all its surfaces. After placing the cube on the loading cell, the cross head was lowered to a height that was just above the cube. The load was zeroed to ensure that at time zero no force was exerted on the cube. Then, the computer program, Partner Version 7.1e WC (materials testing software made for Windows) was programmed to do the remainder of the testing. The program was set-up to apply a force rate of 1.2 kN/second (a common force rate used for cubes of this size) until the cube's ultimate strength was reached. The program output the compressive strength of each of the three cubes in MPa, which was then averaged.

After testing the three cubes to their ultimate strengths, a broken piece from one of the cubes was saved and placed in a glass container filled with isopropanol. The purpose of this was to stop the hydration of the cement piece so that it could be used later in porosity testing. This way, correlations could be made between the compressive strength of the cement and its porosity. The porosity testing procedure is described in the next section.

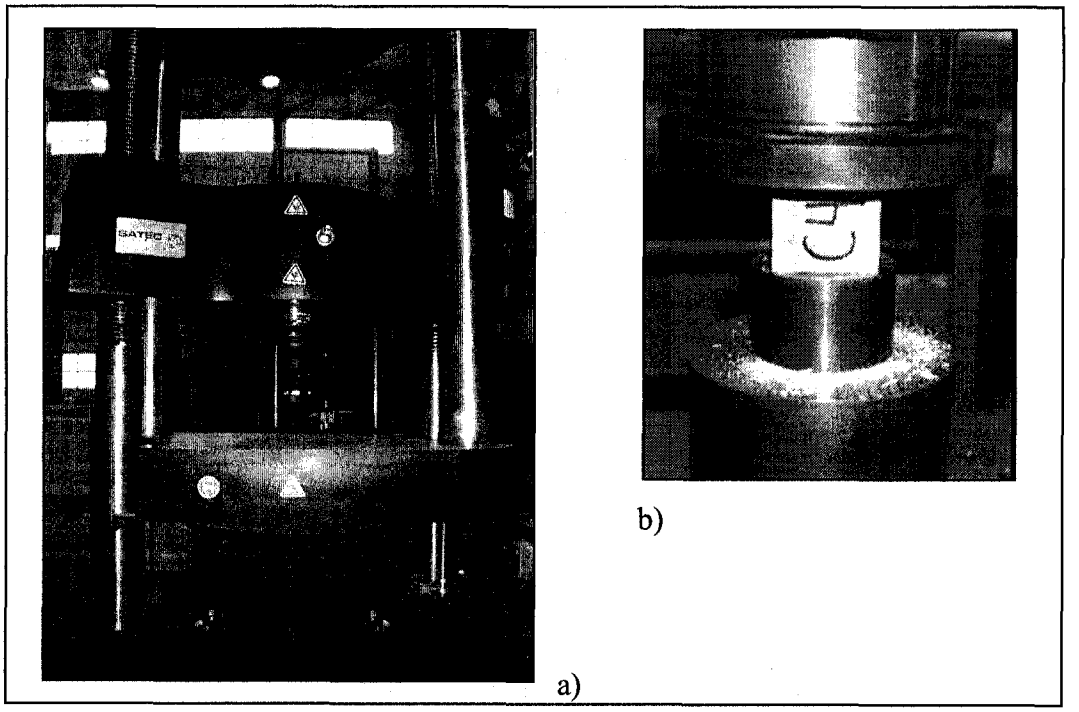

Fig. 5.2-4: a) The Instron Testing Apparatus, b) a cement cube placed within the cross head of the Instron testing apparatus.

5.2.3 Porosity Apparatus and Measurements (at 1, 3, 7, and 28 days)

The set-up for the porosity testing can be seen in Fig. 5.2-5. It consisted of a balance placed on a metal stand. A container of isopropanol was placed directly below the balance. A wire basket was hung from a hook on the base of the balance (which allowed samples to be weighed below the balance).

Each cement sample was submerged in a glass container filled with isopropanol for five days. It was assumed that after this amount of time, all of the pores within the sample were completely saturated with isopropanol. The sample was then taken from the glass container and blotted with a paper towel soaked in isopropanol; this technique is known as surface drying the sample and is used to absorb any excess isopropanol on the surface of the sample. The sample was then placed on the digital balance to measure its mass. This mass was termed the Wet Mass, m_w. The next step was to weigh the saturated sample while it was submerged in isopropanol. In order to weigh the sample while it was submerged, a wire basket was submerged in the container of isopropanol and was hung from the bottom of the balance. The saturated sample was placed inside the wire basket and its mass was measured. This mass was termed the Submerged Mass, m_s. The sample was then taken and placed in a vacuum oven for two days until it was completely dry. Using a vacuum oven allowed the sample to dry in an air-less atmosphere which prevented the sample from reacting with air to form excess calcium carbonate (a process known as carbonation). Once the sample was dry, its mass was then measured on the balance; this mass was termed the Dry Mass, m_d.

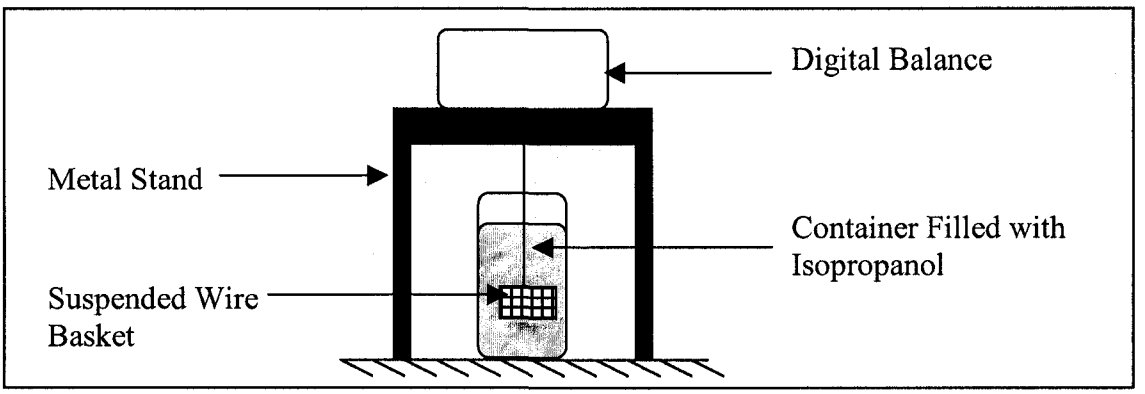

Fig. 5.2-5: The set-up for the porosity testing.

In summary, three mass measurements were made: the Wet Mass, m_w, the Submerged Mass, m_s, and the Dry Mass, m_d. According to mathematician Archimedes, when an item is submerged, the mass of the displaced fluid, m_{disp} is directly proportional to its

volume. From this knowledge, the following set of calculations can be made to determine the sample's porosity:

The mass of the displaced fluid can be calculated by:

$$m_{disp} = m_w - m_s \tag{5.2-1}$$

The volume of the displaced fluid, V_{disp}, can then be calculated by:

$$V_{disp} = \frac{m_{disp}}{\rho_{disp}} \tag{5.2-2}$$

where: ρ_{disp}= the density of the displaced fluid in g/cm^3

And the volume of the displaced fluid is equal to the total volume of the sample:

$$V_{disp} = V_t \tag{5.2-3}$$

In order to calculate the volume of the pores, the mass of fluid in the pores, m_p, must first be calculated:

$$m_p = m_w - m_d \tag{5.2-4}$$

Then the volume of the pores is simply:

$$V_p = \frac{m_p}{\rho_{disp}} \tag{5.2-5}$$

And so the porosity of the sample can then be calculated by dividing Eq. 5.2-5 by Eq. 5.2-3 (as was shown in Eq. 4.2-2.)

Recall Eq. 4.2-2:

$$\varphi = \frac{V_p}{V_t} \tag{4.2-2}$$

where: φ= porosity

V_p= volume of the pores in the sample, m^3

V_t= total volume of the sample, m^3

5.3 AC Impedance Measurements

5.3.1 The AC Impedance Testing Apparatus

A Solartron 1260 Impedance/Gain Analyzer machine (as seen in Fig. 5.3-1) was used for the AC impedance testing. This machine was connected to a computer-based data acquisition system. The data from the testing was collected using the ZPlot software package and viewed using the ZView package (both software packages were products of Scribner Associates, Inc. and were developed specifically for AC impedance measurements).

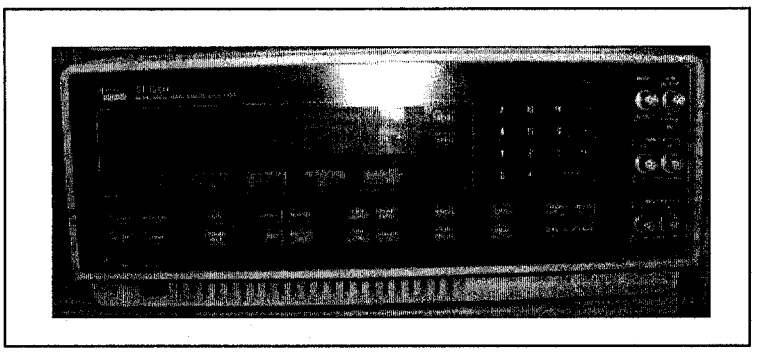

Fig. 5.3-1: The Solartron 1260 Impedance/Gain Analyzer.

An in-circuit test module (which is a device used to output the current provided by the machine) was connected to the Solartron 1260 and then to the sample being tested by the means of two clips. These clips were attached to the electrodes that were cast into the sample mould during the process of mixing and casting the cement sample. It

can be noted that the process of sample preparation is discussed in detail in the next section. Two grounding clips were attached to the module (by the means of wires). When the testing began, the two clips were attached together. This provided a shield against external electromagnetic noise. The module, samples clips and grounding clips can be seen in Fig. 5.3-2.

The ZPlot software controls the different types of variables such as the output frequency, the current amplitude, and the voltage amplitude. The Solartron 1260 can be set to output either a voltage and measure the current to calculate the impedance; or it can be set to output the current and measure the voltage to calculate the impedance. In all testing that was performed, the machine was set to apply a voltage. Running the ZPlot software causes the Solartron 1260 to create a potential difference between the clips attached to the sample's electrodes; this induces a current between the two clips, which runs through the sample.

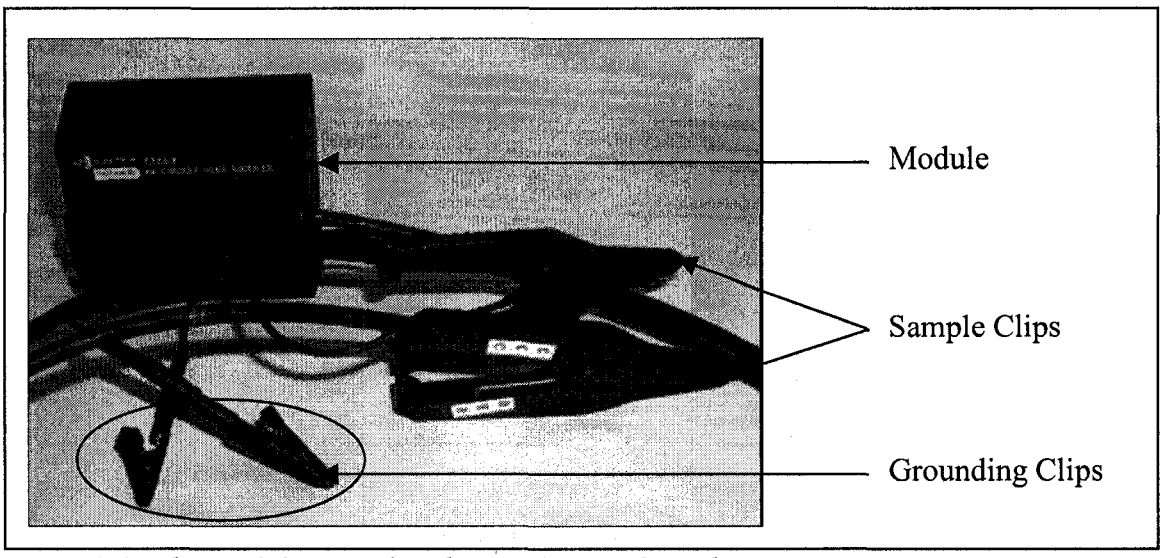

Fig. 5.3-2: The module, samples clips and grounding clips.

5.3.2 AC Impedance Sample Preparation and Sample Testing

The samples for AC impedance testing were cast in plastic cylinders 10 cm long with an inner diameter of 0.96 cm and an outer diameter of 1.30 cm. This meant that the cross sectional area of each sample was 0.72 cm^2. The plastic cylinder was slit at each end in order to facilitate the installation of the electrodes. Each electrode was made by soldering a small stainless steel circular plate (which measured 0.74 cm in diameter) to an electrical wire. After the soldering process, the electrodes were soaked in acetone to remove any grease or dirt that may have accumulated on the electrode as a result of the soldering process. The cement mix was prepared by measuring the appropriate amount of solid materials; and water was added using a pipette at a water/solids ratio of 0.5. The contents were then hand mixed and poured into the plastic cylinder. The mix was cast in three steps and vibrated after each one in order to ensure the removal of any air bubbles. The cylinder was capped with stainless steel plates (measuring 1.15 cm in diameter). The ends of the cylinder were then wrapped in parafilm wax and secured in place with tape. An image of a cement mix cast in a plastic cylinder with electrodes protruding can be seen in Fig. 5.3-3. Next, the sample was wrapped in a wet kimwipe and placed in a plastic container. This ensured that the sample did not dry out during the testing period. The ends of the electrodes were pushed through two small holes in the plastic container to connect with the clips connected to the Solartron 1260 testing device.

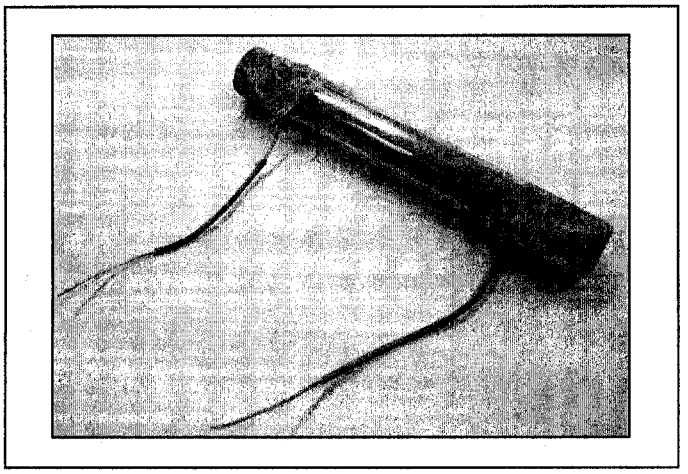

Fig. 5.3-3: A cement sample cast in a plastic cylinder with electrodes protruding.

The first test was conducted immediately after connecting the clips to the electrodes (this first test was considered 'time zero'). The test was set-up to sweep through the frequencies of 1 MHz to 0.1 Hz. The output current started at the highest frequency and decreased to the final lowest output frequency. The software was set-up to perform a test (and sweep through the frequencies) once every hour after time zero for 24 hours. It should be noted that the sample remained cast in the plastic cylinder throughout the testing.

After testing a cement sample, AC impedance data was output and viewed using the ZView software. This software was then used to fit the data from the HFA using the equivalent electric circuit that was shown in Fig 4.3-6. After the fitting process, the ZView software output estimated values for parameters R_1, R_2, C_d, and n. The results will be discussed in Chapter 8.

5.4 Porosity Measurements at early ages (5, 8, 16, 24 hours)

(Note: The collected data is used in conjunction with AC Impedance measurements)

5.4.1 Porosity Sample Preparation

(Note: The Apparatus and Testing Procedures were explained in the Strength and Porosity Measurements section 5.2.3 on page 67.)

Samples for porosity measurements were made to correlate with AC impedance testing. These samples were hand mixed in a plastic container then covered with a plastic cap until the desired hydration time. Samples were hydrated for periods of 5, 8, 16, and 24 hours. At the specified hydration time, the sample was taken from the plastic container and placed in a glass container filled with isopropanol to stop the sample's hydration process. The sample was stored in the isopropanol until its porosity could be tested. The procedure used in the porosity measurements was the same as was conducted for the compression testing samples. It should be noted that the data from these porosity measurements were plotted and fit with a trendline in

order to obtain estimated values for all other hydration times (i.e. 0-4 hours, 6-7 hours, 9-15 hours, and 17-23 hours): this will be discussed in Chapter 8.

5.5 Mercury Intrusion Porosimetry

(Note: The collected data is used in conjunction with AC Impedance measurements.)

5.5.1 Mercury Intrusion Porosimetry Apparatus and Sample Measurements

(Note: There is no sample preparation for the porosimetry measurements because a piece of sample was simply taken from the porosity samples and measured using the technique.)

The objective of the testing, as was described in section 4.4, was to obtain the pore size distribution of six mixes in order determine their mean pore sizes (the selection of samples and the rationale for the selection will be discussed in Chapter 8). A Quantachrome PoreMaster GT mercury intrusion porosimeter was used in the porosimetry measurements. This instrument can be seen in Fig. 5.5-1.

The specimen consisted of a piece of sample that was hydrated for 8 hours, and originally used in the porosity measurements (in section 5.4.). A sample whose mass was between 0.5 g and 0.7 g was placed inside the penetrometer cell and inserted into the machine. The sample was then immersed in liquid mercury. Pressures from zero to approximately 55,000 psi were applied on the contents of the penetrometer cell. This caused the liquid mercury to intrude into the sample's pores. Data for the sample's pore size distribution was recorded using PoreMaster for Windows 5.10 computer software. Plots for the pore size distributions for the six samples can be seen in Fig. 8.7.1.1-1 of the Appendix. The values determined for each sample's mean pore size are presented and discussed in section 8.6.

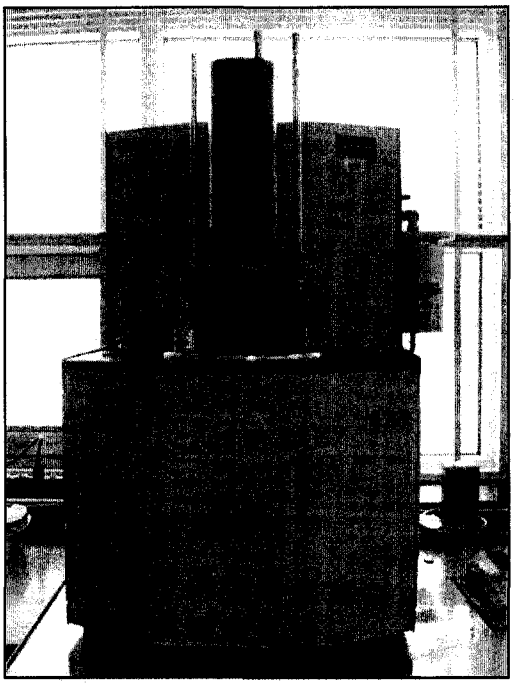

Fig. 5.5-1: The mercury intrusion porosimeter.

Chapter 6

Results and Discussion: Calorimetry Measurements

6.1 Introduction

Calorimetry measurements were obtained for all 18 mixes. The calorimetry results are explained in four sections: first the results from the Alpena CKD mixes, followed by those of the Bath CKD mixes, and then those of the Ashgrove CKD, and Ashgrove CKD with MK mixes. Interpretation of the calorimetry curves involves observing the time (t_p) when the peak value of the heat of hydration occurs. As this peak shifts to lower times, it is interpreted to mean that hydration and setting of the sample have accelerated. Peak shifts to higher times, is interpreted to mean that the hydration and setting of the sample have been retarded.

The results from the calorimetry measurements of the control mixes and mixes containing Alpena CKD, Bath CKD, Ashgrove CKD, and Ashgrove CKD with MK are shown in Figs. 6.2-1, 6.3-1, 6.4-1, and 6.5-1, respectively. The values for the t_p for each mix are shown in Tables 6.2-1, 6.3-1, 6.4-1, and 6.5-1. The results are discussed in the sections that follow.

6.2 Alpena CKD

The additions of 0.1 and 0.2 CC (as can be see in Fig. 6.2-1) both decreased the time to reach the peak, t_p, for the OPC mix. The t_p decreased from 8.5 hours to 5.7 hours with the addition of CC. It decreased further to 4.8 hours with the addition of 0.2 CC. This improvement is in agreement with the XRD results (Chapter 3, section 3.3) and with past research (Sato and Beaudoin, 2006, 2007). The substitution of 30% Alpena CKD slightly retarded the hydration of this mix as compared with the OPC mix

(which was in disagreement with the XRD results presented in Chapter 3 which suggested Alpena may accelerate the hydration of OPC). Alpena CKD is high in sulfate. Therefore this effect is in agreement with results obtained by Heikal et al. (2002). The addition of 0.1 CC to this mix decreased t_p, from 8.9 hours to 5.5 hours. The value of t_p decreased even further with the addition of 0.2 CC to 4.7 hours. This shows that adding CC to the OPC+Alpena CKD mix increased the rate of its reaction. The addition of the CC appears to have a positive effect in accelerating the hydration of all these mixes.

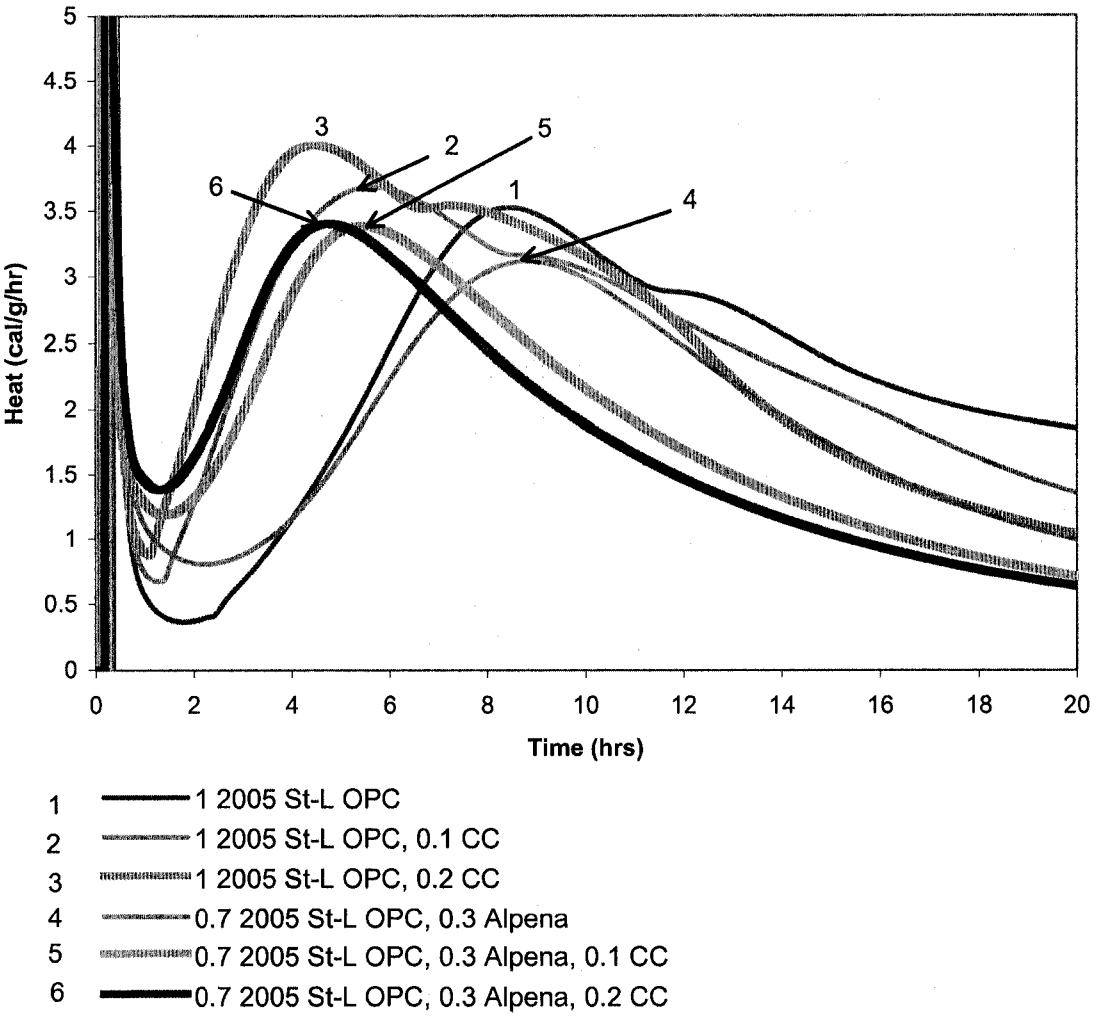

Fig. 6.2-1: Calorimetry results for control mixes with mixes with Alpena CKD.

Table 6.2-1: Values for t_p for control and Alpena CKD mixes.

Mix	t_P (hrs)
OPC	8.5
1 OPC, 0.1 CaCO3	5.7
1 OPC, 0.2 CaCO3	4.8
0.7 OPC, 0.3 Alpena CKD	8.9
0.7 OPC, 0.3 Alpena CKD, 0.1 CC	5.5
0.7 OPC, 0.3 Alpena CKD, 0.2 CC	4.7

6.3 Bath CKD

The substitution of 30% Bath CKD in the OPC mix (as can be see in Fig. 6.3-1) actually showed an improvement in the value of t_p (it went from 8.5 hours to 6.3 hours as seen in Table 6.2-1). This is likely due to the fact that the Bath CKD has a high chloride content which is in agreement with results obtained by Bhatty (1984). The 0.1 and 0.2 additions of CC resulted in further decreases in the t_p times down to 4.9 hours and 4.3 hours, respectively. Once again, the CC additions have accelerated the hydration of the mixes containing CKD and OPC.

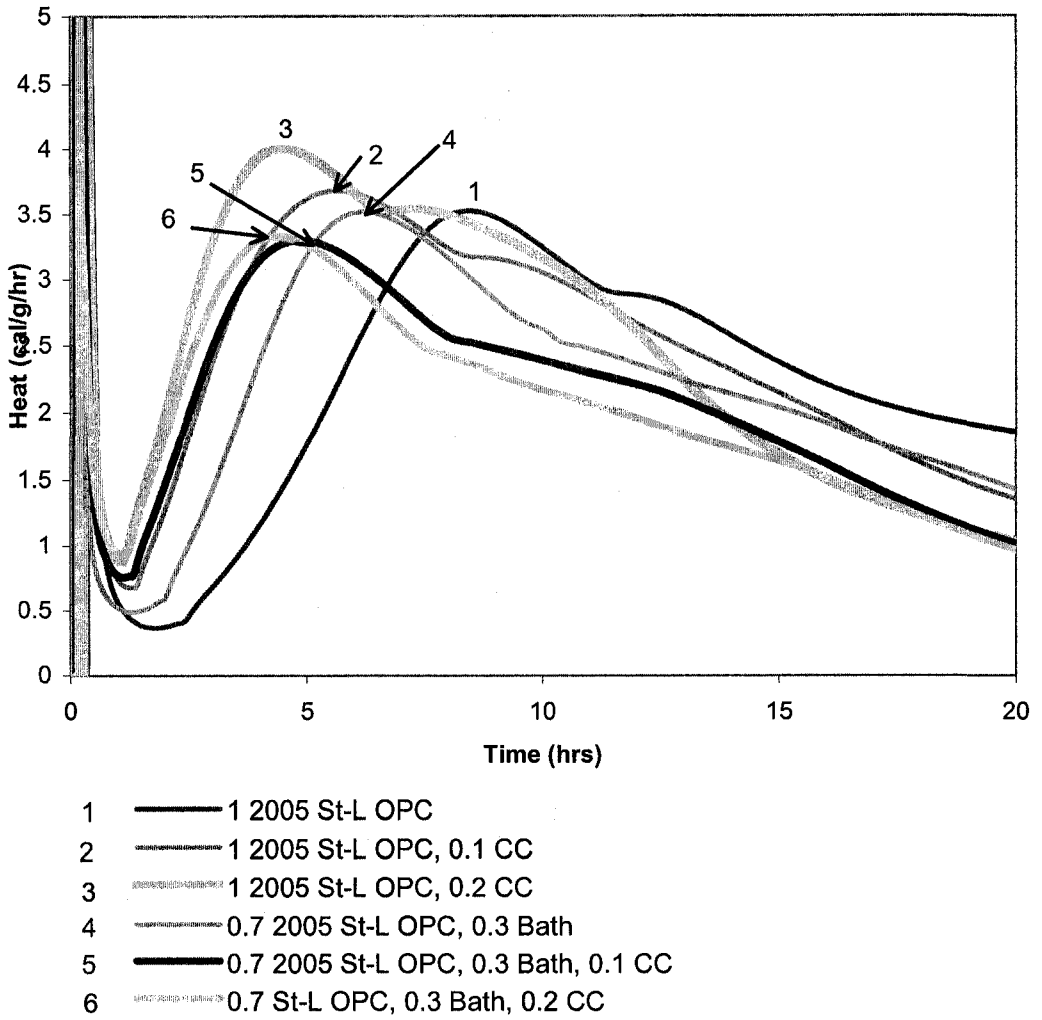

Fig. 6.3-1: Calorimetry results for control mixes with Bath CKD.

Table 6.3-1: Values for t_p for control and Bath CKD mixes

Mix	t_p (hrs)
OPC	8.5
1 OPC, 0.1 CaCO3	5.7
1 OPC, 0.2 CaCO3	4.8
0.7 OPC, 0.3 Bath CKD	6.3
0.7 OPC, 0.3 Bath CKD, 0.1 CC	4.9
0.7 OPC, 0.3 Bath CKD, 0.2 CC	4.3

6.4 Ashgrove CKD

Ashgrove CKD is high in alkali and amorphous compounds therefore it was considered likely to be a very reactive CKD. As can be seen in Fig. 6.4-1, the substitution of Ashgrove CKD to the OPC mix reduced the t_p from 8.5 hours to 7.3 hours (see Table 6.2-1). Its hydration was accelerated less than was seen when Alpena or Bath CKDs were substituted for OPC. This was also indicated by the XRD results. As was the case with both the Alpena and Bath CKDs, the 0.1 and 0.2 additions of CC to the OPC+CKD mix aided in reducing t_p times from 7.3 hours to 5.4 hours and 4.8 hours, respectively. This is also in agreement with the XRD results. Once again, the addition of the CC to the CKD+OPC mix has shown to further accelerate the hydration process.

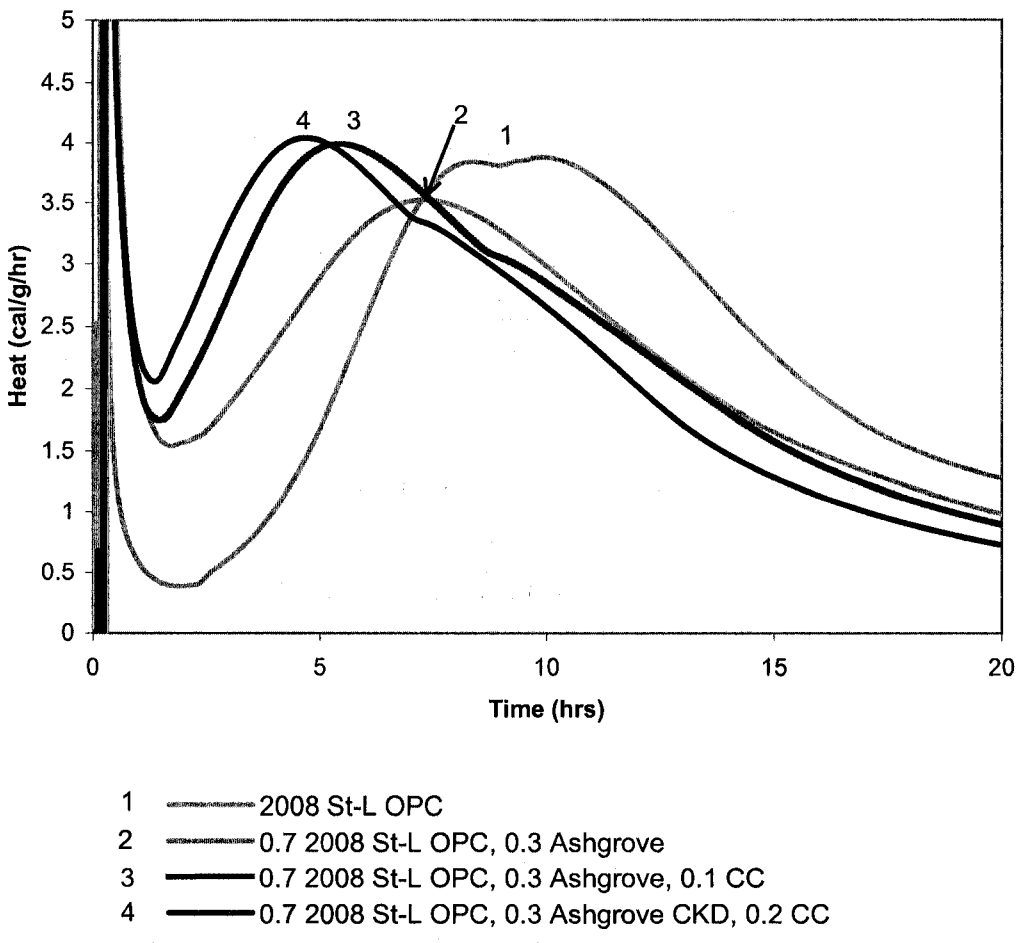

Fig. 6.4-1: Calorimetry results for mixes with Ashgrove CKD.

Table 6.4-1: Values for t_p Ashgrove CKD mixes

Mix	t_p (hrs)
OPC	8.5
0.7 OPC, 0.3 Ashgrove CKD	7.3
0.7 OPC, 0.3 Ashgrove CKD, 0.1 CC	5.4
0.7 OPC, 0.3 Ashgrove CKD, 0.2 CC	4.8

6.5 Ashgrove CKD with MK

The hydration time for the mix with a 30% replacement of OPC with MK showed it accelerated hydration of OPC from 8.5 hours to 5.6 hours. This acceleration is in agreement with research conducted by Justice and Kurtis (2007). The addition of 0.1 CC to this mix reduced its t_p time even further to 4.6 hours, effectively halving the hydration time of the original OPC mix. This shows that MK and CC may both be contributing to the acceleration process. This may be a result of adding a large amount of nucleation sites where reactions are able to take place.

It was expected that the substitution of the Ashgrove CKD with MK would aid in further accelerating its hydration due to its fine particle size. However, the replacement of 15% Ashgrove CKD with MK increased the t_p time from 7.3 hours (see previous Table 6.4-1) to 8.1 hours (see Table 6.5-1). However, it is important to note that hydration was still accelerated when compared with the control OPC mix. The addition of 0.1 and 0.2 CC to this mix aided in greatly reducing the t_p time: from 8.1 hours to 5.3 and 4.4 hours respectively for each CC addition. The results showed that for OPC+Ashgrove CKD+CC mix when the CKD is substituted with MK aids in further reducing the t_p time. The mix containing 0.3 Ashgrove CKD and 0.1 CC (without MK) had a t_p value of 5.4 hours (Table 6.4-1) and when MK was added to this mix a t_p time of 5.3 hours was observed. Also, the addition of 0.2 CC to this mix reduced the t_p time further to 4.6 hours. This indicated that it is the combination of both the MK and CC together that aided in accelerating the hydration of the OPC+Ashgrove CKD mix. This was also in agreement with the XRD results.

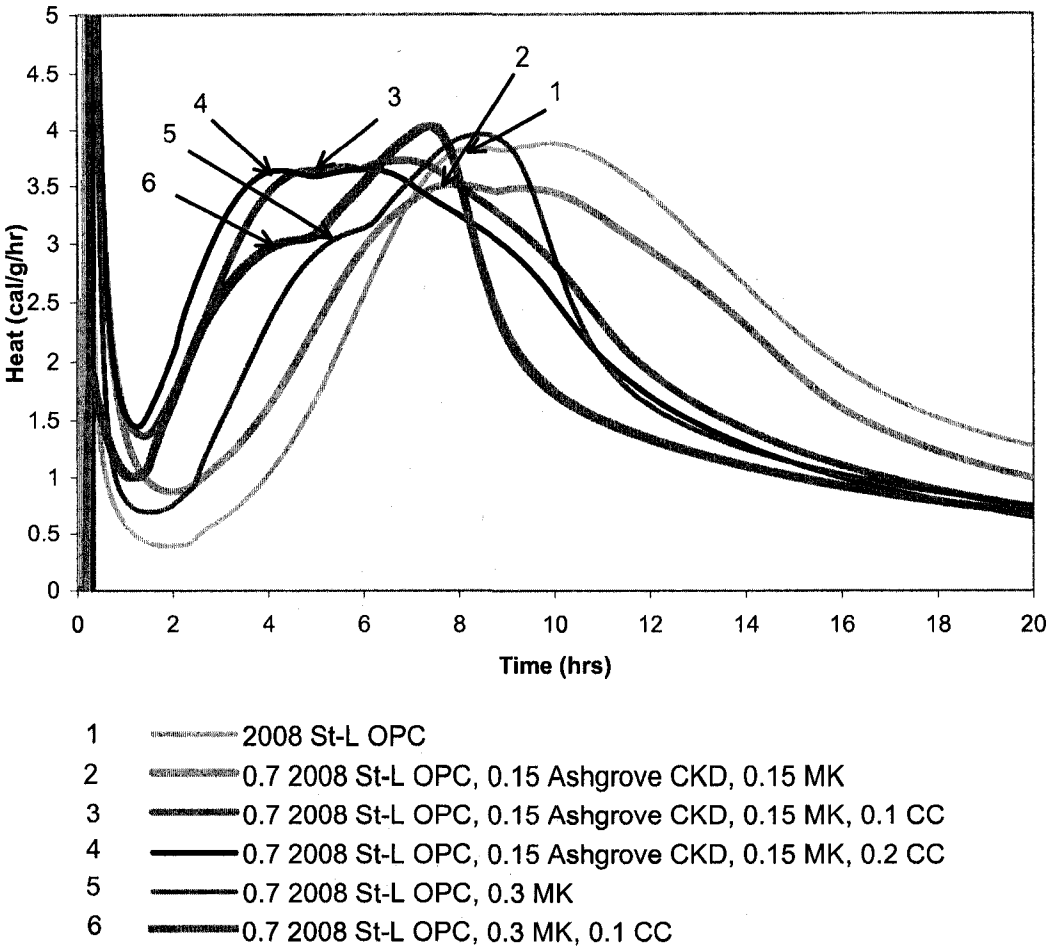

Fig. 6.5-1: Calorimetry results for mixes with Ashgrove CKD and MK.

Table 6.5-1: Values for t_p Ashgrove CKD with MK mixes

Mix	**t_p** (hrs)
OPC	8.5
0.7 OPC, 0.15 Ashgrove CKD, 0.15 MK	8.1
0.7 OPC, 0.15 Ashgrove CKD, 0.15 MK, 0.1 CC	5.3
0.7 OPC, 0.15 Ashgrove CKD, 0.15 MK, 0.2 CC	4.4
0.7 OPC, 0.3 MK	5.6
0.7 OPC, 0.3 MK, 0.1 CC	4.6

6.6 Summary of Calorimetry Results

The promising results of the calorimetry measurements showed that early-age hydration was accelerated with the addition of CC to OPC+CKD mixes. This was in agreement with past research that suggested that the CC accelerated the hydration of cement systems. It was the combination of having both MK and CC present in the Ashgrove CKD mixes that greatly aided in accelerating the hydration process. It is possible that having both of these fine materials, with large surface areas, present added a great number of nucleation sites where reactions are able to occur. This may account for the accelerating effect.

Chapter 7

Results and Discussion: Strength and Porosity Measurements

7.1 Introduction

The strength results will be discussed first as a function of time and second as a function of porosity. The data for both the collected compressive strength and porosity measurements are presented in Table 7.2-1 and 7.2-2 of the Appendix. The results for the compressive strength of the mixes versus time are plotted in Fig.7.2-1 and Fig. 7.2-2. Trendlines were used to fit the compressive strength versus porosity data plotted as a semi-log function. The fit equation along with its corresponding regression value, R^2, can be seen in the Appendix in Table 7.2-3 (it should be noted that some outliers were omitted from the fitting of the data). Fig. 7.3-1, Fig. 7.3-2, Fig. 7.3-2, and Fig. 7.3-4 display the results for the compressive strength versus porosity results.

7.2 Strength vs. Time

7.2.1 Results for Controls, Alpena CKD, and Bath CKD Mixes

The addition of 0.1 CC to the OPC mix resulted in compressive strengths similar to those of the OPC. The addition of 0.2 CC appears to have lowered its strengths. This is not what was expected to occur according to indications by Sato and Beaudoin (2006, 2007).

The substitution of Bath and Alpena CKDs for OPC resulted in lower compressive strengths at all ages. The larger amount of chloride present in the Bath CKD may be one of the reasons its strength was substantially reduced. Past research indicated that

CKDs high in chloride resulted in a sort of crystallization of the hydration products; which leads to an opening of the pore system, causing a reduction of strength (Shoaib et al., 2000). Re-call that Alpena CKD was high in sulfate. There were conflicting reports as to whether a CKD high in sulfate was beneficial or detrimental to OPC strength. Siddique (2006) reported a decrease in strength, while Bhatty (1985) reported an increase. In the current work, the trend seemed to follow the conclusions of Siddique (2006). Sulpho-aluminates (which are known to be responsible for reductions in strength (Siddique, 2006)), due to the presence of the high sulfate content may have reduced the strength of the Alpena mix.

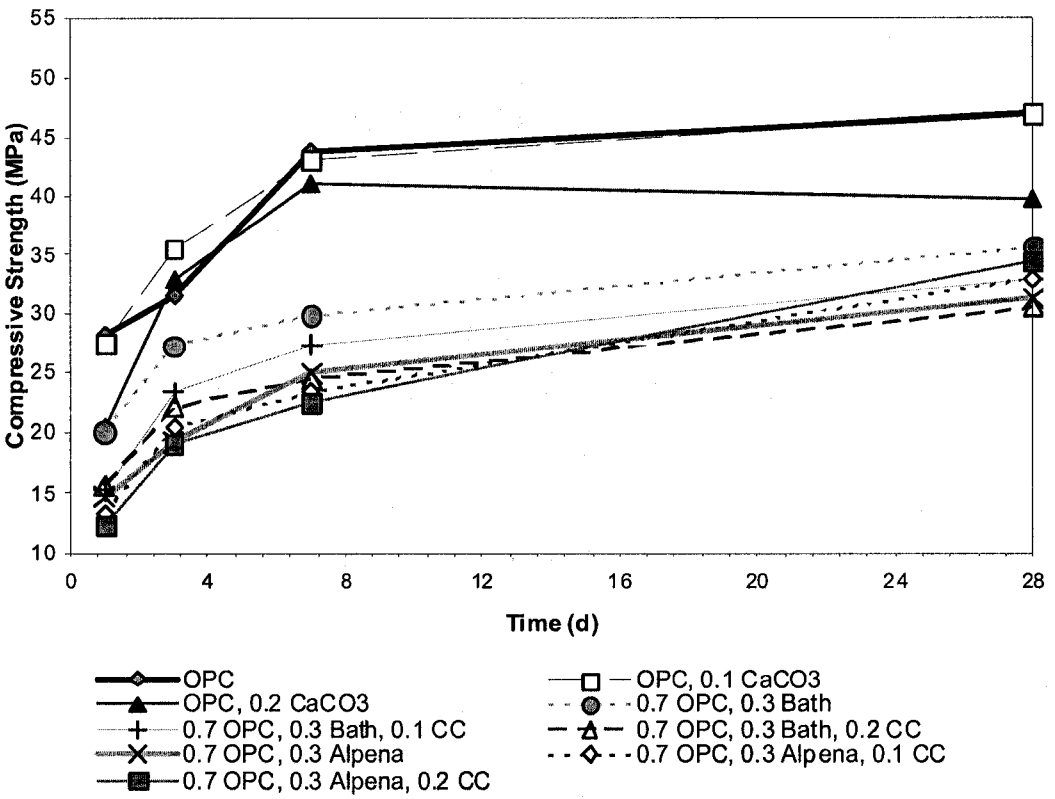

Fig. 7.2-1: Compressive strength results for control, Alpena, and Bath mixes.

The addition of 0.1 CC to the Bath CKD showed compressive strengths that were relatively close to those without any CC. It appears that the detrimental effects due to the high chloride content of this CKD could not be countered by the addition of CC.

The addition of 0.1 CC and 0.2 CC improved the overall strength of the Alpena CKD mix at 28 days. The mix containing no CKD had a 28-day compressive strength of 31.2 MPa, while the OPC+CKD mixes with 0.1 and 0.2 CC additions had 28-day strengths of 33.0 MPa and 34.5 MPa, respectively. This shows that the CC addition to the Alpena CKD aided in its overall strength development at later ages.

7.2.2 Strength vs. Time: Results for Ashgrove CKD with MK

The addition of Ashgrove CKD in the OPC resulted in a decrease in its strength as can be seen in Fig. 7.2-2. This may be due to the large presence of alkalis in this CKD. Shoaib et al. (2000) reported that the presence of alkalis in the cement causes the microstructure of the C-S-H phases to become more heterogeneous and lower the compressive strength. It should be noted, however, that the strength of the OPC decreased much less with the substitution of Ashgrove CKD than with the Bath or Alpena CKDs. The reason is likely due to the composition of the Ashgrove CKD.

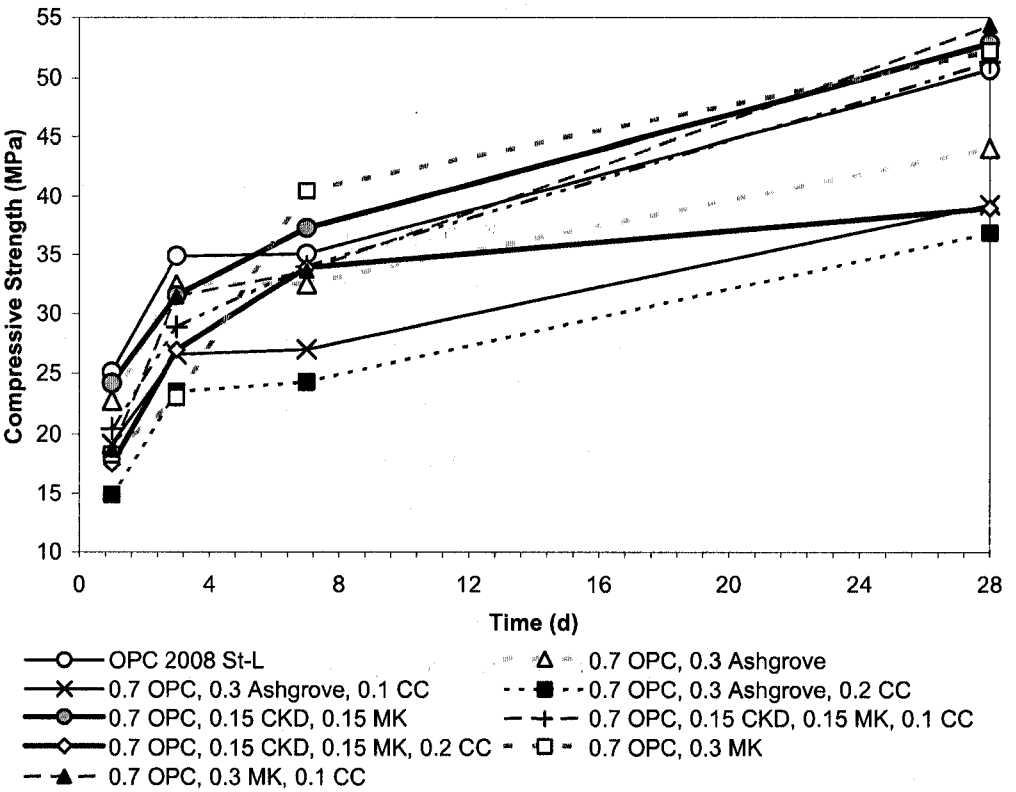

Fig. 7.2-2: Compressive strength results vs. time for Ashgrove CKD and MK.

The Ashgrove CKD mixes with MK and CC faired extremely well. The addition of CC alone to the Ashgrove CKD mix did not aid in its strength development. However, the substitution of Ashgrove CKD with MK showed higher strengths than the OPC mix at 7 days (37.3 MPa vs. 30.2 MPa) and 28 days (52.9 MPa vs. 50.7 MPa). Although the addition of 0.1 CC to that mix lowered its strength values somewhat, they were still an improvement over the OPC mix with higher compressive strengths at 7 days (34.0 MPa) and 28 days (51.3 MPa). The OPC with a 30% substitution of MK proved to be stronger than the OPC mix at 7 days (40.5 MPa) and at 28 days (52.2 MPa). A 0.1 CC addition to this mix resulted in the highest compressive strength of all the mixes at 28 days, i.e. 54.3 MPa.

It is clear that the substitution of CKD with MK was advantageous. The combination of MK and CC could also be advantageous when it comes to strength development of OPC, and OPC with CKD mixes. The fine particle sizes of these additives may have increased the available nucleation sites for reactions to take place. Further, as was suggested previously by Guneyisi et al. (2008), the small particles of MK might have filled the void spaces of the hydrated cement causing the microstructure of the matrix to become denser leading to enhanced strength. Likewise, Ramachandran and Chun-mei (1986) suggested that the pores could be filled with fine-sized high surface area particles of CC thus aiding in strength development.

7.3 Strength vs. Porosity

Conventionally, strength versus porosity plots are plotted with the log-scale of the compressive strength on the y-axis and increasing porosity values are plotted along the x-axis. Plotting strength versus porosity provides a way of looking at the data without time being a factor. Removing the time variable allows other trends to be observed such as the relative strengths at a given porosity and what that might mean with regard to the intrinsic strength of the solid matter.

7.3.1 Results for Controls, Alpena CKD, and Bath CKD Mixes

Trendline curves for the compressive strength versus porosity for the Alpena CKD, and Bath CKD mixes (along with the control mixes) can be seen in Fig. 7.3-1 and Fig. 7.3-2, respectively. In general, at lower porosity values, the strength values appear to be converging. This may indicate that the intrinsic characteristics of the solids in the mixes may be somewhat similar as hydration progresses. It also implies that at later ages (i.e. at decreased porosity) systems containing Alpena and Bath CKDs may have strengths approaching those of OPC. In order to investigate this further, a "zero porosity" strength value was calculated by setting the porosity of the trendline equations equal to zero.

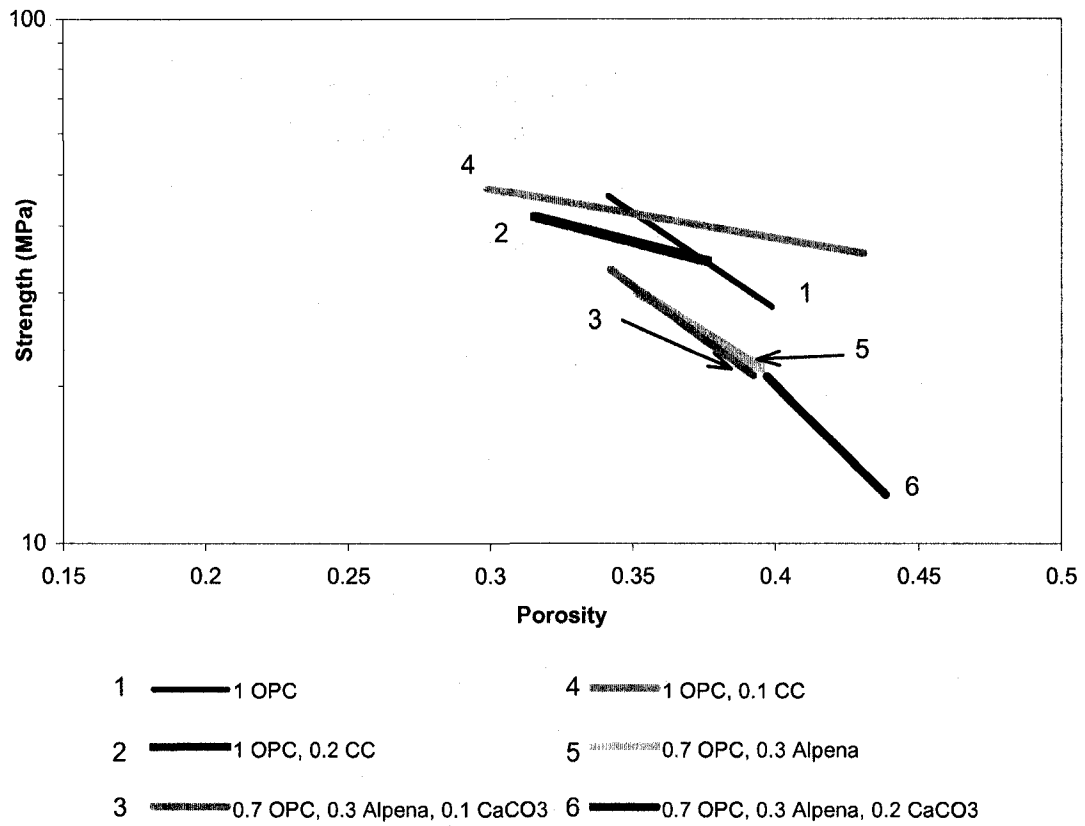

Fig 7.3-1: Compressive Strength vs. Porosity for Alpena CKD mixes.

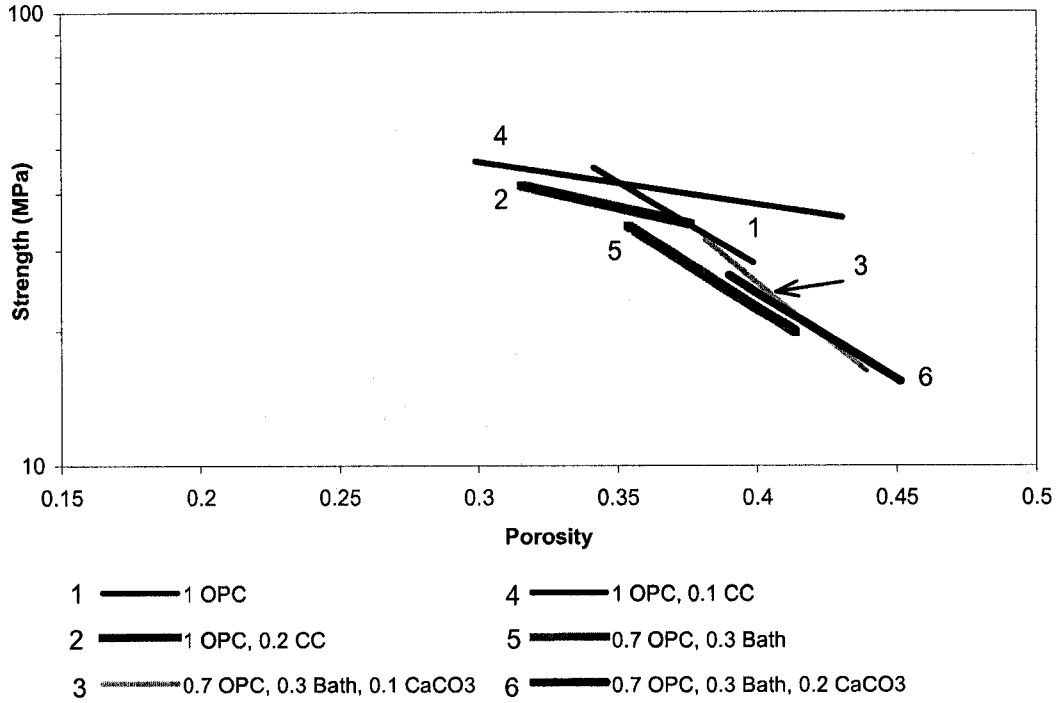

Fig 7.3-2: Compressive Strength vs. Porosity for Bath CKD mixes.

The zero porosity values for the OPC, OPC+Bath CKD, and OPC+Alpena CKD were 776 MPa, 802 MPa, and 450 MPa, respectively, as can be seen in Table 7.3-3. The range of values shows that the strength values for the OPC+CKD mixes may be indeed approaching that of the OPC: perhaps more so for the Bath CKD mix.

The addition of CC to each of the OPC+CKD mixes caused zero porosity strength values to increase. For the OPC+Alpena CKD mix, the addition of 0.1 CC nearly doubled the strength value to 752 MPa; while the addition of 0.2 CC produced a strength value of 3027 MPa. It is known that as porosity decreases, better bonding develops between high density, well crystallized and poorly crystallized materials: consequently resulting in higher strength values (Beaudoin and Feldman, 1975). It was proposed that optimum blends of poorly crystalline and crystalline material can yield maximum strength values. CKDs are known to be less crystalline materials as compared to OPC. This may be the reason such high values were seen when 0.2 CC was added to the OPC+Alpena CKD mix.

In the case of the Bath CKD mixes, the 0.1 concentration of CC showed a much improved strength value (2666 MPa) over the 0.2 CC concentration (849 MPa). It could be that for this particular CKD the 0.1 CC addition provided the optimum mixture of well crystallized materials and poorly crystallized materials. This may mean that, on its own, the Bath CKD perhaps needed only a small concentration of additional crystallized materials to improve its intrinsic strength.

Table 7.3-3: Zero porosity strength values for controls, Alpena CKD and Bath CKD mixes.

Mix	Zero Porosity Strength (MPa)
OPC 2005	776
OPC, 0.1 CC	89
OPC, 0.2 CC	113
0.7 OPC, 0.3 Alpena	450
0.7 OPC, 0.3 Alpena, 0.1 CC	752
0.7 OPC, 0.3 Alpena, 0.2 CC	3027
0.7 OPC, 0.3 Bath	802
0.7 OPC, 0.3 Bath, 0.1 CC	2666
0.7 OPC, 0.3 Bath, 0.2 CC	849

7.3.2 Strength vs. Porosity for Ashgrove CKD, and Ashgrove CKD with MK mixes

The strength versus porosity curves for Ashgrove CKD, and Ashgrove CKD with MK mixes are presented in Fig. 7.3-3 and Fig. 7.3-4, respectively. Visually, these plots are much different from those seen for the Alpena and Bath CKD results. They show a much broader range of porosity for the measured strengths. The curves, as can be seen in Fig. 7.3-3, are generally parallel and not converging as observed for the Alpena CKD and Bath CKD results. The strength values, at a given porosity, for example at 0.25, in decreasing order are as follows (without the mix with 0.2 CC which does not seem to follow the general trend): OPC> OPC+Ashgrove CKD

>OPC+Ashgrove CKD+CC. This indicates that the OPC may have a denser matrix that perhaps becomes less dense with the addition of the Ashgrove CKD.

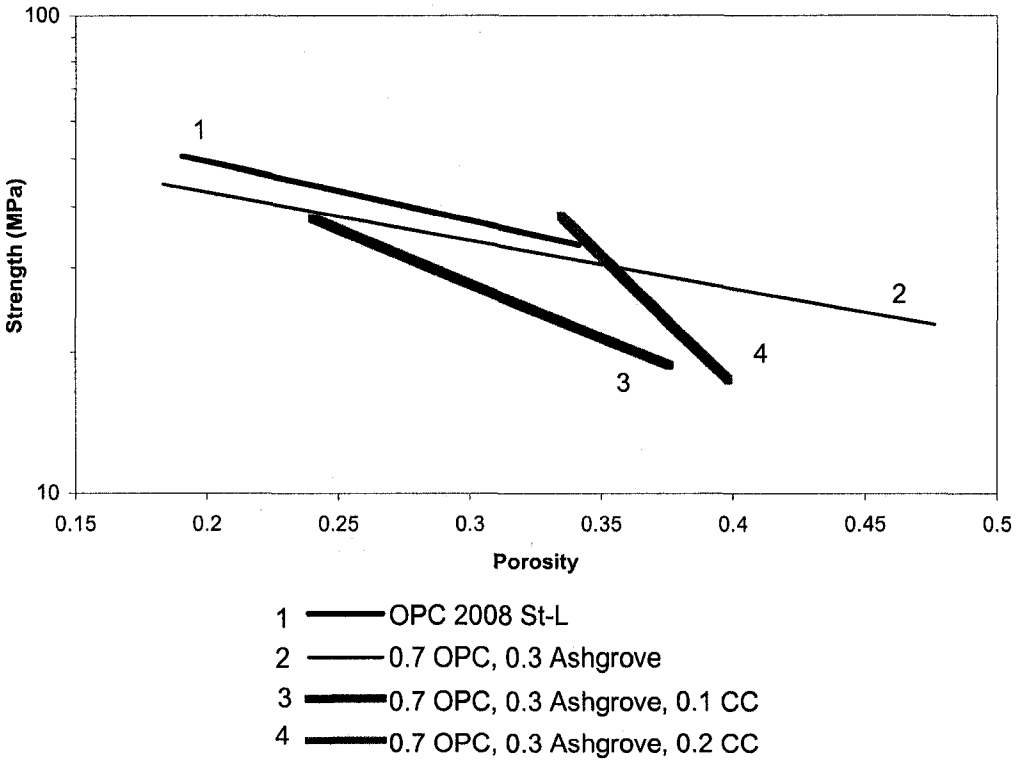

Fig 7.3-3: Compressive Strength vs. Porosity for Ashgrove CKD mixes.

In order to further verify this, the zero porosity strength values were calculated and can be seen in Table 7.3-4. The addition of Ashgrove CKD to the OPC resulted in a decrease of the zero porosity strength value (from 86 MPa to 67 MPa). The reason for this may be due to the fact that Ashgrove CKD is known to be highly amorphous. The addition of 0.1 CC and 0.2 CC increased the zero porosity strength value dramatically to 130 MPa and 2312 MPa, respectively. Once again, the addition of the structured CC particles to the amorphous Ashgrove CKD demonstrated that better bonding is likely to occur at lower porosities. This was shown previously by Beaudoin and Feldman (1975).

Table 7.3-4: Zero porosity strength values for Ashgrove CKD mixes.

Mix	Zero Porosity Strength (MPa)
OPC 2008 St-L	86
0.7 OPC, 0.3 Ashgrove	67
0.7 OPC, 0.3 Ashgrove, 0.1 CC	130
0.7 OPC, 0.3 Ashgrove, 0.2 CC	2312

As for mixes containing Ashgrove CKD and MK lines 1, 2, 3, and 6 seem to be converging (see Fig. 7.3-4) as porosity values decrease. At a particular porosity, for example 0.2, their projected strengths would all be within close proximity of one another. Four of the highest overall compressive strength values of the Ashgrove CKD and Ashgrove CKD with MK mixes were obtained with those mixes. Both of these facts point to the idea that these mixes, on a microscopic scale may have behaved in a similar manner. Their zero porosity strength values are as follows: 86 MPa, 105 MPa, 89 MPa, 192 MPa, respectively, as can be seen in Table 7.3-5. These values, being relative close proximity of one another, further suggest that their microstructures may be similar.

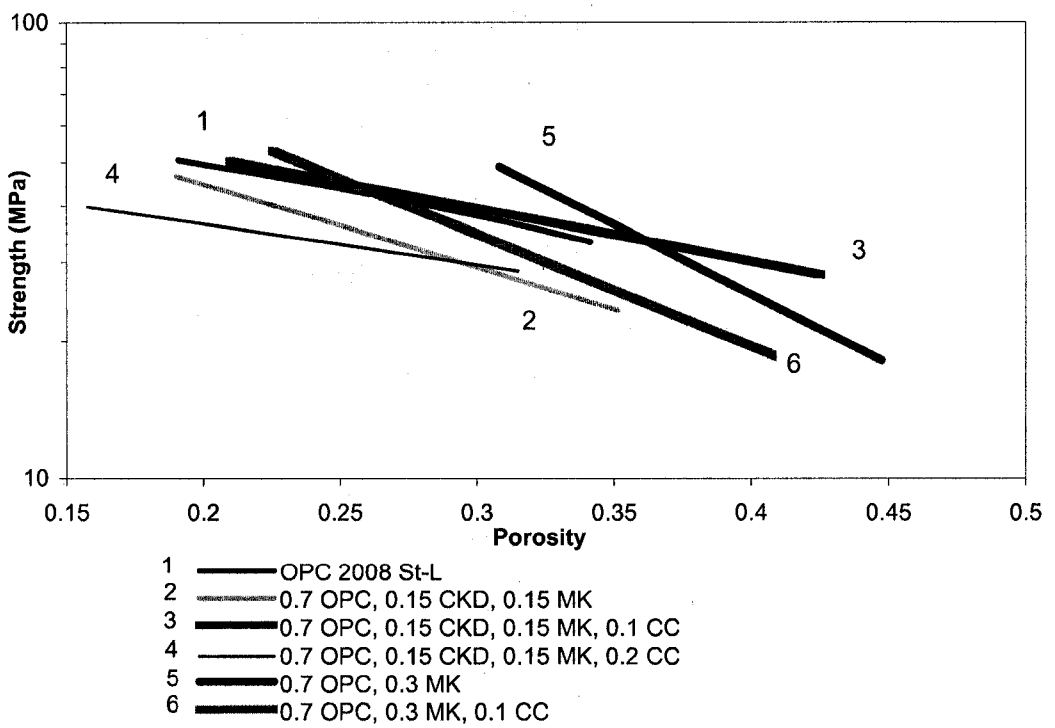

Fig 7.3-4: Compressive Strength vs. Porosity for Ashgrove CKD with MK mixes.

Table 7.3-5: Zero porosity strength values for Ashgrove CKD with MK mixes.

Mix	Zero Porosity Strength (MPa)
OPC 2008 St-L	86
0.7 OPC, 0.3 Ashgrove	67
0.7 OPC, 0.3 Ashgrove, 0.1 CC	130
0.7 OPC, 0.3 Ashgrove, 0.2 CC	2312
0.7 OPC, 0.15 Ashgrove, 0.15 MK	105
0.7 OPC, 0.15 Ashgrove, 0.15 MK, 0.1 CC	89
0.7 OPC, 0.15 Ashgrove, 0.15 MK, 0.2 CC	55
0.7 OPC, 0.3 MK	440
0.7 OPC, 0.3 MK, 0.1 CC	192

7.4 Summary of Strength and Porosity Results

The replacement of OPC with Ashgrove CKD resulted in the highest compressive strength values as compared to those obtained when Alpena and Bath CKDs replaced the OPC. This could be due its high alkali content and the fact that Ashgrove CKD is highly amorphous. It is possible that these two factors led to it being a more reactive CKD. The addition of CC alone to the CKD mixes improved the 28-day compressive strength of the Alpena mix. Further improvement was realized with increasing amounts of added CC. This result was expected for mixes with Bath and Ashgrove CKDs; however it was not the case. The high chloride content of the Bath CKD may have been far too detrimental for the CC to compensate in its strength development. As for the OPC+Ashgrove CKD mixes, the strength was generally on par with the OPC throughout the hydration period. The added CC resulted in lower compressive strengths. They, however, followed the values of the mix without added CC very closely throughout the hydration process.

The substitution of Ashgrove CKD with MK showed a great improvement in compressive strengths over the Ashgrove CKD alone. The results showed that the combination of MK and CC was more advantageous than with CC alone, when it came to strength development of OPC and OPC with Ashgrove CKD mixes.

The strength versus porosity curves showed that mixes containing Alpena and Bath CKDs generally followed a trend of converging toward similar compressive strength values as porosities decreased. This was further demonstrated by calculating zero porosity strength values. The Ashgrove CKD mixes showed that CKD and CC addition lowered strength values at a given porosity. However, zero porosity strength values showed that the intrinsic strengths of the OPC+Ashgrove CKD+CC might be higher than without added CC. It was suggested that the addition of the structured CC particles to the amorphous, poorly crystalline, Ashgrove CKD provides better bonding at lower porosities. This principle was suggested in another study (Beaudoin and Feldman, 1975). Curves for strength versus porosity for the added MK and CC to mixes with Ashgrove CKD revealed relatively higher strengths at lower porosities.

Chapter 8

Results and Discussion: AC Impedance Measurements (with corresponding Porosity and Mercury Intrusion Porosimetry Measurements)

8.1 Introduction

This chapter discusses the results from the following experiments: AC impedance measurements, with corresponding porosity and mercury intrusion porosimetry measurements. First the collected data for the porosity measurements will be shown and then the results from the AC impedance testing will be discussed along with the porosity and mercury porosimetry measurements. The porosity measurements that correspond with the AC impedance testing were measured at 5, 8, 16, and 24 hours. These measurements can be seen in Table 8.1-1 of the Appendix. Trendlines using Excel software were used to fit the data to an appropriate mathematical equation that could be used to appropriately describe the results. This equation was then used to produce a set of data that allowed the porosity values at all other times (i.e. porosity values that occurred at times between those that were physically measured in the lab) to be approximated and used in plots with the AC impedance data. The fit equation, regression values, R^2, and fit data can be seen in Tables 8.1-2 a) to f) of the Appendix while plots of the data are presented in section 8.2.

For the AC impedance results, presented in section 8.3, an idealized set of the output data from the actual testing will be displayed and discussed. The equivalent circuit from Fig. 4.3-7 was used to estimate values for 'n', R_1, and R_2, based on the reasoning provided in section 4.3.6. It was observed that the equivalent circuit fit appropriately fit the raw data. Plots involving the parameters 'n', R_1, and R_2 will be discussed in the sections thereafter. Tables 8.3-1 a) to r) show all the compiled data for values of 'n', R_1, and R_2, and the error values as calculated by the software, can be

seen in the Appendix. Data for the mean pore size diameters, r_o, for the six samples that were tested using mercury intrusion porosimetry are presented in section 8.6.1. This data is used for correlation plots in conjunction with R_2 and porosity values.

8.2 Porosity values at 5, 8, 16 and 24 hours

The results from the porosity measurements performed at 5, 8, 16, and 24 hours are presented in Fig. 8.2-1, Fig 8.2-2, Fig. 8.2-3, and Fig. 8.2-4 for Alpena, Bath, and Ashgrove CKDs, and Ashgrove CKD with MK mixes, respectively. The main purpose of plotting porosity versus time is to ensure that porosity decreases with time: which, as can be seen in all figures, was generally the case. An appropriate trendline was used in fitting the curve so that it can be used in conjunction with the AC impedance data. The trendline fit equation, the regression value, R^2, along with the fit data can be seen in Table 8.2-1 of the Appendix.

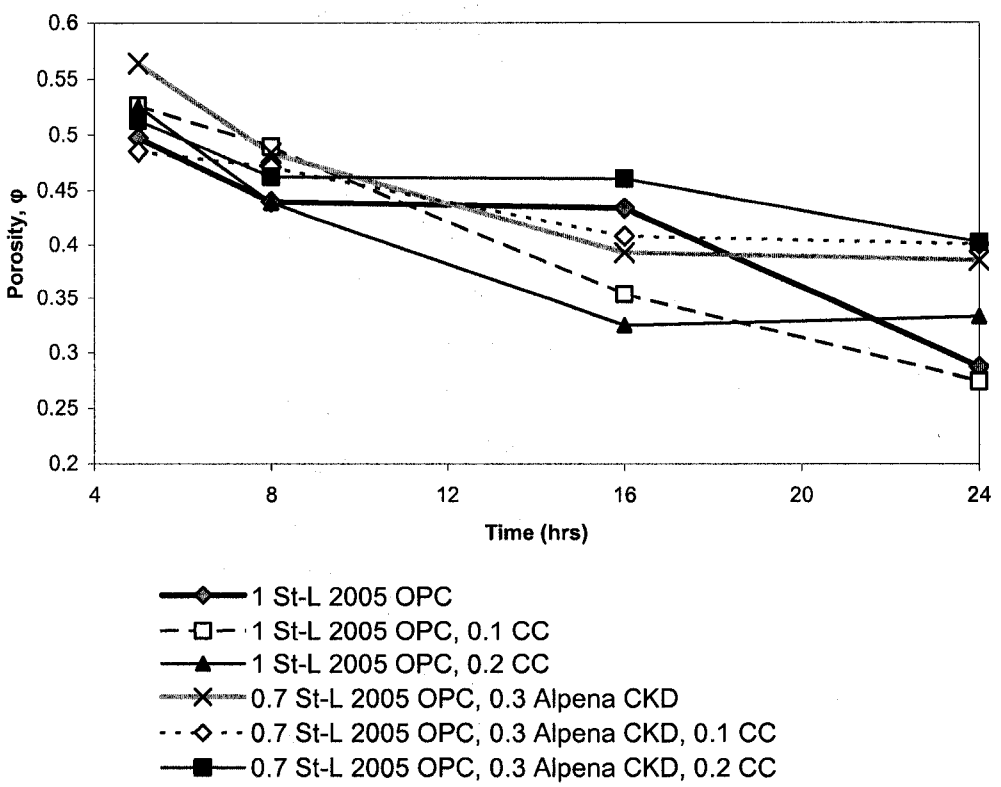

Fig. 8.2-1: Porosity vs. time for the control and Alpena CKD mixes.

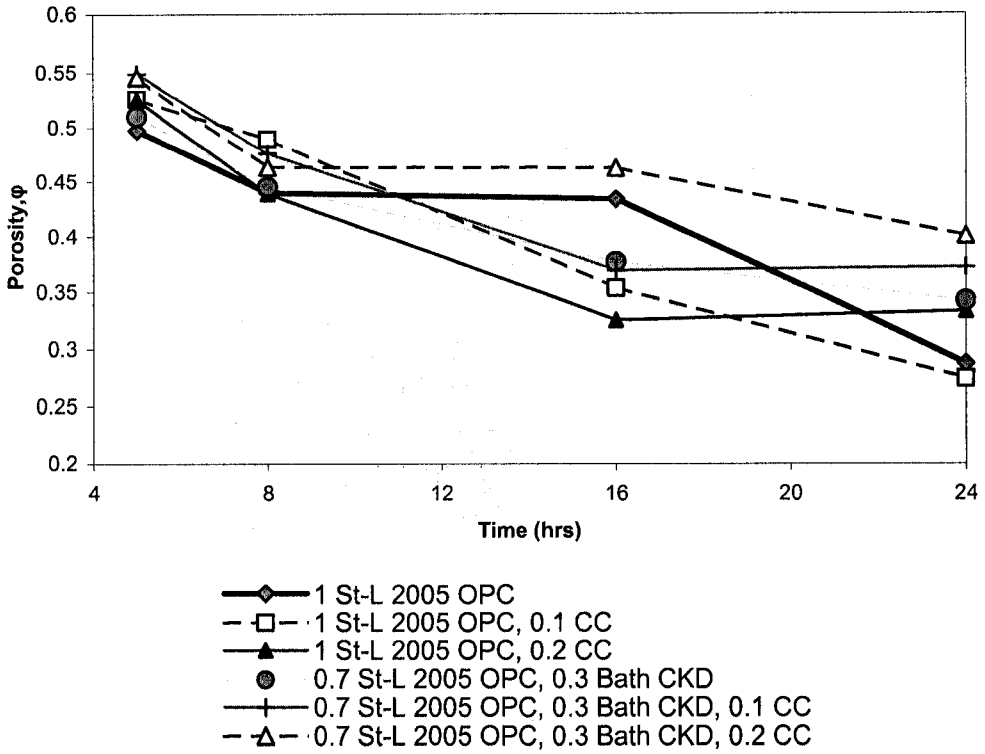

Fig. 8.2-2: Porosity vs. time for the control and Bath CKD mixes.

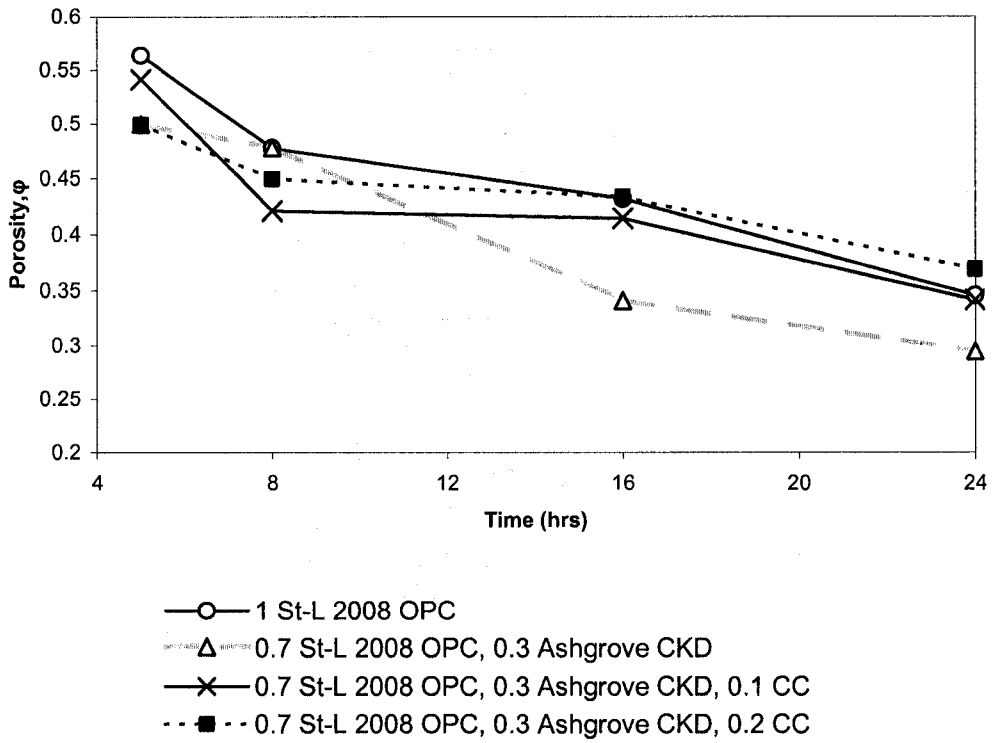

Fig. 8.2-3: Porosity vs. time for the Ashgrove CKD mixes.

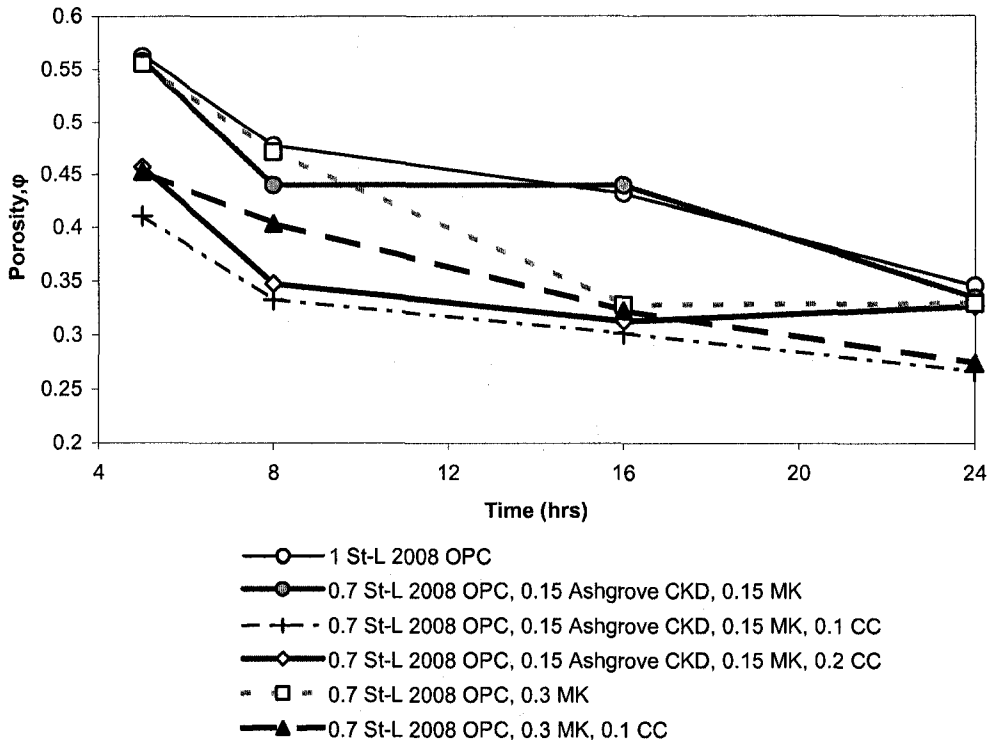

Fig. 8.2-4: Porosity vs. time for the Ashgrove CKD with MK mixes.

8.3 AC Impedance Output Data

Measurements were taken for each cement sample: once at time zero, immediately after the sample was mixed, and then once every hour for the next 24 hours. This meant that 25 AC impedance curves were produced for every mix (there were a total of 18 mixes, meaning 450 curves were produced).

The original results from the AC impedance measurements of each mix displayed a set of arcs of which the high frequency arcs (HFAs) grew with time. For simplicity, a representational set of output curves are presented in Fig. 8.3-1. In this figure the curve t_i represents data at an arbitrary time during the hydration process. Each curve thereafter occurred an hour after the one preceding it. The place the arc first cut the Z' axis, (R_1), the width of the arc (R_2), and the angle with which the arc was depressed below the Z' axis all varied from mix to mix.

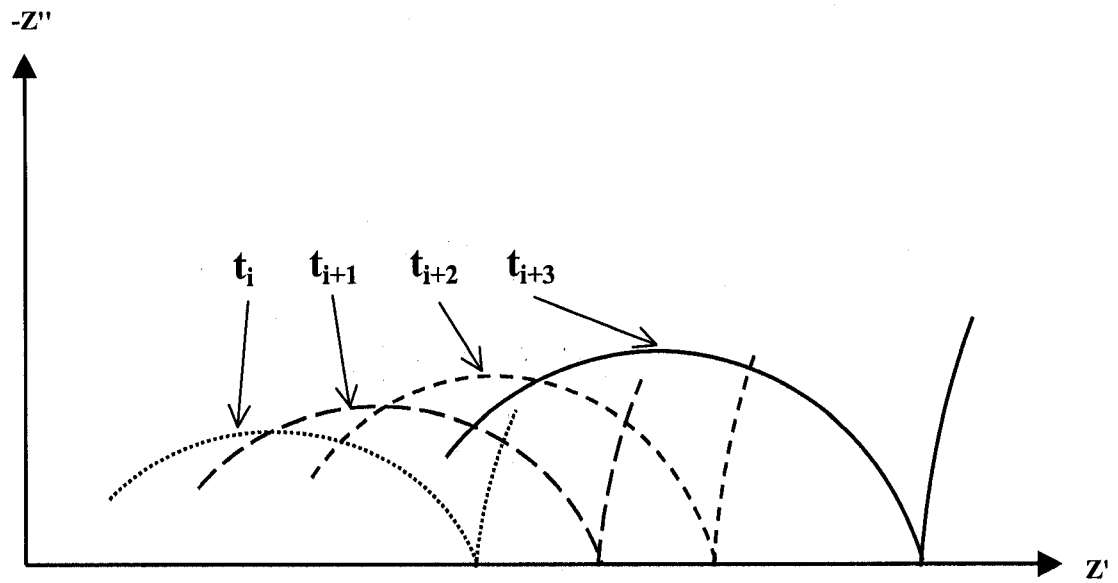

Fig 8.3-1: A set of representational AC impedance output data curves.

To re-iterate, the size of the HFA grew overtime. This result is in agreement with research conducted by McCarter and Brousseau (1990) who found that the HFA of an OPC paste grew as the sample hydrated. The time at which the first arc appeared varied from mix to mix. This is in agreement with past research (Xu et al., 1993). For this reason, the output AC impedance data was carefully examined for each mix to determine the time where the arc was first visible. Then the equivalent circuit and ZView software were used to fit the data in order to estimate values for R_1, R_2, and 'n'. Data for the fitted values of R_1, R_2, 'n', can be seen in Table 8.3-1 a) to r) of the Appendix. It should be noted that the values for C_d, which represents the capacitance due to the solid-liquid interface, although were estimated in conjunction with parameters R_1, R_2, and 'n', were not used or analyzed for this research.

8.4 The Depression Angle Parameter

As was mentioned in Chapter 4, section 4.3.7, research conducted by Gu et al. (1993) is instructive on how to interpret the depression angle parameter versus porosity curves. They reported that a broad pore size distribution results in a wide spread of relaxation times (the length of time for the dipoles of ions inside the pores of the

sample to orientate in order to follow the A.C. signal) which corresponds to a large depression angle, and therefore a small depression angle parameter, 'n'. It follows that a narrow pore size distribution would result in a reduced spread of relaxation times. This would in turn result in a small depression angle, or a large value of the depression angle parameter 'n'. A plot of the results for the depression angle parameter versus porosity can be see in Fig. 8.4-1.

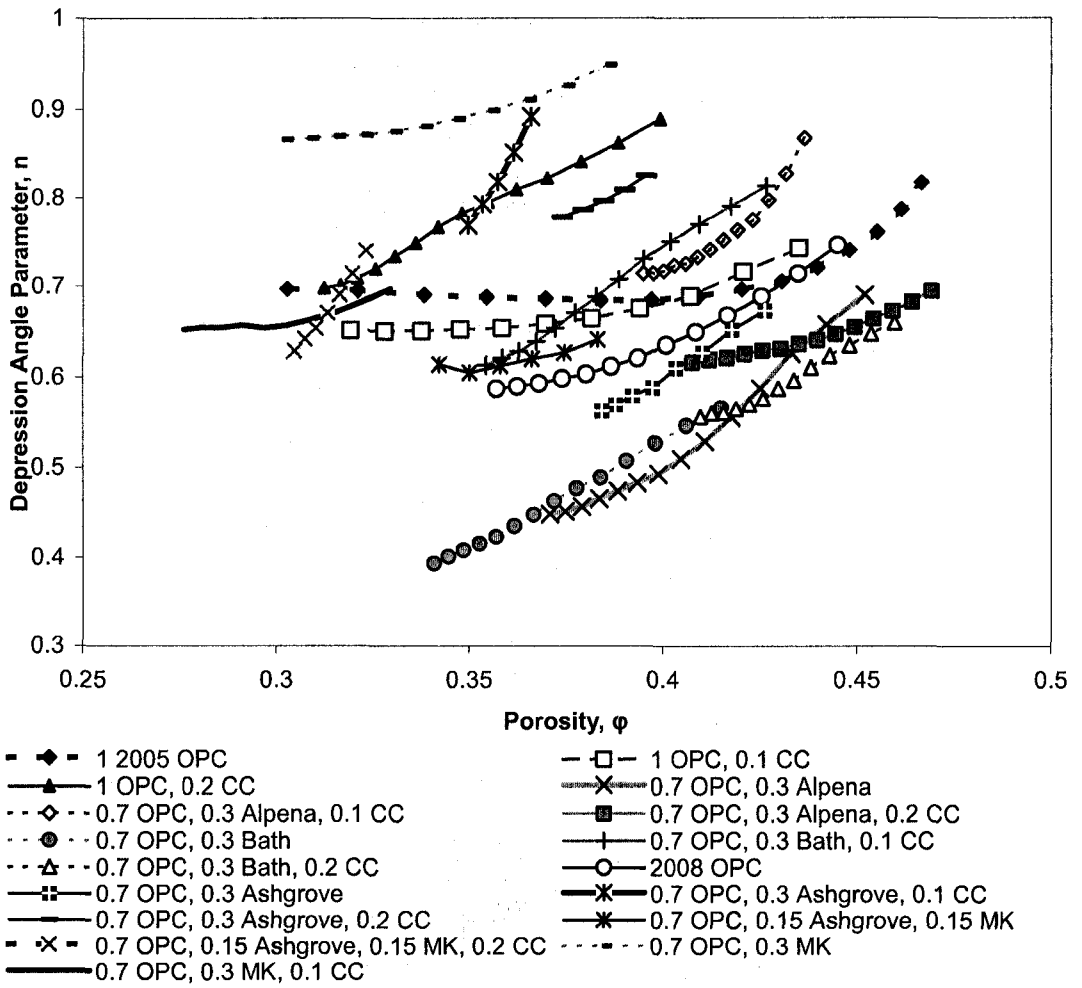

Fig. 8.4-1: The depression angle parameter vs. porosity for the various cement systems investigated.

The values of 'n' increased as porosity increases, as can be see in Fig. 8.4-1. From this it can be concluded that the depression angle decreases as porosity increases. This

suggests that the pore size distribution narrows as the population of large pores increases (with the increase in porosity). Generally, the occurrence of a narrow pore size distribution can occur in different size ranges for different paste systems and hydration times. Therefore, the interpretation of the data relies on previously documented pore structure investigations.

8.4.1 2005 OPC vs. 2008 OPC

The 'n' values for 2005 OPC and 2008 OPC are relatively close, with those of the 2005 OPC being only slightly higher, as can be seen in Fig. 8.4-1. This indicated that they behaved in a similar manner and is in agreement with the conclusion from the oxide analysis (discussed in Chapter 3) that there is no discernable difference in the cement compositions. This meant that relative comparisons between the samples, whether made with 2005 or 2008 OPC were possible.

8.4.2 Substitution of OPC with CKD

In general, the OPC mixes containing CKD (without other additives) had lower values of 'n' than the other mixes. This is observed by locating the following samples in Fig. 8.4-1: 0.7 OPC+0.3 Alpena, 0.7 OPC+0.3 Bath, and 0.7 OPC + 0.3 Ashgrove. This indicated that these mixes had a broader pore size distribution. The order of this trend for the mixes with OPC and CKD is the following: Ashgrove>Bath>Alpena.

8.4.3 Addition of CC to OPC or OPC with CKD

Adding CC to the mixes increased the value of 'n' (therefore decreased the value of the depression angle) when added to mixes containing simply OPC or mixes made up of OPC and CKD. Adding 0.2 CC to a mix containing simply OPC (see the position of curves for samples 2005 OPC and OPC+ 0.2 CC in Fig. 8.1-1) resulted in an increase in the value of 'n'. It was more effective in increasing the value of 'n' than the 0.1 CC addition (see curve for sample 1 OPC + 0.1 CC).

Additions of both 0.1 and 0.2 CC to the mixes of OPC and CKD increased the value of 'n' (and therefore decreased the value of the depression angle). Here it was the 0.1 CC addition that was more effective in increasing the value of 'n'. This can be seen in the figure by comparing the curves for the following mixes: 0.7 OPC+0.3 Ashgrove and 0.7 OPC+0.3 Ashgrove CKD+0.1 CC (and +0.2 CC). The same is true for CKDs Bath and Alpena. The general trend for mixes containing OPC and CKD (in decreasing order) for the increase of 'n' with regard to adding CC, was first mixes that contained Ashgrove CKD, then those containing Bath CKD, followed by those containing Alpena CKD. The corresponding decrease in the depression angle indicates that CC promotes a finer pore structure. This behavior of CC has been documented in published results (Ramachandran and Chun-mei, 1986).

8.4.4 Addition of MK to OPC or OPC and CKD

It is apparent that for a given porosity, adding MK increased the value of 'n' (and therefore decreased the depression angle). An example of this can be seen for a porosity value of φ= 0.37, 'n' for 0.7 OPC+ 0.3 Ashgrove was equal to 0.56 while replacing half of the Ashgrove CKD with MK (see sample 0.7 OPC+0.15 Ashgrove+0.15 MK) resulted in a value for 'n' of 0.64. For a given porosity, a 30% substitution of OPC with MK (see samples 1 2008 OPC and 0.7 OPC+0.3 MK) significantly increased the 'n' therefore significantly reduced the depression angle. The reason is likely the result of the mixes containing both a narrower and finer pore size distribution as past research has suggested (Guneysisi et al., 2008, Khatib and Wild, 1996, and Poon et al., 2001).

8.4.5 Addition of CC to OPC and MK

Adding CC to a mix containing OPC and MK resulted in a decreased value of 'n' and therefore a broadening of the pore size distribution. This is the opposite effect that adding CC had on the results for mixes that contained simply OPC or OPC and CKD.

This showed that the addition of the CC to the OPC+MK mix did not aid in further refining its pore structure.

8.4.6 Summary of the Depression Angle Parameter Results

The substitution of OPC with CKD resulted in decreased 'n' values which corresponded to a broadened pore size distribution. The addition of CC or MK was effective in refining the pore structure of the mixes containing OPC and CKD. The addition of both CC and MK together to an OPC and CKD mix did not show further refinement of the pore structure as compared to when they were present separately.

8.5 The High Frequency Arc Parameter R_1

Studying the results from HFA parameter R_1, aids in the general characterization of the mixes during early-age hydration. In Chapter 4, the parameter R_1 was set to equal NR_L (the resistance due to the pore solution, or liquids, of the cement paste). Xie et al. (1993) define R_L with the following equation:

$$R_L = \frac{\Delta x}{S_1}\frac{1}{\sigma_1} \tag{8.5-1}$$

where: Δx= the width of the N electrical elements (as was first described in Chapter 4, Fig. 4.3-3 a)), mm.

S_1= the area of the liquid phase, mm^2

σ_1= the electrical conductivity of the liquid phase, $\Omega^{-1}m^{-1}$

Xie et al. (1993) define S_1 with Eq. (8.5-2):

$$S_1 = (1-\psi_s)S \tag{8.5-2}$$

where: ψ_s=the area fraction of the solid phase

S= the area of the solid element normal to the electric field, mm^2

From this Eq. 8.5-1 can be re-written to:

$$R_L = \frac{\Delta x}{(1-\psi_S)S}\frac{1}{\sigma_1} \tag{8.5-3}$$

The value for $(1-\psi_s)$ would be equal to the fraction of the liquid phase or its fraction of pores, i.e. its porosity. This means that $1/R_L$ would be directly related to the sample's porosity. And recalling that R_1 was directly related to R_L (from Chapter 4 where R_1 was set to equal NR_L) it follows that $1/R_1$ is directly related to the sample's porosity. Following the same logic, $1/R_1$ is also directly related to the conductivity of the pore solution, σ_1. The pore solution conductivity is dependent on the concentrations of charge carriers in solution. Hydrated ions contribute significantly to the magnitude of the conductivity. It is reasonable to assume that the conductivity of the pore solution is fairly constant during the first ten hours of hydration and that any increase or decrease of conductivity thereafter is not excessive (Taylor, 1997).

The equivalent circuit for the AC impedance output data were used to estimate values for R_1. Then, $1/R_1$ values were plotted versus porosity. These results can be seen in Fig. 8.5-1. The values for $1/R_1$ increase with porosity, as can be seen in Fig. 8.5-1, for all the cement systems and is fairly linear for porosity values greater than around 0.35. This is consistent with what was previously mentioned, i.e. when the conductivity of the pore solution is constant, $1/R_1$ is directly related to porosity. It also follows the assumption that the conductivity of the pore solution is constant for the first ten hours. This also agrees with Eq. 8.5-3 (recalling that R_1 and R_L are also directly proportional). It is important to note that porosity within a cement sample decreases with hydration time and is thus inversely proportional to time.

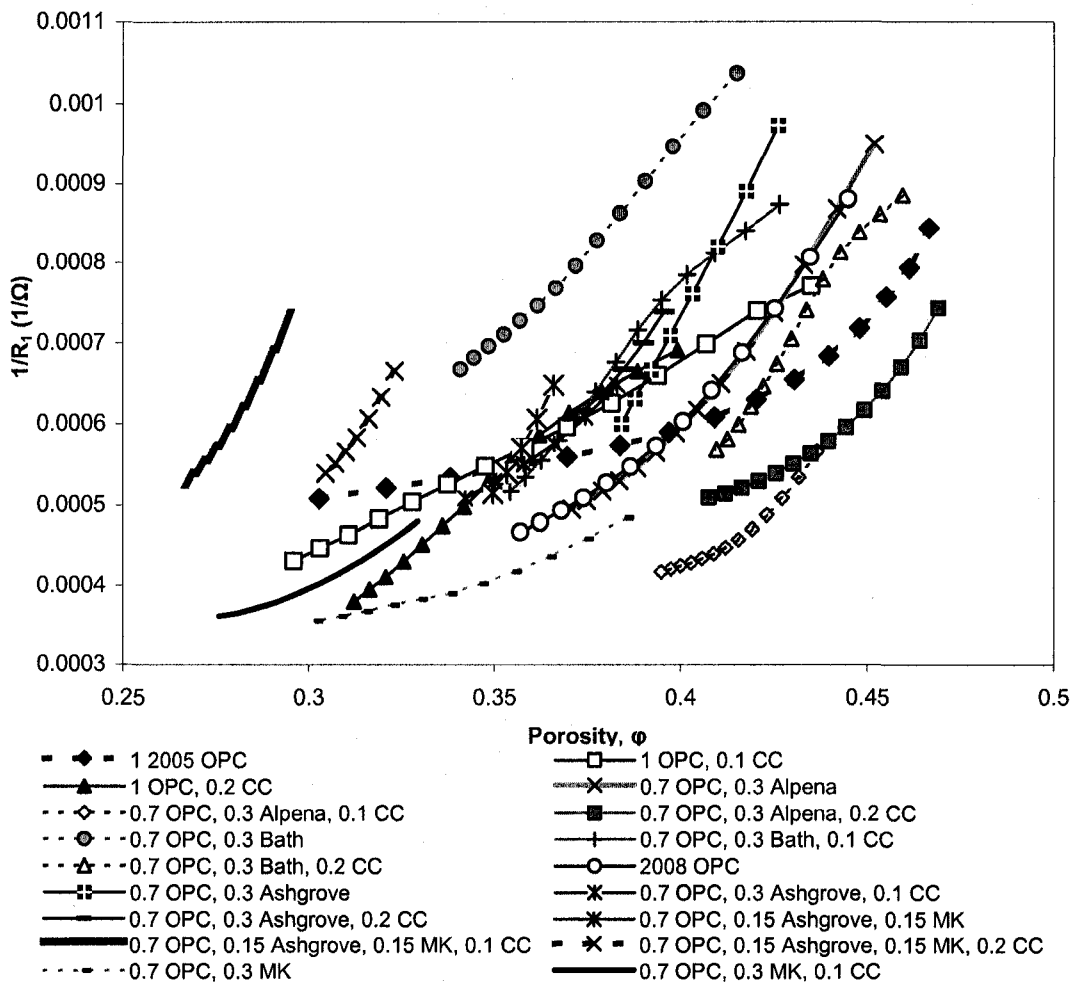

Fig. 8.5-1: $1/R_1$ vs. porosity for the various cement systems investigated.

8.5.1 The Effect of the Addition of CC to OPC

The addition of 0.1 CC increased the $1/R_1$ values and hence the pore solution conductivity of the OPC control sample (see curves for samples 1 2005 OPC and 1 2005 OPC+ 0.1 CC). These results are intermediate to those obtained for the OPC+ Ashgrove CKD+MK and the OPC+MK systems.

8.5.2 The Effect of CKD and CC Addition to OPC

In general, the substitution of OPC with CKD increased its pore solution conductivity. For the mixes containing Alpena CKD or Bath CKD, additions of CC decreased the conductivity of the pore solution. Conductivities for Ashgrove CKD mixes containing added CC increased its conductivity slightly.

8.5.3 The Effect of the Addition of MK to OPC and OCP+CKD Mixes

A 30% substitution of MK in OPC (see mixes 2008 OPC and 0.7 OPC+0.3 MK) resulted in a very low conductivity at porosity values less than 0.35. In this region of porosity values, the curves are generally non-linear. An increased concentration of hydroxide (OH^-) molecules in the pore solution could be responsible for the non-linear result (Taylor, 1997). The addition of CC to the OPC+MK mix (see sample 0.7 OPC+0.3 MK+0.1CC), resulted in slightly higher values of conductivity. Replacing half of the MK with Ashgrove CKD (see 0.7 OPC+0.15 Ashgrove+0.15 MK) resulted in another increase in the conductivity of the mix. The addition of CC to this mix significantly increased its conductivity (see mixes 0.7 OPC+0.15 Ashgrove CKD+0.15 MK+0.1CC and +0.2 CC).

8.5.4 Summary of the Results for the High Frequency Arc Parameter R_1

The pore solution conductivity increased when: 1) OPC was substituted with CKD, 2) MK replaced part of the CKD in the OPC-CKD mix, 3) CC was added to the OPC-CKD-MK mix, and 4) CC was added to the OPC-MK mix. The pore solution conductivity decreased when: 1) MK was substituted for OPC in the OPC mix, and 2) when CC was added to the OPC-CKD mix.

8.6 The High Frequency Arc Diameter R_2

R_2 was first described in Chapter 4 as being the resistance due to the solid-liquid interface within the cement system. As was mentioned in section 4.3.7, graphically R_2 is measured between the points where the depressed high frequency arc first cuts the Z' axis (at R_1) and where it cuts the axis on the right hand side of the arc (as was seen in Fig. 4.3-5). R_2 values were estimated by using the equivalent circuit to fit the output AC impedance data. The HFA for each measurement grew as the sample continued to hydrate, as was seen in section 8.3. This in turn meant that the values for R_2 also grew over time as the sample hydrated. This is in agreement with conclusions Xie et al. (1993) had drawn in past research. Generally, R_2 increases as both the porosity decreases and the hydration progresses (Xu et al., 1993). It is for this reason that R_2 is a good indicator of the progress of the hydration process. Values for R_2 were plotted versus 1/P and can be seen in Fig. 8.6-1. R_2 values increased, as can be seen in this figure, with increasing values of 1/P; this is in agreement with past research that has shown a linear dependence of R_2 and 1/P when the pore solution conductivity is constant (Xu et al., 1993). The assumption that the pore solution conductivity was constant will be further verified and discussed in section 8.7. In order to compare the curves, it was assumed that for greater 1/P values, for which data was not collected, the projected path of the curve would continue the trend as indicated by the data that was collected. It remains to be seen in the results whether R_2 is a good indicator of comparative overall strength development.

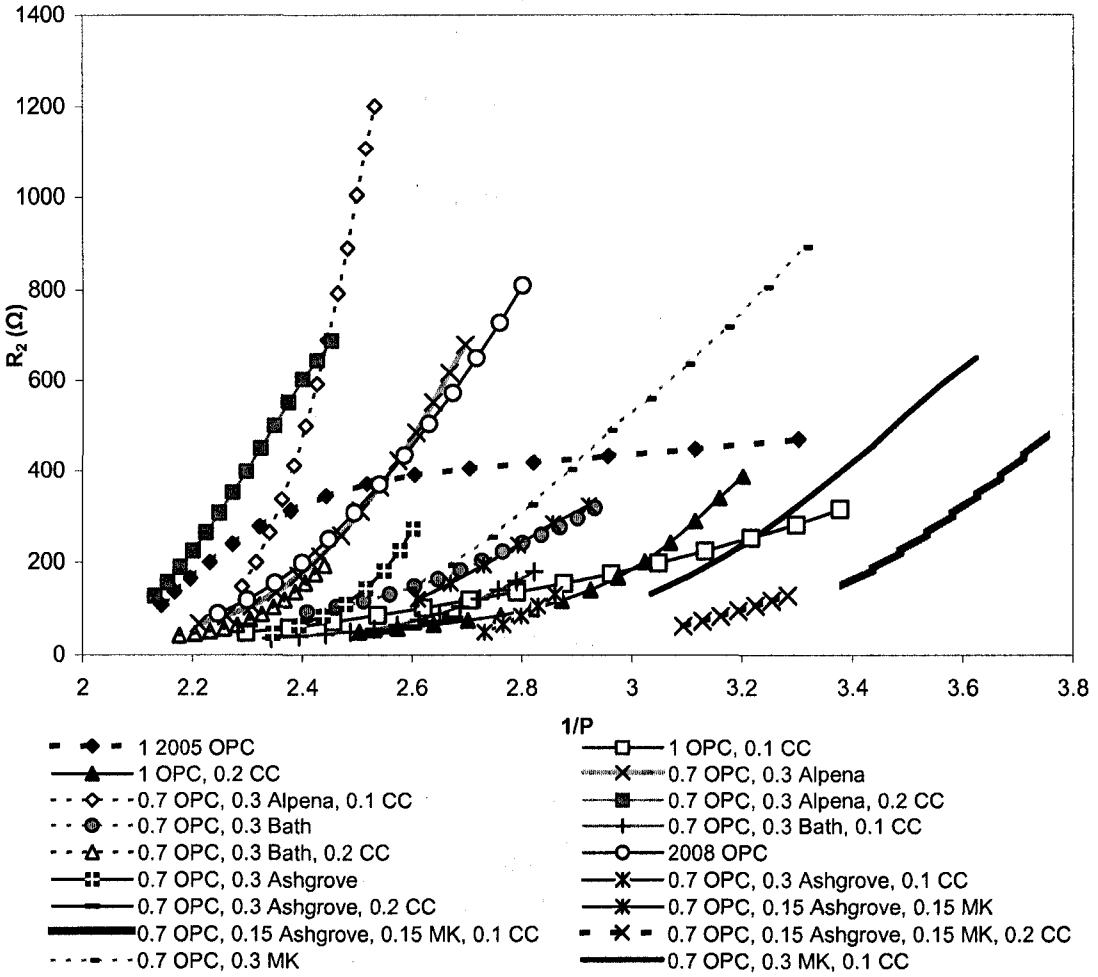

Fig. 8.6-1: R_2 vs. 1/P for the various cement samples investigated.

8.6.1. The Effects of the Substitution of OPC with CKD

The substitution of OPC with Alpena and Bath CKDs produced higher values of R_2; this indicated that a finer pore structure may be formed. The substitution of OPC with Ashgrove CKD decreased the values of R_2.

8.6.2 The Effects of the Addition of CC to OPC-CKD mixes

For the Alpena CKD, the addition of CC to the mix had a significant effect in increasing R_2 in the early stages of hydration. From highest to lowest R_2 values the order is as follows: 0.7 OPC+0.3 Alpena +0.1 CC > 1 2005 OPC > 0.7 OPC+ 0.3

Alpena CKD. The increasing value of R_2 can be interpreted to mean that hydration is occurring earlier when CC is added. This is in agreement with the calorimetry and 28-day compressive strength results that have been presented. It also suggests that a finer pore structure may be formed with the addition of CC. This has been mentioned previously (Ramachandran and Chun-mei 1986, Sato and Beaudoin, 2006, 2007). For CC addition to Bath CKD, the 0.2 CC addition proved to be more effective in increasing the R_2 value than the 0.1 CC addition. These observations are also in agreement with the calorimetry results for the Bath mixes. The reverse effect was observed for Ashgrove CKD. The addition of CC reduced values of R_2, which is not in agreement with the calorimetry results which showed that the addition of CC to OPC+Ashgrove CKD accelerated hydration. It is suggested that pore structure differences may account for these observations.

8.6.3 The Effects of the Addition of CC to OPC-MK and OPC-CKD-MK mixes

The substitution of MK in the OPC mix decreased the R_2 values. The addition of CC to mixes containing MK appears to have a retarding effect at higher values of 1/P. This means that lower values of R_2 were observed when CC was added to mixes containing MK, than when the CC was not present in the mix. The trend for R_2 values is as follows: 2008 OPC> OPC+MK > OPC+ MK+ 0.1 CC > OPC+ Ashgrove+ MK+ 0.1 CC > OPC+ Ashgrove +MK+ 0.2CC. This meant that the addition of CC to the OPC-MK and OPC-CKD-MK mixes did not aid in increasing R_2 values.

8.6.4 Summary Observations of R_2 vs. 1/P Data

It was generally observed that R_2 increased as 1/P increased, and therefore as porosity decreased (indicating the extent of hydration). The calorimetry results showed an accelerated hydration for mixes containing MK, which improved further upon the addition of CC to the mix. Therefore it was thought that R_2 values might increase with the addition of MK and increase further with the addition of CC. However, the

results of R_2, showed that the addition of the MK did not meet these expectations i.e. that it might (on its own and in combination with CC) increase the R_2 values the mixes. Also, because Ashgrove CKD mixes had higher compressive strength throughout the compression testing (i.e. from 1 to 28 days) it was thought that these samples would have higher R_2 values than the mixes with the other CKDs. This was not observed. From this it could be suggested that the R_2 value as a function of porosity alone, is not, necessarily on a comparative basis, a direct indicator of early relative strength. It follows that the intrinsic strength of a sample's matrix (i.e. the zero porosity solid phase) is also a factor to be considered. It would appear that R_2 can only aid as an indicator of strength development within the same cement mix as its porosity and pore size decrease with time.

8.7 Introduction to R_2 versus $1/(P \cdot r_o)$

Research has shown that for samples of hydrated OPC there is a linear dependence of R_2 with $1/(P \cdot r_o)$ assuming a constant pore solution conductivity at a given water/cement ratio (where $P \cdot r_o$ is the product of the porosity and the mean pore size, r_o) (Xu et al., 1993). This linear dependence existed based on the fact that the pore solution remained relatively constant (which was an assumption used in order to relate R_2 to $1/P$ in section 8.6). In order to further research the behavior of the mixes and to verify that the assumption that the pore solution conductivity was relatively constant, data to produce an R_2 vs. $1/(P \cdot r_o)$ plot was obtained.

8.7.1 Data for the Parameters R_2, P, and r_o at 8 Hours Hydration

8.7.1.1 Obtaining r_o

Six samples were tested using mercury intrusion porosimetry. The six samples were chosen based on the fact that their positions in Fig. 8.6-1 were distributed throughout the plot. The following mixes at 8 hours hydration were chosen:

1) 1 2008 OPC
2) 0.7 OPC, 0.3 Bath CKD
3) 0.7 OPC, 0.3 Alpena CKD, 0.2 CC
4) 0.7 OPC, 0.15 Ashgrove CKD, 0.15 MK, 0.1CC
5) 0.7 OPC, 0.3 MK, 0.1 CC
6) 0.7 OPC, 0.3 Alpena CKD, 0.1 CC

Their pore size distributions were produced from these experiments. Plots for the pore size distributions for the six samples can be seen in the Fig. 8.7.1.1-1 of the Appendix. The mean pore size, r_o, for each mix was calculated using Eq. 8.7-1 (which was first introduced in section 4.4). Data for the mean pore sizes can be seen in Table 8.7-1.

$$r_o = \frac{\sum p_i r_i}{\sum p_i} \tag{8.7-1}$$

where: p_i= intrusion volume (%) for a given pressure, i

r_i= pore diameter, μm, for a given pressure, i

8.7.1.2 Obtaining P

It should be noted that for this section of the results, the value of porosity used in the relationship $1/(P \cdot r_o)$ was the porosity value obtained from the mercury porosimetry testing. It was thought to be the most accurate porosity measurement to use in conjunction with r_o. Values for the porosity can be seen in Table 8.7-1.

8.7.1.3 Obtaining R_2

Originally, R_2 values had been estimated by fitting the AC impedance data to the equivalent circuit (which occurred in section 8.3). In order to obtain values for R_2 for 8 hours hydration time the following procedure was used. Trendlines using Excel software were used to fit the output AC impedance data of R_2 values versus time to

mathematical equations from which R_2 values for each mix at 8 hours could be estimated. Values for R_2 at 8 hours hydration can be seen in Table 8.7-1. The trendline equations with respective regression values, R^2, can be seen in Table 8.7-2 in the Appendix.

8.7.2 Results for R_2 versus $1/(P \cdot r_o)$

Data collected for the various parameters can be seen in Table 8.7-1. Fig. 8.7-1 shows a plot of R_2 vs. $1/(P \cdot r_o)$.

Table 8.7-1: Values for R_2, r_o, P, 1/P, $1/(P \cdot r_o)$

Sample	Fitted R_2 (Ω)	r_o (μm)	P	1/P	$1/Pr_o$
2008 St-L OPC	26.1	7.7E-02	5.8E-01	1.7	22.5
0.7 OPC, 0.3 Bath	54.3	3.0E-02	3.5E-01	2.8	93.6
0.7 OPC, 0.3 Alpena, 0.2 CC	65.9	1.8E-02	4.2E-01	2.4	135.6
0.7 OPC, 0.15 Ashgrove, 0.15 MK, 0.1CC	22.0	1.7E-02	4.6E-01	2.2	125.2
0.7 OPC, 0.3 MK, 0.1 CC	16.2	1.1E-02	3.6E-01	2.8	244.7
0.7 OPC, 0.3 Alpena, 0.1 CC	48.3	1.8E-02	4.9E-01	2.0	112.0

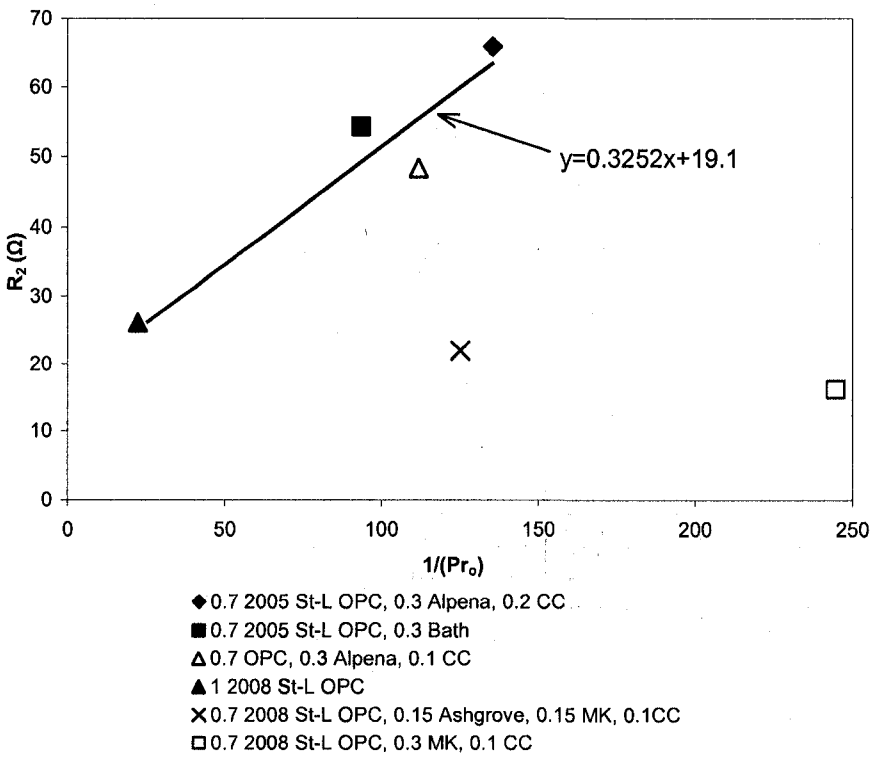

Fig. 8.7-1: R_2 vs. $1/(P \cdot r_o)$ for selected cement systems.

The data showed an indication of the linear dependence of R_2 and $1/(P \cdot r_o)$ (in agreement with results from Gu et al., 1993) for the following mixes: OPC+Alpena CKD +CC (0.1 and 0.2), OPC, and OPC+ Bath CKD. The equation for the linear trendline that was fit to this data is noted on the figure. More data would need to be collected in order to make firm conclusions from this relationship; however it would seem that the assumption of the pore solution conductivity being fairly constant during the first few hours of hydration is indeed valid. The two mixes containing MK (OPC+ Ashgrove CKD+ MK+CC and OPC+MK+CC) resulted in two data points that were displaced to lower values of R_2. These other two data points may be forming a separate line. The porosimetry data indicated that these systems contained a larger amount of pores that were greater than 1 μm. In addition, the OPC+Ashgrove CKD+MK+CC had greater than 10% porosity in this pore size region. Therefore, this second line may form for samples with this type of matrix (i.e. containing MK) and that contain larger pores.

Chapter 9

Concluding Remarks and Recommendations for Future Research

9.1 General Comments

The four main objectives of this study have been met. Re-call that the main objectives were as follows: 1) to determine the effects that the addition of nano-calcium carbonate (CC) and metakaolinite (MK) had on the OPC-CKD system with emphasis on early hydration (through calorimetry) and strength development (descriptors of the latter include the strength-porosity relationship, strength, and porosity measurements), 2) to use AC impedance methods coupled with porosity and mercury porosimetry measurements as a means of further investigating the early-age hydration behavior of the binary, ternary, quaternary systems containing CKD, 3) to assess the influence of CKD composition on the early hydration kinetics of the systems, and 4) to assess the compatibility of MK in cement systems containing CKD.

The findings of the study are summarized in five sub-sections. The contributions are discussed in terms of the aforementioned objectives. The first three sections are: 1) calorimetry measurements, 2) strength and porosity measurements, and 3) AC impedance measurements (with corresponding porosity and porosimetry measurements). The fourth and fifth sections are devoted to further summarizing and discussing the overall conclusions of the study and presenting recommendations for future research.

9.2 Conclusions Based on Calorimetry Measurements

The conclusions resulting from the calorimetry measurements are the following:

1. The replacement of OPC with CKD accelerated the hydration of the system when Bath CKD or Ashgrove CKD was present. The replacement of OPC

with Alpena CKD retarded the hydration of the OPC-CKD system. Re-call that Bath CKD was high in chloride and low in alkali; Ashgrove CKD was high in alkali; and Alpena CKD was high in both sulfate and alkali.

2. The addition of nano-calcium carbonate to each OPC-CKD system accelerated its hydration process, effectively halving the hydration time.
3. The addition of the CC to the OPC+CKD+MK system greatly accelerated the hydration of this system. A further improvement was seen with higher concentrations of added CC.
4. The combination of OPC+Ashgrove CKD+MK, had a longer hydration time than the OPC+CKD mix, but had an accelerating effect when compared with the hydration time of the control OPC mix.
5. It was apparent that the CC particles acted as nucleation sites that promoted the acceleration of hydration of the pastes (as evidenced by XRD measurements and SEM images). The XRD measurements also supported the view that MK particles could possibly be behaving as nucleation sites. The SEM imaging in this case was not conclusive.

9.3 Conclusions Based on Strength and Porosity Measurements

The conclusions resulting from the strength and porosity measurements along with the strength-porosity relationships are the following:

1. The replacement of OPC with each type of CKD, as expected, decreased the strength of the system throughout the hydration process.
2. The addition of the CC particles to the OPC+Alpena CKD system aided in improving its 28 day strength. The strength of Bath CKD and Ashgrove CKD mixes with added CC did not improve.
3. The substitution of Ashgrove CKD with MK substantially improved its strength resulting in a higher 28-day strength than the control OPC mix. The OPC+Ashgrove CKD+MK+ 0.1 CC also showed a higher 28 day strength than the control OPC mix. It was, however, not as significant as the system without the CC.

4. The strength versus porosity curves showed some indication that it is likely that a combination of ill-crystallized, amorphous materials, and structured, crystalline materials is necessary to achieve optimum strength values. This was in agreement with the research of Beaudoin and Feldman (1975). This was demonstrated using the zero porosity strength values calculated from the strength-porosity curve obtained by trendline fitting of the data.

9.4 Conclusions Based on AC Impedance Measurements

The conclusions from the AC impedance measurements (along with corresponding porosity and porosimetry measurements) are the following:

1. The depression angle parameter, 'n', analysis showed that the replacement of OPC with CKD resulted in a broad pore size distribution. The addition of CC or MK was shown to be effective in refining the pore structure (i.e. increasing the relative population of small pores) of the OPC-CKD system. The addition of both CC and MK together in an OPC+CKD system did not show further refinement of the pore structure as compared to when they were added separately. The fact that MK refined the pore structure of the OPC+CKD system is in line with the compression strength values which showed that MK addition to the OPC+CKD system greatly increased its strength. Linking these two results, suggests that the MK may indeed be filling the voids of the system, creating a denser structure, resulting in an increase in its strength values. This is also in agreement with XRD measurements which showed that the addition of MK to the OPC-CKD system possibly accelerated the hydration. Re-call that the XRD results showed an increase in the amount of $Ca(OH)_2$ when the MK particles were added to the mix. This suggested an acceleration of the hydration of this system.
2. The pore solution conductivity (shown in sections 8.6, and further verified in section 8.7, to be proportional to the high frequency arc parameter R_1, estimated from the AC impedance data) increased when: 1) OPC was replaced

with CKD, 2) when MK replaced part of the CKD in the OPC-CKD mix, 3) when CC was added to the OPC-CKD-MK mix, and 4) when CC was added to the OPC-MK mix. It decreased when CC was added to the OPC-CKD mix. The pore solution conductivity is dependent on the concentrations of charge carriers in solution. Hydrated ions contribute significantly to the magnitude of the conductivity. The R_1 values generally reflect the alkalinity of the CKD in the system. It is clear that the conductivity values alone are not satisfactory descriptors of system performance. Nevertheless, as an initial screening test for CKD selection, conductivity measurements may have merit.

3. The R_2 value for a particular system generally increases with hydration time. It is also dependent on pore structure parameters and to some extent variations in pore solution conductivities. It was therefore expected that the R_2 value, which is the resistance due to the solid-liquid interface of the system, would be a good indicator of relative hydration progression and strength development that could be compared amongst different cement systems. It was suggested that the intrinsic strength of a sample's matrix (meaning the zero porosity solid phase) was also a factor that must be considered when comparing systems. As was previously discussed in the strength-porosity results, zero porosity strength values (obtained by extrapolation) were helpful in further demonstrating this point. There may be other R_2-pore structure relationships dependent on intrinsic strength. It was established that the pore structure dependence of R_2 i.e. the relation between R_2 and the product of porosity and mean pore size was apparently valid for different OPC-CKD systems. This did not apply to the OPC-CKD or OPC systems containing MK and CC. It is clear that additional pore structure characterization measurements would be required to explain the effect of MK and CC. It may be related to the intrinsic properties of the solid and the nature of the interface (vis-a-vis the bonding environment) in these systems.

9.5 Summary

The following is a summary of the specific findings that have been presented:

1. Overall, the calorimetry measurements showed that both the CC additions to the OPC+CKD systems and Ashgrove CKD in combination with MK additions were effective in producing hydration times that were less (implying acceleration) than the OPC control mix.
2. The strength values of the OPC-CKD system decreased least when Ashgrove CKD was used. Re-call that the Ashgrove CKD, was highly amorphous and high in alkali. It is perhaps the best combination when it comes to replacement of OPC with CKD.
3. Although the CC was effective in accelerating the hydration process of the OPC+CKD, and OPC+CKD+MK systems, it was the OPC+CKD+MK system that was the most effective in improving strength values (higher than the control system). Also, the calculation of zero porosity strength values was useful in observing the intrinsic strengths of the solid material.
4. A linkage between the AC impedance depression angle parameter, 'n', and strength values is apparent. It is suggested that the MK addition to the OPC+CKD system refined its pore structure (increasing the population of small pores) leading to an increase in strength values. This is in agreement with previous research on other OPC pastes (Guneyisi et al., 2008 and Khatib and Wild, 1996).
5. SEM imaging and XRD measurements indicated that CC addition to the systems studied possibly acts as a source of nucleation sites. It was difficult to view MK particles acting as nucleation sites with SEM imaging. The qualitative XRD results, however, supported this possibility.

9.6 Recommended Future Research

The objectives of this study were generally met. Future research, however, is needed in order to more substantially validate and extend the results obtained. The recommended future research areas are as follows:

1. The addition of MK to the OPC+CKD system showed promise as an effective supplementary cementing material. The addition provided an accelerated hydration time compared to the OPC control mix, refined pore structure (greater population of small pores), and improved the strength of the system. In this system the addition was perhaps more effective than the addition of the CC. Further research would be useful in verifying the results that showed the effectiveness of partial replacement of the CKD, in the OPC+CKD system, with MK.
2. Highly amorphous CKDs high in alkali (such as the Ashgrove CKD) should be further investigated in longer-term studies in combination with CC and supplementary cementing materials (for example, MK) as this CKD showed the least amount of strength decrease when added to the OPC.
3. It would be worthwhile to further investigate CKDs high in sulfate and high in alkali (such as the Alpena CKD) which showed an increase in strength values when CC was added to the system. Perhaps investigating a system that replaces part of such a CKD in the OPC+CKD system with MK would also be of value.
4. It should be noted that CKDs high in chloride (such as the Bath CKD) do not seem to be beneficial in the OPC+CKD system nor in the OPC+CKD+CC system. The high chloride content in the CKD appears to be too detrimental to the structure of the system to be of particular use. Therefore further research is not recommended with such a CKD.

References

Al-Harthy, A.S., Taha, R., Al-Maamary, F. (2003), "Effect of cement kiln dust (CKD) on mortar and concrete mixtures," Construction and Building Materials, Vol 17 (5), pp. 353-360.

ASTM Standard C109, (2008), "Standard Test Method For Comperssive Strength of Hydraulic Cement Mortars (Using 2-in or 50-mm Cube Specimens)". ASTM International, West Conshohocken, PA, www.astm.org.

ASTM Standard C150, (2007), "Standard Specification for Portland Cement". ASTM International, West Conshohocken, PA, www.astm.org.

ASTM C305, (2006), "Standard Practice for Mechanical Mixing of Hydraulic Cement Pastes and Mortars of Plastic Consistency". ASTM International, West Conshohocken, PA, www.astm.org.

ASTM Standard C511, (2003), "Standard Specification for Mixing Rooms, Moist Cabinets, Moist Rooms, and Water Storage Tanks Used in the Testing of Hydraulic Cements and Concretes." ASTM International, West Conshohocken, PA, www.astm.org.

ASTM Standard D5050, (2008), "D5050: Standard Guide for Commercial Use of Lime Kiln Dusts and Portland Cement Kiln Dusts." ASTM International, West Conshohocken, PA, www.astm.org.

Beaudoin, J.J., (1979), "Porosity measurement of some hydrated cementitious systems by high pressure mercury intrusion- microstructural limitations", Cement and Concrete Research, Vol 9, pp. 771-781.

Beaudoin, J.J., and Feldman, R.F. (1975), "A study of mechanical properties of autoclaved calcium silicate systems," Cement and Concrete Research, Vol 5, pp. 103-118.

Bhatty, M.S.Y. (1984), "Use of cement-kiln dust in blended cements," World Cement, Vol 15 (4), pp.126-8 and 131-4.

Bhatty, M.S.Y. (1985), "Kiln Dust Cement Blends Evaluated," Rock Products, Vol 88 (10) pp. 47-65.

BS EN 197-1, "Cement composition, specifications, and conformity criteria for common cements," British Standard, (2000).

CSA A3000-08, "Cementitious materials compendium". Canadian Standards Association (2008).

De Silva, P.S., and Glasser, F.P. (1990), "Hydration of cements based on metakaolin: thermochemistry," Advance in Cement Research, Vol. 3 (12), pp.167-177.

Dyer, T.D., Halliday, J.E., Dhir, R.K. (1999), "An investigation of the hydration chemistry of ternary blends containing cement kiln dust," Material Science, Vol 34, 20, pp.109-110.

Feldman, R.F., and Beaudoin, J.J. (1976), "Microstructure and strength of hydrated cement," Cement and Concrete Research, Vol 6, pp. 389-400.

Gu, P., Xu, Z., Xie, P., Beaudoin, J.J., and Low, N.M.P. (1993), "Application of A.C. Impedance Techniques in Studies of Porous Cementitious Materials (II): Relationship Between ACIS Behaviour and the Porous Microstructure," Cement and Concrete Research, Vol 23, pp.853-862.

Note: Gu et al. (2) (1993) was used in referencing this document in the text.
Gu, P., Xie, P., Beaudoin, J.J., Brousseau, R. (1993), "A.C. Impedance Spectroscopy (II): Microstructural Characterization of Hydrating Cement-Silica Fume Systems," Cement and Concrete Research, Vol 23, pp. 157-168.

Gu, P., Xie, P., Beaudoin, J.J. (1994), "Investigation of the retarding effect of superplasticizers on cement hydration by impedance spectroscopy and other methods," Cement and Concrete Research, Vol. 24, pp. 433-442.

Guneyisi, E., Gesoglu, M., and Mermerdas, K. (2008), "Improving strength, drying shrinkage, and pore structure of concrete using metakaolin," Materials and Structures, Vol 41 (5), pp. 937-949.

Heikal, M, Aiad, I., Helmy, M.I., (2002), "Portland cement clinker, granulated slag and by-pass cement kiln dust composites", Cement and Concrete Research. Vol 32 (11), pp.1805-1812.

Hooton, R.D., Nokken, M., Thomas, M.D.A. (2007). "Portland-Limestone Cements: State-of-the-Art Report and Gap Analysis for CSA A 3000". Cement Association of Canada.

Ingram, K.D., and Daugherty, K.E. (1991), "A review of limestone additions of Portland cement and concrete," Cement and Concrete Composites, Vol 13, pp. 165-170.

Justice, J.M., Kurtis, K.E. (2007), "Influence of metakaolin surface area on properties if cement-based materials," ASCE Journal of Materials in Civil Engineering. Vol 19 (9), pp. 762-771.

Khatib, J.M., and Wild, S. (1996), "Pore Size Distribution of Metakaolin Paste," Cement and Concrete Research. Vol 26 (10) pp. 1545-53.

Konsta-Gdoutos, M.S., Shah, S.P. (2003), "Hydration and properties of novel blended cements based on cement kiln dust and blast furnace slag," Cement and Concrete Research Vol 33, (8), pp. 1269-76.

Kumar, R. and Bhattacharjee, B. (2003), "Porosity, pore size distribution and in situ strength of concrete," Cement and Concrete Research, Vol. 33, pp. 155-164.

Lagier, F., and Kurtis, K.E. (2007), "Influence of Portland cement composition on early age reactions with metakaolin," Cement and Concrete Research, Vol 37, pp. 1411-1417.

Malhotra, V.M. (1987), *Supplementary Cementing Materials for Concrete.* Canadian Government Publishing Centre.

McCarter, W.J., and Brousseau, R. (1990), "The A.C. response of hardened cement paste," Cement and Concrete Research, Vol 20, pp. 891-900.

Mehta, J.K. and Monteiro, P.J.M. (2006). *Concrete Microstructure, Properties, and Materials,* McGraw-Hill 3rd Ed.

Nagaraj, T.S., and Banu, Z. (1996), "Generalization of Abram's Law," Cement and Concrete Research, Vol 26 (6), pp. 993-942.

Odler, I., and Robler, M. (1985), "Investigations on the relationship between porosity, structure, and strength of hydrated Portland cement pastes II: Effect of pore structure and or degree of hydration," Cement and Concrete Research, Vol 15, pp.401-410.

Poon, C.S., Lam, L., Kou, S.C., Wong, Y.L., and Wong, R. (2001), "Rate of pozzolanic reaction of metakaolinite in high performance cement pastes," Cement and Concrete Research. Vol 31, pp. 1301-6.

Péra, J., Husson, S., and Guilhot, B. (1999), "Influence of finely ground limestone on cement hydration," Cement and Concrete Composites, Vol 21, pp. 99-105.

Pratt, P.L., and Ghose, A. (1983), "Electron microscope studies of Portland cement microstructures during setting and hardening," Philosophical Transactions of the Royal Society of London, Vol A310, pp. 93-103.

Ramachandran, V.S. and Chun-mei, Z. (1986), "Influence of CaCO3 on hydration and microstructural characteristics of Tricalcium silicate," Il Cemento, Vol 3, pp. 129-152.

Ramachandran, V.S., Feldman, R.F., and Beaudoin, J.J. (1981), *Concrete Science*, Heyden & Son Ltd., London UK.

Rojas, M.F., and Cabrera, J. (2002), "The effect of temperature on the hydration rate and stability of the hydration phases of metakaolin-lime-water systems," Cement and Concrete Research, Vol 32, pp. 133-138.

Rostasy, F.S., Weib, R., and Wiedmann, G. (1980), "Changes of pore structure of cement mortars due to temperature," Cement and Concrete Research, Vol. 10, pp. 157-164.

Sato, T. (2002), "An AC Impedance Spectroscopy Study of the Freezing-Thawing Durability of Wollastonite Micro-Fibre Reinforced Cement Paste," Master's Thesis, University of Ottawa, Ottawa, Canada.

Sato, T. (2006), "Applications of Nanotechnology for the Sustainable Development of Cement-based Materials", PhD Thesis, University of Ottawa, Ottawa, Canada.

Sato, T., and Beaudoin, J.J. (2006), "The effect of nano-sized $CaCO_3$ addition on the hydration of OPC containing high volumes of ground granulated blast-furnace slag," 2nd International RILEM Symposium on Advances in Concrete through Science and Engineering (Quebec City), pp. 355-366.

Sato, T. and Beaudoin, J.J. (2007), "The effect of nano-sized CaCO3 addition on the hydration of cement paste containing high volumes of fly ash," 12th International Congress on the Chemistry of Cement (Montreal, QC, 2007). pp. 1-12.

Sereda, J.P. (1972), "Significance of microhardness of porous inorganic materials," Cement and Concrete Research, Vol 2, pp. 717-729.

Shoaib, M., Balaha, M.M., and Abdel-Rahman, A.G. (2000), "Influence of cement kiln dust substitution on the mechanical properties of concrete," Cement and Concrete Research, Vol. 30, pp. 371-377.

Siddique. R. (2006), "Utilization of cement kiln dust (CKD) in cement mortar and concrete- an overview", Resources, Conservation and Recycling, Vol 48, pp. 315-338.

Skalny, J. and Mindness, S. (1995), *Materials Science of Concrete IV*, The American Ceramic Society.

Soroka, I., and Setter, N. (1976), "The effect of fillers on strength of cement mortars", Cement and Concrete Research, Vol 7, pp. 449-456.

Taylor, H.F.W. (1997). *Chemistry of Cement.* Academic Press, London.

Wang, K., Shah, S.P., and Mishulovich, A. (2004), "Effects of curing temperature and NaOH addition on hydration and strength development of clinker-free CKD-fly ash binders," Cement and Concrete Research, Vol. 34, pp. 299-309.

Xie, P., Gu, P., Xu, Z., and Beaudoin, J.J. (1993). "A Rationalized A.C. Impedance Model for Microstructural Characterization of Hydrating Cement Systems," Cement and Concrete Research, 2, Vol 23, pp. 359-367.

Xu, Z., Gu, P., Xie, P., and Beaudoin, J.J. (1993), "Applications of A.C. impedance techniques in studies of porous cementitious materials (II): Relationship between ACIS behaviour and the porous microstructure," Cement and Concrete Research, Vol. 23, pp. 853-862.

Appendix

Table 3.2-1: Oxide analyses of the raw materials

Oxides	2005 OPC (% weight)	2008 OPC (% weight)	Bath (% weight)	Alpena (% weight)	Ashgrove (% weight)
Na_2O	0.1	0.09	--	0.31	0.27
MgO	1.99	1.86	2.18	1.03	1.89
K_2O	1.01	1.08	1.76	6.28	7.84
CaO	63.45	63.08	51.77	45.09	49.08
Al_2O_3	4.66	4.34	3.88	4.66	3.24
SiO_2	18.97	19.5	18.01	13.41	11.51
P_2O_5	0.13	0.13	--	0.083	0.07
SO_3	3.52	3.31	3.65	16.68	4.95
TiO_2	0.016	0.15	--	0.457	0.17
Fe_2O_3	1.64	2.57	2.88	1.75	1.59
MnO	0.03	0.04	--	--	0.04
Zr_2O	0.01	0.01	--	--	--

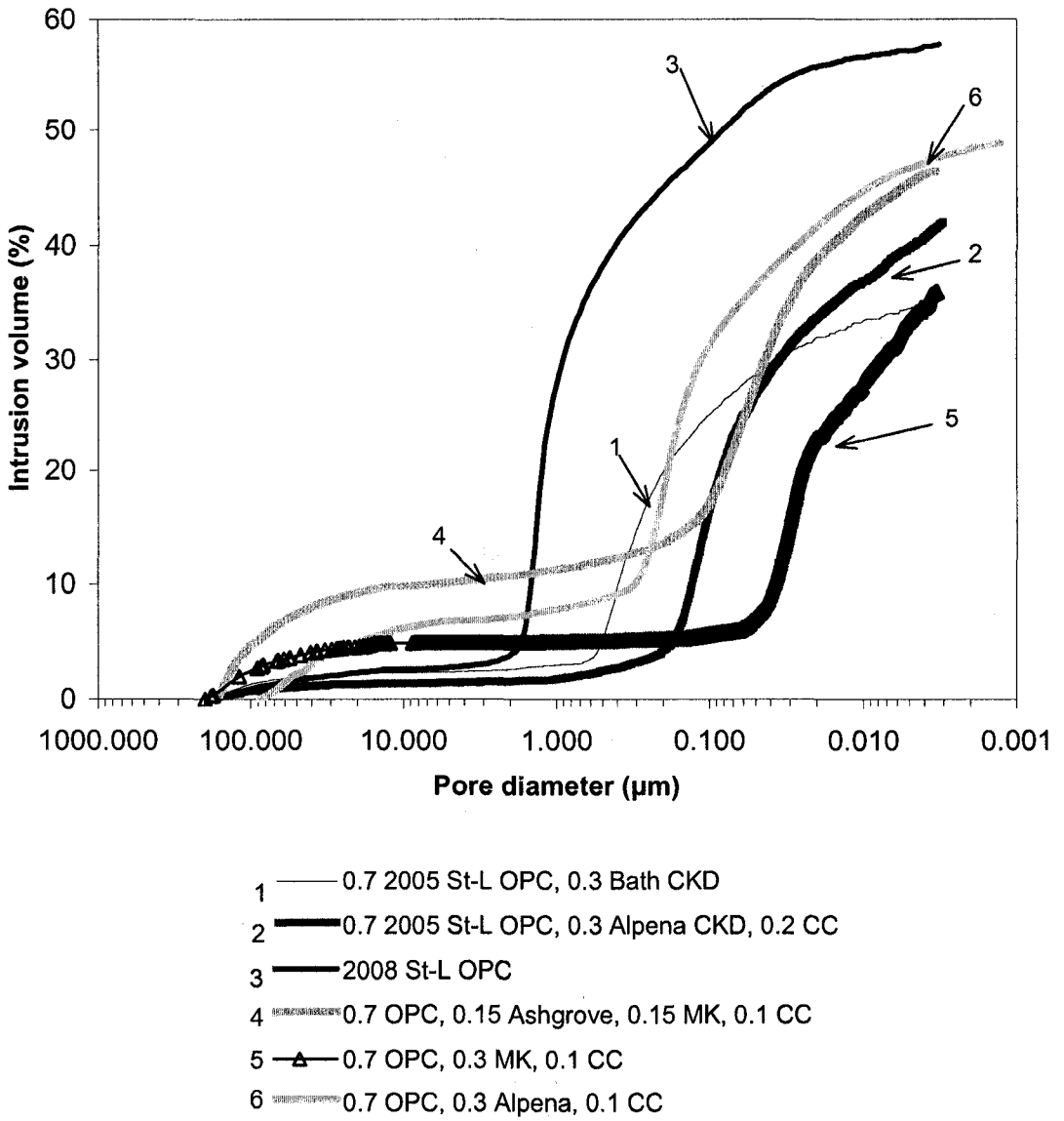

Fig. 8.7.1.1-1: Pore size distribution curves for the six samples tested with the mercury intrusion porosimeter.

Table 7.2-1: Compressive strength data for all mixes at 1, 3, 7, 28 d

Mix	time (d)			
	1	3	7	28
	Compressive Strength (MPa)			
OPC 2005 St-L	28.2	31.4	43.9	46.9
OPC, 0.1 CC	27.5	35.5	43.2	47.0
OPC, 0.2 CC	20.5	32.8	41.1	39.9
0.7 OPC, 0.3 Bath	20.2	27.2	29.8	35.6
0.7 OPC, 0.3 Bath, 0.1 CC	15.3	23.4	27.3	33.0
0.7 OPC, 0.3 Bath, 0.2 CC	15.6	22.1	24.5	30.4
0.7 OPC, 0.3 Alpena	14.7	19.3	24.9	31.2
0.7 OPC, 0.3 Alpena, 0.1 CC	13.4	20.5	23.3	33.0
0.7 OPC, 0.3 Alpena, 0.2 CC	12.4	19.0	22.6	34.5
OPC 2008 St-L	25.1	34.9	35.1	50.7
0.7 OPC, 0.3 Ashgrove	22.8	32.5	32.6	44.1
0.7 OPC, 0.3 Ashgrove, 0.1 CC	19.2	26.6	27.0	39.3
0.7 OPC, 0.3 Ashgrove, 0.2 CC	14.9	23.5	24.3	36.9
0.7 OPC, 0.15 Ashgrove, 0.15 MK	24.2	31.5	37.3	52.9
0.7 OPC, 0.15 Ashgrove, 0.15 MK, 0.1 CC	20.4	28.9	34.0	51.3
0.7 OPC, 0.15 Ashgrove, 0.15 MK, 0.2 CC	17.5	26.9	33.9	39.0
0.7 OPC, 0.3 MK	18.3	23.1	40.5	52.2
0.7 OPC, 0.3 MK, 0.1 CC	18.7	31.4	33.6	54.3

Table 7.2-2: Porosity data for all mixes at 1, 3, 7, 28 d

Mix	time (d)			
	1	3	7	28
	Porosity			
OPC 2005 St-L	0.399	0.329	0.341	0.342
OPC, 0.1 CC	0.437	0.431	0.338	0.299
OPC, 0.2 CC	0.384	0.377	0.346	0.315
0.7 OPC, 0.3 Bath	0.414	0.373	0.367	0.354
0.7 OPC, 0.3 Bath, 0.1 CC	0.439	0.414	0.382	0.390
0.7 OPC, 0.3 Bath, 0.2 CC	0.451	0.396	0.397	0.390
0.7 OPC, 0.3 Alpena	0.402	0.387	0.395	0.351
0.7 OPC, 0.3 Alpena, 0.1 CC	0.499	0.392	0.384	0.342
0.7 OPC, 0.3 Alpena, 0.2 CC	0.438	0.397	0.398	0.398
OPC 2008 St-L	0.329	0.320	0.341	0.191
0.7 OPC, 0.3 Ashgrove	0.476	0.303	0.269	0.183
0.7 OPC, 0.3 Ashgrove, 0.1 CC	0.376	0.301	0.294	0.240
0.7 OPC, 0.3 Ashgrove, 0.2 CC	0.399	0.386	0.340	0.334
0.7 OPC, 0.15 Ashgrove, 0.15 MK	0.352	0.275	0.212	0.190
0.7 OPC, 0.15 Ashgrove, 0.15 MK, 0.1 CC	0.289	0.426	0.338	0.210
0.7 OPC, 0.15 Ashgrove, 0.15 MK, 0.2 CC	0.343	0.315	0.275	0.158
0.7 OPC, 0.3 MK	0.447	0.349	0.324	0.308
0.7 OPC, 0.3 MK, 0.1 CC	0.411	0.309	0.251	0.225

Table 7.2-3: Trendline fit equations for strength vs. porosity (data covers 1, 3, 7, 28 days testing) with corresponding R^2 value for all mixes.

Mix	Trendline Fit Equation	R^2
OPC 2005	$776e^{-8.3088x}$	0.981
OPC, 0.1 CC	$88.882e^{-2.1315x}$	1.000
OPC, 0.2 CC	$113.17e^{-3.1697}$	0.628
0.7 OPC, 0.3 Bath	$802.04e^{-8.9364x}$	0.970
0.7 OPC, 0.3 Bath, 0.1 CC	$2665.8e^{-11.617x}$	0.844
0.7 OPC, 0.3 Bath, 0.2 CC	$848.7e^{-8.88434x}$	0.844
0.7 OPC, 0.3 Alpena	$449.6e^{-7.6869x}$	0.551
0.7 OPC, 0.3 Alpena, 0.1 CC	$752.33e^{-9.1288x}$	0.988
0.7 OPC, 0.3 Alpena, 0.2 CC	$3027e^{-12.537x}$	0.909
OPC 2008 St-L	$85.778e^{-2.7607x}$	1.000
0.7 OPC, 0.3 Ashgrove	$67.193e^{-2.2585x}$	0.999
0.7 OPC, 0.3 Ashgrove, 0.1 CC	$130.6e^{-5189x}$	0.960
0.7 OPC, 0.3 Ashgrove, 0.2 CC	$2311.9e^{-12.259x}$	0.843
0.7 OPC, 0.15 Ashgrove, 0.15 MK	$105.06e^{-4.2713x}$	0.894
0.7 OPC, 0.15 Ashgrove, 0.15 MK, 0.1 CC	$88.8e^{-2.7037x}$	0.982
0.7 OPC, 0.15 Ashgrove, 0.15 MK, 0.2 CC	$55.292e^{-2.0626x}$	0.836
0.7 OPC, 0.3 MK	$439.91e^{-7.1253x}$	0.984
0.7 OPC, 0.3 MK, 0.1 CC	$191.85e^{-5.7118x}$	0.995

Table 8.1-1: Porosity measurements for all cement systems 5, 8, 16, and 24 hours (this data was used in conjunction with AC impedance results).

Time (hrs)	2005 OPC	OPC, 0.1 CC	OPC, 0.2 CC
	Porosity		
5	0.497	0.526	0.526
8	0.440	0.489	0.439
16	0.434	0.354	0.325
24	0.287	0.274	0.334
Time (hrs)	0.7OPC, 0.3Bath	0.7OPC,0.3Bath,0.1CC	0.7OPC,0.3Bath,0.2CC
	Porosity		
5	0.510	0.549	0.546
8	0.446	0.476	0.463
16	0.377	0.369	0.462
24	0.342	0.372	0.401
Time (hrs)	0.7OPC, 0.3Alpena	0.7OPC,0.3Alpena,0.1CC	0.7OPC,0.3Alpena,0.2CC
	Porosity		
5	0.564	0.485	0.513
8	0.484	0.471	0.462
16	0.392	0.408	0.461
24	0.385	0.400	0.403
Time (hrs)	0.7OPC, 0.3Ashgrove	0.7OPC,0.3Ashgrove,0.1CC	0.7OPC,0.3Ashgrove,0.2CC
	Porosity		
5	0.499	0.541	0.499
8	0.478	0.421	0.449
16	0.341	0.414	0.433
24	0.295	0.341	0.369
Time (hrs)	0.7OPC, 0.15Ash,0.15MK	0.7OPC,0.3Ash,0.15MK,0.1CC	0.7OPC,0.3Ash,0.15MK,0.2CC
	Porosity		
5	0.559	0.411	0.457
8	0.440	0.333	0.348
16	0.440	0.302	0.313
24	0.335	0.267	0.327
Time (hrs)	0.7OPC, 0.3MK	0.7OPC, 0.3MK, 0.1 CC	2008 OPC
	Porosity		
5	0.555	0.453	0.564
8	0.471	0.404	0.477
16	0.328	0.323	0.432
24	0.330	0.274	0.346

Table 8.1-2 a): Trendline Equations, R^2 values, and data for first 24 hours porosity: control mixes.

Trendline Equation	$0.0005x^2+0.0053x+0.4636$	$0.0003x^2-0.0212x + 0.632$	$0.8505x^{-0.3153}$
R^2	0.923	0.9957	0.921
Time (hrs)	2005 OPC	1 OPC, 0.1 CC	1 OPC, 0.2 CC
1	0.468	0.611	0.851
2	0.472	0.591	0.684
3	0.475	0.571	0.602
4	0.477	0.552	0.549
5	0.478	0.534	0.512
6	0.477	0.516	0.483
7	0.476	0.498	0.460
8	0.474	0.482	0.441
9	0.471	0.466	0.425
10	0.467	0.450	0.412
11	0.461	0.435	0.399
12	0.455	0.421	0.389
13	0.448	0.407	0.379
14	0.440	0.394	0.370
15	0.431	0.382	0.362
16	0.420	0.370	0.355
17	0.409	0.358	0.348
18	0.397	0.348	0.342
19	0.384	0.338	0.336
20	0.370	0.328	0.331
21	0.354	0.319	0.326
22	0.338	0.311	0.321
23	0.321	0.303	0.316
24	0.303	0.296	0.312

Table 8.1-2 b): Trendline Equations, R^2 values, and data for first 24 hours porosity: Bath CKD mixes.

Trendline Equation	$0.8304x^{-0.2537}$	-0.0601Ln(x)+0.5859	$0.5283e^{-0.0108x}$
R^2	0.998	0.936	0.841
Time (hrs)	0.7 OPC, 0.3 Bath	0.7 OPC, 0.3 Bath, 0.1 CC	0.7 OPC, 0.3 Bath, 0.2 CC
1	0.830	0.586	0.523
2	0.696	0.544	0.517
3	0.628	0.520	0.511
4	0.584	0.503	0.506
5	0.552	0.489	0.501
6	0.527	0.478	0.495
7	0.507	0.469	0.490
8	0.490	0.461	0.485
9	0.476	0.454	0.479
10	0.463	0.448	0.474
11	0.452	0.442	0.469
12	0.442	0.437	0.464
13	0.433	0.432	0.459
14	0.425	0.427	0.454
15	0.418	0.423	0.449
16	0.411	0.419	0.444
17	0.405	0.416	0.440
18	0.399	0.412	0.435
19	0.393	0.409	0.430
20	0.388	0.406	0.426
21	0.384	0.403	0.421
22	0.379	0.400	0.417
23	0.375	0.397	0.412
24	0.371	0.395	0.408

Table 8.1-2 c): Trendline Equations, R^2 values, and data for first 24 hours porosity: Alpena CKD mixes.

Trendline Equation	$0.8304x^{-0.2537}$	-0.0601Ln(x)+.5859	$0.5283e^{-0.0108x}$
R^2	0.957	0.950	0.856
Time (hrs)	0.7 OPC, 0.3 Alpena	0.7 OPC, 0.3 Alpena, 0.1 CC	0.7 OPC, 0.3 Alpena, 0.2 CC
1	0.830	0.586	0.523
2	0.696	0.544	0.517
3	0.628	0.520	0.511
4	0.584	0.503	0.506
5	0.552	0.489	0.501
6	0.527	0.478	0.495
7	0.507	0.469	0.490
8	0.490	0.461	0.485
9	0.476	0.454	0.479
10	0.463	0.448	0.474
11	0.452	0.442	0.469
12	0.442	0.437	0.464
13	0.433	0.432	0.459
14	0.425	0.427	0.454
15	0.418	0.423	0.449
16	0.411	0.419	0.444
17	0.405	0.416	0.440
18	0.399	0.412	0.435
19	0.393	0.409	0.430
20	0.388	0.406	0.426
21	0.384	0.403	0.421
22	0.379	0.400	0.417
23	0.375	0.397	0.412
24	0.371	0.395	0.408

Table 8.1-2 d): Part 1: Trendline Equations, R^2 values, and data for first 24 hours porosity: Ashgrove CKD mixes and the control OPC.

Trendline Equation	-0.127Ln(x) + 0.7606	$0.0004x^2 - 0.0224x + 0.614$
R^2	0.956	0.979
Time (hrs)	2008 OPC	0.7 OPC, 0.3 Ashgrove
1	0.761	0.669
2	0.673	0.648
3	0.621	0.628
4	0.585	0.608
5	0.556	0.589
6	0.533	0.571
7	0.513	0.554
8	0.497	0.538
9	0.482	0.522
10	0.468	0.507
11	0.456	0.493
12	0.445	0.480
13	0.435	0.468
14	0.425	0.456
15	0.417	0.445
16	0.408	0.435
17	0.401	0.426
18	0.394	0.418
19	0.387	0.410
20	0.380	0.403
21	0.374	0.397
22	0.368	0.392
23	0.362	0.388
24	0.357	0.384

Table 8.1-2 d): Part 2: Trendline Equations, R^2 values, and data for first 24 hours porosity: Ashgrove CKD mixes.

Trendline Equation	$0.7746x^{-0.2503}$	$0.5246e^{-0.0141x}$
R^2	0.859	0.925
Time (hrs)	0.7 OPC,0.3 Ashgrove,0.1 CC	0.7 OPC, 0.3 Ashgrove, 0.2 CC
1	0.775	0.517
2	0.651	0.510
3	0.588	0.503
4	0.547	0.496
5	0.518	0.489
6	0.495	0.482
7	0.476	0.475
8	0.460	0.469
9	0.447	0.462
10	0.435	0.456
11	0.425	0.449
12	0.416	0.443
13	0.408	0.437
14	0.400	0.431
15	0.393	0.425
16	0.387	0.419
17	0.381	0.413
18	0.376	0.407
19	0.371	0.401
20	0.366	0.396
21	0.362	0.390
22	0.357	0.385
23	0.353	0.379
24	0.350	0.374

Table 8.1-2 e): Part 1: Trendline Equations, R^2 values, and data for first 24 hours porosity: Ashgrove CKD wtih MK mixes.

Trendline Equation	$0.5873e^{-0.0225x}$	$0.597x^{-0.2537}$
R^2	0.838	0.952
Time (hrs)	0.7 OPC, 0.15 Ashgrove, 0.15 MK	0.7 OPC, 0.15 Ashgrove, 0.15MK, 0.1CC
1	0.574	0.597
2	0.561	0.501
3	0.549	0.452
4	0.537	0.420
5	0.525	0.397
6	0.513	0.379
7	0.502	0.364
8	0.491	0.352
9	0.480	0.342
10	0.469	0.333
11	0.459	0.325
12	0.448	0.318
13	0.438	0.311
14	0.429	0.306
15	0.419	0.300
16	0.410	0.295
17	0.401	0.291
18	0.392	0.287
19	0.383	0.283
20	0.374	0.279
21	0.366	0.276
22	0.358	0.273
23	0.350	0.269
24	0.342	0.267

Table 8.1-2 f): Part 2, Continued: Trendline Equations, R^2 values, and data for first 24 hours porosity: Ashgrove CKD with MK mixes.

Trendline Equation	$0.5876x^{-0.2068}$	-0.1551Ln(x)+0.7947	-0.114Ln(x) + 0.6382
R^2	0.728	0.941	0.999
Time (hrs)	0.7OPC, 0.15Ashgrove, 0.15MK, 0.2CC	0.7 OPC, O.3 MK	0.7 OPC, 0.3 MK, 0.1 CC
1	0.588	0.795	0.638
2	0.509	0.687	0.559
3	0.468	0.624	0.513
4	0.441	0.580	0.480
5	0.421	0.545	0.455
6	0.406	0.517	0.434
7	0.393	0.493	0.416
8	0.382	0.472	0.401
9	0.373	0.454	0.388
10	0.365	0.438	0.376
11	0.358	0.423	0.365
12	0.351	0.409	0.355
13	0.346	0.397	0.346
14	0.340	0.385	0.337
15	0.336	0.375	0.329
16	0.331	0.365	0.322
17	0.327	0.355	0.315
18	0.323	0.346	0.309
19	0.320	0.338	0.303
20	0.316	0.330	0.297
21	0.313	0.322	0.291
22	0.310	0.315	0.286
23	0.307	0.308	0.281
24	0.305	0.302	0.276

Table 8.3-1 a) to -r): AC impedance spectra data: values for R_1, R_2, and n along with their respective errors for each mix.

Table 8.3-1 a)

Sample: 2005 OPC						
time (hrs)	R_1 (Ω)	R_1 % Error	R_2 (Ω)	R_2 % Error	n	n % Error
10	1184	0.53	108	6.99	0.818	5.91
11	1260	0.59	137	6.41	0.787	5.29
12	1320	0.65	165	6.12	0.762	4.95
13	1392	0.72	200	5.82	0.741	4.58
14	1462	0.80	240	5.60	0.721	4.32
15	1527	0.87	277	5.48	0.706	4.13
16	1587	0.92	312	5.31	0.697	3.94
17	1643	0.97	343	5.23	0.689	3.82
18	1695	1.00	371	5.14	0.685	3.70
19	1743	1.00	391	4.99	0.684	3.57
20	1786	0.97	406	4.80	0.686	3.42
21	1828	0.96	419	4.67	0.688	3.31
22	1873	0.92	433	4.48	0.691	3.16
23	1918	0.89	448	4.25	0.695	2.98
24	1967	0.87	469	4.06	0.697	2.84

Table 8.3-1 b)

Sample: 2005 OPC, 0.1 CC						
time (hrs)	R_1 (Ω)	R_1 % Error	R_2 (Ω)	R_2 % Error	n	n % Error
11	1296	0.39	49.2	14.70	0.828	14.23
12	1351	0.41	58.7	13.36	0.8	12.90
13	1430	0.45	71.6	12.21	0.767	11.71
14	1515	0.48	86.3	11.18	0.744	10.58
15	1598	0.51	102	10.52	0.717	9.79
16	1675	0.58	120	10.32	0.689	9.39
17	1750	0.62	136	10.00	0.676	8.84
18	1824	0.67	155	9.63	0.665	8.29
19	1901	0.70	175	9.17	0.658	7.67
20	1983	0.74	198	8.72	0.654	7.05
21	2068	0.77	224	8.30	0.653	6.46
22	2156	0.81	252	7.95	0.651	5.96
23	2235	0.85	282	7.64	0.65	5.55
24	2318	0.89	314	7.35	0.651	5.16

Table 8.3-1 c)

Sample: 2005 OPC, 0.2 CC						
time (hrs)	R_1 (Ω)	R_1 % Error	R_2 (Ω)	R_2 % Error	n	n % Error
11	1446	0.34	50.2	14.82	0.89	12.49
12	1503	0.36	57.9	13.90	0.862	11.80
13	1563	0.37	65.9	13.02	0.842	11.07
14	1630	0.39	75.1	12.20	0.823	10.35
15	1705	0.41	85.6	11.24	0.81	9.44
16	1796	0.43	99.7	10.36	0.795	8.54
17	1900	0.45	118	9.41	0.782	7.56
18	2007	0.49	141	8.66	0.767	6.75
19	2106	0.53	168	8.13	0.749	6.13
20	2213	0.59	201	7.68	0.734	5.57
21	2322	0.66	242	7.37	0.72	5.11
22	2432	0.73	290	6.98	0.709	4.63
23	2529	0.78	339	6.56	0.701	4.16
24	2630	0.81	388	6.15	0.698	3.77

Table 8.3-1 d)

Sample: 0.7 OPC, 0.3 Bath						
time (hrs)	R_1 (Ω)	R_1 % Error	R_2 (Ω)	R_2 % Error	n	n % Error
11	964	0.46	92.9	10.38	0.566	10.60
12	1008	0.50	104	10.10	0.546	10.37
13	1056	0.54	117	9.82	0.527	10.11
14	1107	0.59	132	9.61	0.508	9.92
15	1158	0.64	149	9.45	0.49	9.76
16	1207	0.70	164	9.26	0.478	9.55
17	1256	0.77	183	9.21	0.463	9.47
18	1301	0.85	204	9.21	0.449	9.43
19	1339	0.92	223	9.31	0.436	9.50
20	1374	1.01	242	9.48	0.424	9.63
21	1407	1.07	259	9.53	0.416	9.66
22	1436	1.13	276	9.56	0.409	9.67
23	1466	1.20	295	9.63	0.401	9.70
24	1498	1.29	318	9.65	0.393	9.66

Table 8.3-1 e)

Sample: 0.7 OPC, 0.3 Bath, 0.1CC						
time (hrs)	R_1 (Ω)	R_1 % Error	R_2 (Ω)	R_2 % Error	n	n % Error
12	1144	0.30	36.2	17.90	0.814	15.38
13	1189	0.32	40.7	17.15	0.791	14.91
14	1231	0.34	45.2	16.48	0.77	14.47
15	1274	0.37	49.9	16.21	0.751	14.33
16	1327	0.39	56	15.72	0.731	13.97
17	1396	0.44	64.6	15.30	0.708	13.61
18	1478	0.49	75.8	14.56	0.689	12.85
19	1563	0.55	89.1	13.89	0.671	12.04
20	1645	0.63	105	13.50	0.653	11.41
21	1724	0.71	122	13.19	0.639	10.79
22	1799	0.81	141	13.03	0.628	10.25
23	1869	0.89	160	12.72	0.621	9.64
24	1933	0.99	180	12.73	0.613	9.26

Table 8.3-1 f)

Sample: 0.7 OPC, 0.3 Bath, 0.2CC						
time (hrs)	R_1 (Ω)	R_1 % Error	R_2 (Ω)	R_2 % Error	n	n % Error
12	1129	0.41	42.7	18.37	0.66	17.36
13	1160	0.44	46.8	17.89	0.648	16.87
14	1191	0.48	51.2	17.53	0.635	16.48
15	1229	0.52	56.8	17.06	0.623	15.91
16	1283	0.57	65	16.41	0.611	15.03
17	1349	0.66	76.4	16.09	0.597	14.31
18	1417	0.74	89	15.53	0.588	13.34
19	1483	0.85	104	15.42	0.576	12.69
20	1547	0.95	119	15.09	0.57	11.84
21	1609	1.07	137	14.95	0.565	11.15
22	1667	1.18	156	14.68	0.561	10.42
23	1719	1.31	176	14.60	0.56	9.83
24	1758	1.43	194	14.64	0.556	9.46

Table 8.3-1 g)

Sample: 0.7 OPC, 0.3 Alpena						
time (hrs)	R_1 (Ω)	R_1 % Error	R_2 (Ω)	R_2 % Error	n	n % Error
11	1052	0.46	67.7	12.71	0.691	12.33
12	1151	0.50	84.4	11.62	0.658	11.31
13	1254	0.57	106	10.83	0.626	10.49
14	1355	0.68	136	10.35	0.588	9.92
15	1449	0.82	171	10.09	0.556	9.49
16	1538	1.00	212	10.02	0.529	9.14
17	1621	1.20	258	9.89	0.51	8.69
18	1696	1.44	310	9.94	0.493	8.37
19	1767	1.62	364	9.70	0.484	7.85
20	1829	1.85	423	9.62	0.474	7.47
21	1885	2.08	485	9.55	0.466	7.14
22	1931	2.43	551	9.85	0.457	7.05
23	1977	2.69	617	9.86	0.452	6.82
24	2019	2.94	680	9.90	0.449	6.65

Table 8.3-1 h)

Sample: 0.7 OPC, 0.3 Alpena, 0.1CC						
time (hrs)	R_1 (Ω)	R_1 % Error	R_2 (Ω)	R_2 % Error	n	n % Error
12	1766	0.53	148	7.86	0.868	5.32
13	1871	0.66	200	7.36	0.828	4.77
14	1964	0.82	264	7.05	0.797	4.33
15	2048	0.99	335	6.84	0.775	3.97
16	2123	1.14	412	6.51	0.764	3.59
17	2185	1.31	498	6.29	0.753	3.31
18	2233	1.55	592	6.35	0.742	3.20
19	2271	1.77	691	6.28	0.733	3.05
20	2300	2.02	793	6.27	0.726	2.94
21	2331	2.19	891	6.11	0.724	2.80
22	2351	2.48	1005	6.16	0.717	2.74
23	2372	2.65	1107	6.03	0.715	2.64
24	2392	2.72	1201	5.74	0.714	2.49

Table 8.3-1 i)

Sample: 0.7 OPC, 0.3 Alpena, 0.2 CC						
time (hrs)	R_1 (Ω)	R_1 % Error	R_2 (Ω)	R_2 % Error	n	n % Error
11	1344	0.89	128	10.93	0.695	8.19
12	1421	1.02	157	10.56	0.683	7.54
13	1492	1.15	189	10.26	0.673	6.97
14	1559	1.29	225	9.98	0.664	6.48
15	1620	1.46	264	9.87	0.655	6.13
16	1676	1.63	306	9.73	0.647	5.80
17	1727	1.82	351	9.69	0.64	5.55
18	1773	2.01	399	9.63	0.636	5.33
19	1814	2.23	450	9.64	0.631	5.14
20	1853	2.42	499	9.57	0.629	4.97
21	1886	2.64	551	9.60	0.626	4.85
22	1916	2.83	603	9.53	0.621	4.73
23	1944	2.91	644	9.29	0.619	4.58
24	1961	3.10	689	9.30	0.616	4.50

Table 8.3-1 j)

Sample: 2008 OPC						
time (hrs)	R_1 (Ω)	R_1 % Error	R_2 (Ω)	R_2 % Error	n	n % Error
12	1135	0.57	89.3	9.33	0.747	8.36
13	1239	0.65	119	8.41	0.714	7.26
14	1346	0.73	155	7.67	0.689	6.33
15	1453	0.82	198	7.04	0.668	5.54
16	1558	0.91	250	6.57	0.649	4.93
17	1658	1.01	307	6.20	0.635	4.43
18	1746	1.13	370	5.95	0.621	4.06
19	1826	1.23	435	5.71	0.612	3.73
20	1895	1.36	503	5.60	0.604	3.51
21	1963	1.45	573	5.40	0.599	3.28
22	2025	1.56	650	5.26	0.593	3.09
23	2085	1.64	729	5.05	0.59	2.89
24	2139	1.73	811	4.88	0.588	2.73

Table 8.3-1 k)

Sample: 0.7 OPC, 0.3 Ashgrove						
time (hrs)	R_1 (Ω)	R_1 % Error	R_2 (Ω)	R_2 % Error	n	n % Error
17	1027	0.44	46.9	14.77	0.673	14.34
18	1123	0.52	63.8	12.59	0.652	11.76
19	1218	0.61	84.9	11.48	0.627	10.24
20	1313	0.71	111	10.52	0.61	8.87
21	1409	0.87	145	10.11	0.589	8.04
22	1500	0.98	182	9.36	0.579	7.01
23	1584	1.12	226	8.96	0.57	6.33
24	1665	1.25	273	8.57	0.563	5.76

Table 8.3-1 l)

Sample: 0.7 OPC, 0.3 Ashgrove, 0.1CC						
time (hrs)	R_1 (Ω)	R_1 % Error	R_2 (Ω)	R_2 % Error	n	n % Error
20	1543	0.393	50.2	17.39	0.892	14.163
21	1650	0.449	66.1	15.294	0.852	12.337
22	1754	0.522	85	14.013	0.818	11.036
23	1851	0.595	107	12.932	0.793	9.8496
24	1942	0.688	132	12.32	0.769	9.0243

Table 8.3-1 m)

Sample: 0.7 OPC, 0.3 Ashgrove, 0.2 CC						
time (hrs)	R_1 (Ω)	R_1 % Error	R_2 (Ω)	R_2 % Error	n	n % Error
20	1353	0.44	42.8	20.56	0.826	18.28
21	1428	0.48	51	18.82	0.81	16.52
22	1498	0.52	60.1	17.38	0.797	14.98
23	1563	0.55	69.6	16.11	0.787	13.59
24	1622	0.59	79.5	15.27	0.778	12.58

Table 8.3-1 n)

Sample: 0.7 OPC, 0.15 Ashgrove, 0.15 MK						
time (hrs)	R_1 (Ω)	R_1 % Error	R_2 (Ω)	R_2 % Error	n	n % Error
19	1543	0.98	121	15.72	0.641	13.09
20	1643	1.19	156	15.13	0.627	11.76
21	1737	1.41	194	14.65	0.62	10.62
22	1816	1.67	237	14.48	0.613	9.83
23	1887	1.96	285	14.50	0.605	9.23
24	1966	2.04	323	13.76	0.614	8.49

Table 8.3-1 o)

Sample: 0.7OPC,0.15Ashgrove,0.15MK,0.1CC						
time (hrs)	R_1 (Ω)	R_1 % Error	R_2 (Ω)	R_2 % Error	n	n % Error
16	1355	1.57	151	18.99	0.542	16.85
17	1444	1.81	185	17.62	0.548	14.46
18	1528	1.97	223	16.13	0.559	12.27
19	1606	2.08	262	14.71	0.573	10.47
20	1679	2.16	303	13.51	0.587	9.08
21	1743	2.22	346	12.50	0.596	8.03
22	1798	2.28	387	11.71	0.604	7.24
23	1851	2.39	433	11.20	0.609	6.67
24	1901	2.47	480	10.64	0.615	6.14

Table 8.3-1 p)

Sample: 0.7OPC,0.15Ashgrove,0.15MK,0.2CC						
time (hrs)	R_1 (Ω)	R_1 % Error	R_2 (Ω)	R_2 % Error	n	n % Error
18	1502	0.41	62.8	19.09	0.741	17.89
19	1579	0.44	73	17.43	0.714	16.54
20	1649	0.47	83.9	16.28	0.691	15.55
21	1714	0.51	95.4	15.26	0.671	14.60
22	1766	0.55	107	14.56	0.654	13.88
23	1812	0.58	118	13.84	0.642	13.12
24	1852	0.62	129	13.42	0.629	12.62

Table 8.3-1 q)

Sample: 0.7OPC, 0.3 MK						
time (hrs)	R_1 (Ω)	R_1 % Error	R_2 (Ω)	R_2 % Error	n	n % Error
14	2063	0.48	142	7.79	0.948	4.13
15	2179	0.56	193	6.91	0.926	3.41
16	2291	0.66	254	6.38	0.91	2.96
17	2392	0.75	324	5.88	0.899	2.58
18	2483	0.84	403	5.47	0.89	2.28
19	2563	0.93	488	5.12	0.882	2.05
20	2611	1.01	559	4.93	0.876	1.92
21	2661	1.07	636	4.70	0.872	1.79
22	2718	1.12	719	4.42	0.87	1.65
23	2767	1.18	806	4.22	0.868	1.55
24	2814	1.18	893	3.86	0.867	1.40

Table 8.3-1 r)

Sample: 0.7OPC, 0.3 MK, 0.1 CC						
time (hrs)	R_1 (Ω)	R_1 % Error	R_2 (Ω)	R_2 % Error	n	n % Error
15	2080	0.80	133	14.82	0.697	11.16
16	2195	0.97	170	14.30	0.683	9.94
17	2302	1.18	215	14.06	0.671	9.01
18	2401	1.43	267	14.01	0.663	8.26
19	2487	1.67	324	13.79	0.657	7.56
20	2564	1.94	389	13.61	0.654	6.94
21	2639	2.15	453	13.22	0.657	6.36
22	2690	2.46	525	13.24	0.654	6.00
23	2735	2.69	592	12.97	0.654	5.63
24	2764	2.90	651	12.81	0.652	5.37

Table 8.7-2: Trendline equations and R^2 values for the six samples used in the R_2 vs $1/(Pr_o)$ analysis for estimating R_2 values at 8 hours.

Mix	R^2	Trendline Equation
2008 OPC	0.996	$0.034x^{3.1953}$
0.7 OPC, 0.3 Bath	0.999	$1.8986x^{1.6128}$
0.7 OPC, 0.3 Alpena, 0.2 CC	0.998	$0.695x^{2.1887}$
0.7 OPC, 0.15 Ashgrove, 0.15 MK, 0.1 CC	0.996	$0.0604x^{2.8358}$
0.7 OPC, 0.3 MK, 0.1 CC	0.995	$0.0131x^{3.4248}$
0.7 OPC, 0.3 Alpena, 0.1 CC	0.992	$0.0915x^{3.0151}$